DUBNA

CIFRA

VIII International Pontecorvo Neutrino Physics School

Proceedings

of the Student Poster Session

Edited by F. Šimkovic

JOINT INSTITUTE FOR NUCLEAR RESEARCH

VIII INTERNATIONAL PONTECORVO NEUTRINO PHYSICS SCHOOL

Sinaia, Romania
September 1–10, 2019

Proceedings of Student Poster Session

Edited by F. Šimkovic

Dubna 2020

УДК 539.123(063)539.1.07(063)
ББК 22.382.4я431
22.381.5я431
I69

The financial support was provided by grants of the JINR Directorate and the Plenipotentiaries of the Governments of the Czech Republic and Romania, by the programme of cooperation between JINR and Comenius University in Bratislava, and by IEAP CTU in Prague, and by European Regional Development Fund — project No.EF16_019/0000766.

Composed by *A. Babič* and *A. V. Malykh.*

Title page design by *A. V. Malykh.*

The contributions are reproduced directly from the originals presented by the Organizing Committee.

VIII International Pontecorvo Neutrino Physics School (Sinaia, Romania,
I69 September 1–10, 2019): Proceedings of Student Poster Session / Ed. F. Šimkovic. — Dubna: JINR, 2020. — 190 p.

ISBN 978-5-9530-0538-8

The VIII International Pontecorvo Neutrino Physics School, which was organized by the Joint Institute for Nuclear Research in Dubna, International Centre for Advanced Training and Research in Physics in Bucharest, Czech Technical University, Charles University in Prague, and Comenius University in Bratislava, was held at Hotel International, Sinaia mountain resort (Romania), on September 1–10, 2019.

The School covered a broad range of topics in neutrino physics and neutrino cosmology. The purpose of the School was to review the present status of experimental and theoretical neutrino physics. Twenty-two outstanding lecturers drew attention of 78 students and young scientists to prominent neutrino physics experiments and unsolved problems concerning fundamental properties and interactions of neutrinos. Three evening discussion sessions were organized covering problems of oscillation mechanism, the effect of matter, and the nature of neutrino masses. Thirty-five students and young scientists presented results of their research during the Student Poster Session, 17 of them contributed to this Proceedings.

УДК 539.123(063)539.1.07(063)
ББК 22.382.4я431
22.381.5я431

ISBN 978-5-9530-0538-8

Organizing Committee

Chairman:

V.A. Matveev (JINR, Dubna)

Scientific program:

S.M. Bilenky (JINR, Dubna)

Vice-chairmen:

A.G. Olshevskiy (JINR, Dubna)
S. Stoica (CIFRA, Bucharest)
I. Štekl (CTU, Prague)
F. Šimkovic (Comenius U., Bratislava/JINR, Dubna)

Members:

V.A. Bednyakov (JINR, Dubna)
R. Leitner (Charles U., Prague)
C. Giunti (U. of Torino)
V.B. Brudanin (JINR, Dubna)
E.A. Kolganova (JINR, Dubna)

Secretaries:

A. Babic (JINR, Dubna)
D. Ali (Bucharest)
A. Neacsu (CIFRA, Bucharest)
O. Nitescu (CIFRA, Bucharest)
C. Militaru (CIFRA, Bucharest)

VIII International Pontecorvo Neutrino Physics School

September 3 – September 10, 2019
Sinaia, Romania

http://theor.jinr.ru/~neutrino/19/

Introduction to ν-physics — Samoil Bilenky (JINR Dubna)
Theory of ν-masses and mixing — Alexei Smirnov (MPI Heidelberg)
ν-oscillation phenomenology — Boris Kayser (Fermilab)
ν oscillations experiments:
- Solar ν-experiments — Oleg Smirnov (JINR Dubna)
- Atmospheric ν-experiments — Juan Pablo Yanez (Univ. of Alberta)
- Accelerator ν-experiments — Maury Goodman (Argonne National Lab)
- Reactor ν-experiments — Dmitry Naumov (JINR Dubna)

Spectra of ν's from reactor — Anna Hayes (Los Alamos National Lab)
Light sterile neutrinos
- theory — Carlo Giunti (INFN)
- experiments — Yuri Shitov (JINR Dubna)

Heavy sterile neutrinos — Dmitry Gorbunov (INR RAS Moscow)

Measurement of ν-mass — Kathrin Valerius (KIT in Karlsruhe)
0νββ-decay experiments — Andrea Giuliani (CSNSM in Paris)
0νββ-decay NME's — Javier Menendez (Univ. of Tokyo)
Coherent scattering of ν's — Henry Wong (Academia Sinica, Taipei)
ν-nucleus interactions — Jan Sobczyk (Univ. of Wroclaw)
Leptogenesis — Pasquale Di Bari (Univ. of Southampton)
ν-telescopes — Nathan Whitehorn (Univ. of California)
ν-properties from cosmology — Richard Battye (Univ. of Manchester)
Dark matter searches — Suchita Kulkarni (HEPHY Vienna)
Physics of gravitational waves — Imre Bartos (Univ. of Florida)
Everything about Higgs boson — Gheorghe Mitselmakher (Univ. of Florida)
Statistics for ν-experiments — Thomas Schwetz (KIT in Karlsruhe)

VIII International Pontecorvo Neutrino Physics School (group photo)

Contents

POSTER SESSION

PREFACE

GENERAL INFORMATION

The VIII International Pontecorvo Neutrino Physics School continued the tradition of the Pontecorvo Neutrino Physics Schools, which were held in Dubna, Alushta, Horny Smokovec and Prague in 1998, 2003, 2007, 2010, 2012, 2015 and 2017. The information about all editions of the Pontecorvo Schools can be reached through the web site http://pontecorvosch.jinr.ru.

The Pontecorvo Schools were initiated by Samoil Bilenky to commemorate the eminent neutrino physicist Bruno Pontecorvo (called Mr. Neutrino), whose pioneering scientific contributions go on shaping modern neutrino physics. Bruno Pontecorvo was working in Dubna within the period 1950–1993, where in 1957 he suggested the idea of neutrino oscillations, a phenomenon which was experimentally discovered about 40 years later and which remains one of the most intriguing subjects of the modern particle physics. The growing number of School participants demonstrates that neutrino studies attract more and more young people nowadays.

The Pontecorvo School series is now enjoying a period of rapid development and worldwide interest to open problems of neutrino physics. We still do not know the number of neutrino species, the absolute neutrino masses, the size of any leptonic CP violation and the characteristic nature of the neutrino. Improving our understanding of neutrino mass and its origin is so important, when it comes to some of the big unanswered question in physics today. Neutrino physics is receiving more and more attention as a source of information on new physics beyond the Standard Model being a benchmark for new theory in elementary particles and for the understanding of the Universe evolution. Neutrino physics is a window on the knowledge of the infinitely small and on the infinitely large. Due to unwillingness of neutrinos to interact with matter, the study of their properties requires the construction of extremely large detectors placed usually in environments with very low natural radioactivity and shielded from the cosmic radiation.

It is noteworthy that there were some highlights in the history of the Pontecorvo Schools. For instance, within the 2017 edition, organized by the Institute of Experimental and Applied Physics (Czech Technical University in Prague) and its Director Ivan Štekl, there were two lectures dedicated to the discovery of gravitational waves and given by Barry Barish (Caltech) who was awarded for this result the 2017 Nobel Prize in Physics, together with R. Weiss and K. Thorne, just one month after the end of the School.

The source of our special pride is that it was the second Nobel Prize winner among the lecturers of the Pontecorvo Schools. The first one was Takaaki Kajita (University of Tokyo) who received the 2015 Nobel Prize in Physics for the discovery of neutrino oscillations, which show that neutrinos have mass. In 2007, in Alushta, Professor Kajita talked about these research results in his lecture on the physics of atmospheric neutrinos.

PRESENT SCHOOL

The VIII International Pontecorvo Neutrino Physics School took place in the beautiful mountain resort Sinaia in the Prahova river valley in Romania from 1 to 10 September 2019.

The VIII Pontecorvo Neutrino Physics School covered a broad range of topics in neutrino physics, astroparticle physics and cosmology. The purpose of the School was to review the latest achievements in above mentioned fields, both from theoretical and experimental points of view.

ORGANIZERS

The VIII Pontecorvo Neutrino Physics School was organized by the International Centre for Advanced Training and Research in Physics (Măgurele-Bucharest, Romania) in cooperation with the Joint Institute for Nuclear Research (Dubna, Russia), Institute of Experimental and Applied Physics (Czech Technical University in Prague, the Czech Republic), Charles University in Prague (the Czech Republic) and Comenius University in Bratislava (Slovakia).

The funding for the School was provided by the grants of the JINR Directorate and the Plenipotentiaries of the Governments of the Czech Republic, Romania, as well as by the program of cooperation between JINR and Comenius University in Bratislava, IEAP CTU in Prague, and European Regional Development Fund-Project No. EF16_019/0000766.

VENUE

The town of Sinaia, also known as "Pearl of the Carpathians," is a famous tourist attraction, not far from the geographical center of Romania, near the historical border between the principalities of Transylvania and Wallachia, within walking distance of Peleș Castle, one of the World Heritage Sites. The venue of the School was Hotel International, a four-star complex where all participants were accommodated.

PROGRAM OF THE SCHOOL

In the formation of the Pontecorvo School programmes, much credit goes to Samoil Bilenky, an outstanding expert and international authority in neutrino physics, well acquainted with the subject and the scientists working in all fields related to neutrinos. He is not only the founder of the School but also its permanent organizer, the scientific programme supervisor, and excellent lecturer.

Program of the School covered modern topics of neutrino physics, astrophysics and cosmology:

- Theory of neutrino mixing and masses
- Solar, atmospheric, reactor and geo neutrino experiments
- Direct neutrino mass measurements
- Neutrinoless double-beta decay (theory and experiment)
- Neutrino-nucleus interactions
- Sterile neutrinos
- Neutrino cosmology and astronomy
- Dark matter
- Leptogenesis and baryogenesis

- Gravitational waves
- Statistics for nuclear and particle physics

LECTURERS AND LECTURES AT THE SCHOOL

The members of the Organizing Committee Samoil Bilenky, Rupert Leitner, Fedor Šimkovic and Alexander Olshevskiy succeeded to invite the most knowledgeable experts in corresponding areas who delivered high quality lectures for the wide audience: undergraduates, PhD students, postdocs, and also some members of academic staff.

During 9 working days outstanding lecturers from the field of neutrino physics, astroparticle physics and cosmology drew attention of the students and young scientists to prominent neutrino physics experiments and unsolved problems concerning fundamental properties and interactions of neutrinos.

The 23 leading scientists presented their lectures on various neutrino topics: neutrino mixing and masses, neutrino oscillations, interactions with nuclei, sterile neutrinos, and neutrino detectors. Some related topics were also introduced, like double-beta decay, gravitational waves, dark matter, and leptogenesis. The wide range of subject matters backed up both the theoretical and experimental aspects of this field.

- Samoil Bilenky (JINR, Dubna)
  Introduction to neutrino
- Alexei Smirnov (MPI, Heidelberg)
  Theory of ν-masses and mixing
- Boris Kayser (Fermilab)
  ν-oscillation phenomenology
- Oleg Smirnov (JINR, Dubna)
  Solar ν-experiments
- Juna Pablo Yanez (Univ. of Alberta)
  Atmospheric ν-experiments
- Maury Goodman (Argonne National Laboratory)
  Accelerator ν-experiments
- Dmitry Naumov (JINR, Dubna)
  Reactor ν-experiments
- Anna Hayes (Los Alamos National Laboratory)
  Spectra of ν's from reactor
- Carlo Giunti (INFN, Torino)
  Light sterile ν's: theory
- Yuri Shitov (JINR, Dubna)
  Light sterile ν's: experiments
- Dmitry Gorbunov (INR RAS, Moscow)
  Heavy sterile ν's
- Kathrin Valerius (KIT in Karlsruhe)
  Measurement of ν-mass

- Andrea Giuliani (CSNSM in Paris)
  $0\nu\beta\beta$*-decay experiments*
- Javier Menendez (Univ. of Barcelona)
  $0\nu\beta\beta$*-decay nuclear matrix elements*
- Henri Wong (Academia Sinica, Taipei)
  Coherent ν*-nucleus elastic scattering*
- Jan Sobczyk (Wroclaw University)
  ν*-nucleus interaction*
- Pasquale Di Bari (Univ. of Southampton)
  Leptogenesis
- Richard Battye (Univ. of Manchaster)
  ν*-properties from cosmology*
- Suchita Kulkarni (HEPHY, Vienna)
  Dark matter searches
- Nathan Whitehorn (Univ. of California)
  ν*-telescopes*
- Imre Bartos (Univ. of Florida)
  Physics of gravitational waves
- Guenakh Mitselmakher (Univ. of Florida)
  Everything about Higgs boson
- Thomas Schwetz (KIT in Karlsruhe)
  Statistics for ν*-experiments*

A special session was held in memory of Bruno Pontecorvo, where the participants watched the film about this outstanding scientist, and Samoil Bilenky shared his memories about this man, whose scientific achievements and human qualities largely affected the currently formed image of Dubna, JINR, and world science.

Moreover, the scientific program of the School would not have been complete without the evening exercise sessions. Under the guidance of the top experts (Samoil Bilenky, Boris Kayser and Alexei Smirnov), the School listeners had the opportunity to solve various interesting problems in neutrino physics, reaching the level often beyond regular textbooks. These tasks were related to the neutrino oscillation mechanism, MSW effect on mixing parameters in matter, and Majorana nature of massive neutrinos. These events were found very useful to stimulate vitality for discussion, dialogue and debate on the topic covered.

PARTICIPANTS:

The 77 listeners attending the School were from all over the world: 22 of them came from JINR and Russia; 34 of them were from the JINR Member States, namely Belarus, the Czech Republic, Poland, Romania, Slovakia and Ukraine; and 21 of them arrived from China, Finland, France, Germany, India, Italy, Spain and the United Kingdom. The priority for participation in the school was given to the applicants with a strong neutrino physics background and interests.

According to the established School format, all the attendees were encouraged to participate in the discussions and informal exchanges of ideas during the breaks and after the lectures.

ACCOMMODATION:

Accommodation of all participants was organized in the beautiful Hotel International in Sinaia, where was also the venue of the School. The hotel offered 3 nice restaurants and catering facilities, an indoor pool and a spa center, and an entertainment center (bowling lanes, billiards tables, etc). From the rooms of Hotel International participants admired the views of the surrounding mountains.

POSTER SESSION:

On the last working day, within a special session, 35 of the participants presented their posters in a 3-minute talk. In spite of limited time they managed to deliver to the audience the main message covered in their posters, which were hanging at the wall of the Lecture Hall during the whole period of the School. Seventeen students and researchers contributed to this Proceedings of the student poster session.

EXCURSION

The picturesque mountain scenery emphasized the pleasant atmosphere of the School. It was the day off, when the School listeners had two full-day trips to choose from. The first one brought them to the Râșnov Fortress and Bran Castle (the latter is famous for

its Dracula legends). The second one let them go hiking in Bucegi Mountains up to 2000 meters above sea level.

The rich social program was concluded by a farewell dinner with traditional Romanian food, live music and dance, in a special place in surrounding mountains.

SUMMARY

There was a lot of positive feedback from the School participants. The beautiful location, comfortable venue, thought-out arrangements, outstanding lecturers, informative lectures were of high value for them. Besides, rich scientific and inspirational social communication let the listeners establish personal and professional contacts and made it possible to remain connected afterwards. This all means that the VIII Pontecorvo Neutrino Physics School was a great success.

THE NEXT EDITION OF PONTECORVO SCHOOL

The first School was held in Dubna. An important role in its organization was played, in addition to Samoil Bilenky, by the former Director of the JINR (Dubna), Alexei Sissakian, and Svetlana Ivanova. The next four Schools were organized in the beautiful JINR sea resort in Alushta, Crimea (`http://pontecorvosch.jinr.ru`). Since 2007, the former Director of the Laboratory of Nuclear Problems, Alexander Olshevskiy, fostered mainly the development of the Pontecorvo Schools.

Starting in 2015, the School geography has grown wide as Ivan Štekl (Czech Technical University in Prague) and Fedor Šimkovic (Comenius University in Bratislava) have joined actively the organization of the Schools, emphasizing their international character and increasing mutual fruitful cooperation with the JINR Member States. The sixth School moved to Horný Smokovec, High Tatras mountain region of Slovakia (`http://theor.jinr.ru/~neutrino15/`) and the seventh School was held in Prague, the capital of the Czech Republic (`http://theor.jinr.ru/~neutrino17/`). After a while, the Organizing Committee was extended again, and this time by the Romanian colleague Sabin Stoica and a prominent Italian neutrino physicist Carlo Giunti. The eighth School was successfully organized in the mountain resort Sinaia, in the Prahova region of Romania (`http://theor.jinr.ru/~neutrino19/`).

The preparation of the next Schools has already started. Firstly, the forthcoming IX Pontecorvo School is set to take place in Bratislava, the beauty on the Danube in Slovakia. Secondly, considering the very special occasion in 2023, the 110th anniversary of the birth of Bruno Pontecorvo, the X Pontecorvo School will be held in Italy.

THE JINR EDUCATIONAL POLICY

The School participants learned about the most challenging recent subjects in Neutrino Physics, as well as about ongoing and upcoming opportunities for participating in neutrino physics research, particularly in the Neutrino Program at the Dzhelepov Laboratory of Nuclear Problems, JINR. This Program is being carried out together with other research institutes of the Czech Republic, Poland, Romania, Russia and Slovakia.

The Pontecorvo Schools remain one of the key cornerstones of the scientific and educational philosophy at JINR, a worldwide-acknowledged research center. Moreover, it is obvious that the future JINR success significantly depends on new generations of young motivated researchers. That is why the JINR University Center, together with Ivan Štekl and Stanislav Pakuliak, developed effective stage-by-stage educational programs, in particular short and long-term summer practices, summer schools, and postdoc positions, to attract talented young researchers to JINR and give them every support and confidence.

Colloquiums in honor of Samoil Bilenky on occasion of his jubilee

Samoil Bilenky

Samoil Bilenky was born in Zmerinka, a town in the Ukrainian Republic of the USSR, on May 23, 1928. He graduated from MEPhI (Moscow Engineering Physics Institute) in 1952. The supervisor of his diploma thesis was Isaak Pomeranchuk, who recommended him for position in Dubna institute. His scientific and academic career started there in 1952.

Being a member different research groups he studied various problems of elementary particle physics. He contributed significantly to the following subjects: i) *Polarization effects in particle collisions.* An important achievement was the discovery of a general connection between polarization effects and internal parities of particles. ii) *Neutral current effects.* The investigation of P-violating effects in deep in-elastic scattering of polarized muons by nucleons inspired the realization of an experiment at CERN. iii) *Physics of massive and mixed neutrinos.* In a deep and fruitful collaboration with Bruno Pontecorvo, which started in 1975, the general theory of neutrino mixing and neutrino oscillations was developed.

Samoil Bilenky is one of the most cited physicists working in the JINR Dubna. He published together with his collaborators more than 400 papers with above 28 thousand citations (Hirsch index 82 following https://inspirehep.net). The important results were summarized in several review articles. From them very well known are those published in Physics Reports in 1977 (together with Bruno Pontecorvo) and in Review of Modern Physics in 1987 (together with Serguey Petcov). Samoil Bilenky is considered to be one of the most prominent neutrino physicists nowadays.

During a period of 30 years Samoil Bilenky delivered lectures for the courses of the physics of electroweak interactions, quantum mechanics and scattering theory at the Department of Elementary Particles, Moscow State University. He managed to publish the following six excellent books: 1) *Introduction to Feynman diagrams* (in Russian, Moscow Atomizdat, 1971; in English, Pergamon Press, 1974); 2) *Introduction to the physics of electroweak interactions* (in Russian, Moscow Energoatomizdat, 1980; in English, Pergamon Press, 1981); 4) Introduction to scattering theory (in Russian, Moscow University, 1985); 5) *Introduction to Feynman diagrams and electroweak interaction physics* (in Russian, Moscow Energoatomizdat, 1990; in English, Editions Frontiers, 1994), 6) *Introduction to the Physics of Massive and Mixed Neutrinos* (in English, Springer, 2010).

Many of the PhD students of Samoil Bilenky (Dmitry Bardin, Serguey Petcov, N. Shumeiko, Victor Semikoz, Fedor Šimkovic and others) became very well known scientists.

Celebration in Prague

On Wednesday, 23rd of May 2018, the "Celebrating Neutrinos" Colloquium took place in Hrzánský palace in honor of Samoil Bilenky's jubilee.

The event started with a welcome presentation of the director of the IAEP CTU in Prague, Ivan Štekl. Then, former students, collaborators, friends and relatives delivered their talks as follows: i) Ivan Štekl (IAEP, CTU in Prague): *Welcome*; ii) Serguey Petcov (SISSA Trieste): *Being a Student of S. M. Bilenky at JINR, Dubna*; iii) Jiřii Hošek (ÚJV Řež): *Fatal influence*; iv) Wanda Alberico (INFN Torino): *My teacher Samoil (The many*

things I learned from him); v) Elena Christova (Bulgarian Academy of Sciences): *On the 3D partonic structure of the nucleon*; vi) Fedor Šimkovic (Comenius University and JINR Dubna): *Weak, but important, interactions with Samoil*; vii) Gabriela Motz: *Weak interactions leading to lifelong entanglemen*; viii) Walter Grimus (Univ. of Vienna): *Samoil as a "Schrödinger Guest Professor" in Vienna*; ix) Jaroslav Cvach (Inst. of Physics of CAS): *Passion for mountains*; x) Mikhail Bilenky: *On studies of regulation of gene expression*; xi) Samoil Bilenky (JINR Dubna): Neutrino in my life; xii) Rupert Leitner (Charles Univ. in Prague): *Conclusion*. Afterwards, participants of the event moved to the Restaurant Bellavista, where a warm and friendship discussions continued.

Celebration in Dubna

On 20 June, the jubilee seminar dedicated to the jubilee anniversary of the birthday of Samoil Bilenky was held at the JINR Scientists' Club. It was organized by the Bogoliubov Laboratory of Theoretical Physics and the Dzhelepov Laboratory of Nuclear Problems. The celebration event was opened by the Director of the BLTP, Dmitry Kazakov. Samoil Bilenky in his turn dedicated his speech to the subject of his long-term research and called it *Neutrino in my life*.

Carlo Giunti (INFN Torino), a close collaborator of Samoil Bilenky, devoted his presentation to achievements and tasks of neutrino physics. The topic of contribution of Samoil Bilenky to studies of the mysterious particle was continued by his student and colleague Fedor Šimkovic (BLTP JINR and Comenius University). Alexander Ol-

shevskiy (DLNP, JINR Dubna) presented the JINR neutrino programme to colleagues, friends, and students of Samoil Mihelevich. The director of the JINR Dubna, Victor Matveev, concluded the scientific part of the seminar, heartily congratulated Samoil Bilenky and presented to him a photo album printed by the JINR Publishing Department and prepared by the JINR Scientific Information Department. The event finished with a banquet with a friendly and informal discussions. Among the participants of this celebration were scientists from Dubna (Dmitry Peshehonov etc.), Moscow (Mikhail Krivoruchenko, Boris Martemyanov, Leonid Ponomariov, Alexander Studenikin etc.) and Caltech (Petr Vogel).

To the pleasant atmosphere of these celebrations contributed also Samoil Bilenky's wife Sophia and son Mikhail, who delivered an interesting talk about gene research. He is an example of the versatility of the best particle physicists, that can change to the study of a subject as different as biology and publish valuable papers in prestigious journals as Nature. Let us recall that the author of the picturesque pictures symbolizing each new edition of the Pontecorvo School is Mikhail Bilenky.

Colleagues and many friends over the world heartily congratulated Samoil Bilenky on his jubilee and wish him sound health and new outstanding achievements in science.

Bruno Pontecorvo: Pioneer of Neutrino Oscillations

S. M. Bilenky

Joint Institute for Nuclear Research, 141980 Dubna, Russia

Figure 1. Bruno Pontecorvo (B. P.).

Bruno Pontecorvo (B. P.) was born on August 22, 1913, in Pisa (Marina di Pisa), Italy. His father was an owner of a textile factory founded by Pellegrino Pontecorvo, Bruno's grandfather. After the war, for many years the factory was closed and the building was not used. Today, it is a home of the Pisa department of INFN. The square in front of the building is called *Largo di Bruno Pontecorvo.*

There were eight children in the family: five brothers and three sisters, all of them were very successful. Guido (the eldest brother) became a famous biologist, Bruno became a famous physicist and Gillo was a very well known film director.

B. Pontecorvo joined the Faculty of Engineering at the University of Pisa. He had good marks, but he did not like mechanical drawing. After two years, he decided to study physics. From his autobiography: *My brother Guido declared authoritatively: "Physics! I would like to say that you must go to Rome. In Rome there are Fermi and Rasetti."* B. Pontecorvo passed an exam with Fermi and Rasetti. After the exam, Fermi made the following remark: *"While there is only one physics, today's physicists are divided into two categories: theorists and experimentalists. If a theorist is not gifted with extraordinary abilities, his work is pointless. As to the experimental physics, there are opportunities for some useful work even for an averagely skilled individual."* After

Figure 2. **Left panel**: B. P. with wife Marianna and first-born son Gil (Paris, 1940).
Right panel: B. P. with brother Gillo (Moscow, 1961).

the exam B. Pontecorvo was accepted to the Faculty of Physics and Mathematics at the University of Rome with specialization in experimental physics. First as a student and later as a researcher, from 1931 till 1936 Bruno worked in the Fermi group (famous *gruppo dei "ragazzi di via Panisperna"*) with Fermi, Rasetti, Amaldi and Segrè.

In 1934, Amaldi and B. Pontecorvo performed a series of experiments aimed at the measurement of radioactivity of different elements irradiated by neutrons. They observed that if the distance between the source and the detector is small and they are enclosed in lead, some irregularities occurred; in particular, the inverse-square law $1/r^2$ was not valid. Amaldi and Pontecorvo were sure that this effect had something to do with the lead. They told about their results to Fermi and Rasetti; Rasetti did not believe the results and Fermi did not seem much interested. In fact, this impression was wrong. Fermi had been thinking about the anomalies and a few days later he proposed to do an experiment with paraffin (and water) placed between the source and the detector. The effect was enormous: radioactivity was hundreds of times larger than before. When they discovered this effect, Fermi stopped the excitement of his colleagues and said a famous phrase: *"Let's go and have a lunch."* After the lunch, Fermi explained everything: this effect was due to the slowing down of neutrons caused by their scattering on protons in the paraffin (water). Bruno remembered that Fermi said: *"How stupid of us to have discovered this phenomenon by chance and not having been able to predict it!"* The effect of slowing down of neutrons opened the road to all applications of neutrons (reactors, radioisotopes in medicine, atomic bombs). Professor Corbino convinced the group (E. Fermi, E. Amaldi, B. Pontecorvo., E. Segrè, F. Rasetti, and D'Agostino) to secure a patent for this invention.

In 1936, B. P. received a prize of the Italian Ministry of Education and went for Paris to work with F. Joliot-Curie. In Paris, he studied nuclear isomers, i.e., metastable nuclear states with high spins. He performed the first experiments aimed at the observation of conversion electrons in decays of isomers, produced nuclear isomers in process of the irradiation of nuclei by high-energy photons (nuclear phosphorescence), etc. For the study of the nuclear isomerism, B.Pontecorvo was awarded the Curie-Carnegie prize. Fermi congratulated him with excellent results, which made him very happy and proud (Bruno joked that Fermi, who usually called him a great champion, had respect to him

only as a tennis expert).

In 1940, before the Germans occupied Paris, B. Pontecorvo escaped together with his family (wife and son) to US. From 1940 to 1942, he worked in a private oil company in Oklahoma. He developed a method of neutron well logging for oil (and water) prospering. This was the first practical application of neutrons. The method of neutron well logging is widely used nowadays.

In 1943, B. Pontecorvo took the position of a researcher in the Anglo-Canadian Uranium Project in Canada (first, in Montreal Research Laboratory and afterwards in the Chalk River Laboratory). He was a scientific leader of the project of the research reactor which was built in 1945 and was the first nuclear reactor outside of USA.

In Canada, B. Pontecorvo started his research in the elementary particle physics. Soon after the publication of the famous Fermi's paper on the theory of the β decay (1934), Bethe and Pierls estimated the cross section of the interaction of the postulated by Pauli neutrino with a nucleus. The estimated cross section was extremely small; at $\sim$ MeV energies: $\sigma < 10^{-44}\,\mathrm{cm}^2$. For many years the neutrino was considered an "undetectable particle."

Pontecorvo was the first physicist who challenged this opinion. He proposed the first method of neutrino detection [1] (Canada, 1946), based on the observation of the decay of daughter nucleus produced in the reaction: $\nu + (A, Z) \longrightarrow e^- + (A, Z+1)$. As the most promising he considered the process $\nu_e + {}^{37}\mathrm{Cl} \longrightarrow e^- + {}^{37}\mathrm{Ar}$, which has the following advantages:

- C_2Cl_4 is a cheap, non-inflammable liquid.
- ${}^{37}\mathrm{Ar}$ nuclei are unstable (K-capture) with a convenient half-life (34.8 days).
- A few atoms of ${}^{37}\mathrm{Ar}$ (rare gas), produced during the exposition time, can be extracted from a large detector.
- K-capture is accompanied with the energy release of 2.8 keV. This gives a possibility to use low-background proportional counters.

The Pontecorvo Cl-Ar radiochemical method was used by R. Davis in the first experiment on the detection of solar neutrinos. In 2002, R. Davis was awarded the Nobel Prize for the discovery of solar neutrinos. Furthermore, the radiochemical method of neutrino detection based on observation of the reaction $\nu_e + {}^{71}\mathrm{Ga} \longrightarrow e^- + {}^{71}\mathrm{Ge}$, proposed by V. Kuzmin, was used in the GALLEX/GNO and SAGE solar neutrino experiments in which the most abundant pp neutrinos were detected.

In order to detect neutrinos, it was necessary to find intensive neutrino sources. In the seminal Chalk-River paper [1], Pontecorvo paid attention to the following sources: the Sun, the nuclear reactors, and the radioactive materials produced inside the reactors. In 1948, he invented the low-background proportional counter with high amplification. This counter proved crucial for the detection of solar neutrinos in the Homestake , GALLEX and SAGE solar neutrino experiments.

After the famous Conversi–Pancini–Piccioni experiment (1947), from which it followed that the muon weakly interacts with nuclei, B. Pontecorvo together with E. Hincks started a series of brilliant pioneering experiments on the investigation of the fundamental properties of muon. They proved that:

1. The charged particle emitted in the muon decay is an electron.


Figure 3. **Left panel**: B. P. with N. S. Isaeva and B. G. Kadyshevskij (Dubna, 1964).
Right panel: B. P. with sons Tito (left) and Antonio (Dubna, 1960s).

2. The muon decays into three particles.
3. The muon does not decay into an electron and a photon.

B. Pontecorvo suggested that the muon is a particle with spin $1/2$ and the muon capture by a proton is accompanied by an emission of a neutrino: $\mu^- + p \longrightarrow \nu + n$. He was the first who paid attention of the deep analogy between the electron and muon [2]. He compared the probabilities of the processes: $\mu^- + (A, Z) \longrightarrow \nu + (A, Z-1)$ and $e^- + (A, Z) \longrightarrow \nu + (A, Z-1)$, and concluded that the coupling constants which characterize the strength of these two processes are of the same order of magnitude: *"There is a fundamental analogy between the β processes and the absorption of muons."* In 1947, B. Pontecorvo was the first who came to the idea of universal weak interaction of e-ν and μ-ν pairs. Later, the idea of e-μ universality was proposed by Puppi, Klein, Tiomno and Wheeler.

In 1950, B. Pontecorvo together with his wife and three sons decided to go from England to USSR. He started to work in Dubna, which at that time hosted the largest accelerator in the world (460 MeV, later upgraded to 680 MeV). Pontecorvo and his group carried out different at this accelerator: experiments on the investigation of the production of π^0 mesons in neutron-proton and neutron-nucleus collisions, on pion-nucleon scattering and others.

B. Pontecorvo always thought about the neutrino. Towards the end of the 1950's in Dubna a project of a meson factory was prepared (unfortunately it was not realized). In connection with this project, Bruno considered a feasibility of neutrino experiments with neutrinos originating from the decays of pions and kaons produced at high-intensity accelerators. At that time neutrinos had been discovered in the famous Reines and Cowan reactor experiment. B. Pontecorvo came to conclusion that experiments with accelerator neutrinos are possible (independently, M. A. Markov and M. Schwartz came to the same conclusion). He started to think about fundamental problems of neutrino physics which could be solved in such experiments. Bruno always remembered that people who worked with muons in early days had in mind that neutrinos which are produced together with electron and muon (electron and muon neutrinos, ν_e and ν_μ) could be different particles. In 1958, Feinberg showed that if ν_e and ν_μ are identical, the probability of the process: $\mu \longrightarrow e + \gamma$, calculated within the theory with W-boson and

cut-off, should be many orders of magnitude higher than the existed at that time upper bound. B. Pontecorvo was the first who understood that experiments with high-energy neutrinos from the $\pi \longrightarrow \mu + \nu_\mu$ decays allow to probe the existence of the second type of neutrino in a direct, model-independent way [3]. His proposal was realized in the famous Brookhaven experiment (1962) in which it was proved that $\nu_\mu \neq \nu_e$. In 1988, Lederman, Schwartz and Steinberger, the participants of the Brookhaven experiment, were awarded the Nobel Prize for *"the discovery of the muon neutrino leading to the classification of elementary particles into families."*

We come now to a very bright and courageous idea of B. Pontecorvo which led to the creation of a new modern field of neutrino physics, to the idea of neutrino masses, mixing and oscillations. Bruno came to the idea of neutrino oscillations in 1957-58. He was impressed by a possibility of $K^0 \rightleftarrows \overline{K^0}$ oscillations suggested by Gell-Mann and Pais. This suggestion was based on the following:

1. K^0 and $\overline{K^0}$ are different particles. They have different strangeness ($+1$ and -1, respectively). The strangeness is conserved in strong interactions.
2. Weak interactions do not conserve the strangeness. As a result, K^0 and $\overline{K^0}$ are "mixed" particles and transitions between them in the vacuum become possible.

In 1957, B.Pontecorvo put the following question: *"Are there other "mixed" neutral particles (not necessarily elementary ones) which are not identical to their corresponding antiparticles and for which the particle-antiparticle transitions are not strictly forbidden?"* He came to the conclusion that muonium (μ^+e^-) to antimuonium (μ^-e^+) are such systems and considered muonium $\rightleftarrows$ antimuonium oscillations [4]. At that time it was not known that ν_e and ν_μ are different particles. Pontecorvo suggested that the transitions $(\mu^+e^-) \rightleftarrows (\mu^-e^+)$ are *"induced by the same interaction which is responsible for the μ decay:"* $(\mu^+e^-) \rightarrow \nu + \overline{\nu} \rightarrow (\mu^-e^+)$. Note that the experiments searching for the muonium-antimuonium transitions, proposed by Pontecorvo , are going on at present. They provide a sensitive way of obtaining information about interaction in which the flavor lepton numbers are changed by two units.

B. Pontecorvo was also thinking about the neutrino. At that time it was established that neutrino is a two-component particle and is described by the two-component neutrino theory. According to this theory, only the left-handed neutrino ν_L and right-handed antineutrino $\overline{\nu}_R$ exist in the Nature (let us stress that only one type of neutrino was known at that time). Transitions between them are forbidden by the conservation of angular momentum. A rumor helped Bruno realized his idea of neutrino oscillations in case of one neutrino flavor. In 1957, R. Davis was searching for ^{37}Ar production in the process: $\overline{\nu}_{\text{reactor}} + {}^{37}\text{Cl} \longrightarrow e^- + {}^{37}\text{Ar}$. A rumor that Davis had observed such "events" reached Pontecorvo . He suggested that these "events" could be due to neutrino oscillations, i.e., transitions of reactor antineutrinos into the right-handed neutrinos on their way from the reactor to the detector. He published the first paper dedicated to neutrino oscillations in 1958 [5]. In this paper, he wrote: *"The neutrino may be a particle mixture, and consequently there is a possibility of real neutrino-antineutrino transitions in vacuum, provided that the lepton (neutrino) charge is not conserved. This means that the neutrino and antineutrino are mixed particles, i.e., a symmetric and antisymmetric combination of two truly neutral Majorana particles ν_1 and ν_2."* And further in the paper: *"This*

possibility became of some interest in connection with new investigations of inverse β processes." B. Pontecorvo considered a transition: $\overline{\nu}_R \to \nu_R$ (and similarly $\nu_L \to \overline{\nu}_L$), i.e., he had to assume that the lepton number is not conserved and that in addition to $\overline{\nu}_R$ and ν_L, quanta of the left-handed neutrino field $\nu_L(x)$, ν_R and $\overline{\nu}_L$, quanta of the right-handed neutrino field $\nu_R(x)$, existed as well. According to the two-component neutrino theory only the field $\nu_L(x)$ enters the weak-interaction Lagrangian. Thus, according to this theory ν_R and $\overline{\nu}_L$ must be non-interacting "sterile" particles. In order to explain the Davis "events", B. Pontecorvo had to assume that *"a definite fraction of particles (ν_R) can induce the reaction."*

In the 1958 paper Pontecorvo pointed out that due to neutrino oscillations in the experiment of Reines and Cowan a deficit of antineutrino events will be observed: *"The cross section of the process $\overline{\nu} + p \longrightarrow e^+ + n$ with $\overline{\nu}$ from the reactor must be smaller than expected. This is due to the fact that the neutral lepton beam, which at the source is capable of inducing the reaction, changes its composition on the way from the reactor to the detector."*

Later, the anomalous "events" in the Davis experiment disappeared and only an upper bound for the cross section of the reaction $\overline{\nu} + {}^{37}\mathrm{Cl} \longrightarrow e^- + {}^{37}\mathrm{Ar}$ was obtained. B. Pontecorvo understood that ν_R and $\overline{\nu}_L$ (if they exist) must be non-interacting, sterile particles. The terminology "sterile neutrino," which is standard nowadays, was introduced by him.

Starting from this paper, all his life B. Pontecorvo believed in the existence of neutrino oscillations. He wrote: *"The effects of transformation of the neutrino into antineutrino and vice versa may be unobservable in the laboratory, but will certainly occur, at least, on an astronomical scale."*

The next paper on neutrino oscillations was written by B. Pontecorvo in 1967 [6]. At that time, the phenomenological V – A theory was established, $K^0 \rightleftarrows \overline{K^0}$ oscillations were observed, and it was proved that (at least) two types on neutrinos ν_e and ν_μ exist in nature. In this paper he discussed the transitions between active neutrinos $\nu_\mu \rightleftarrows \nu_e$ and also transitions $\nu_e \rightleftarrows \overline{\nu}_{eL}$ and $\nu_\mu \rightleftarrows \overline{\nu}_{\mu L}$, which transform *"the active particles into particles which, from the point of view of ordinary weak processes, are sterile."* He pointed out that not only the disappearance of ν_μ, but also the appearance of ν_e can be observed. In the case of transitions of the active neutrinos into the sterile ones, only disappearance of the initial active neutrinos can be observed.

In the 1967 paper, B. Pontecorvo discussed the effect of neutrino oscillations for the solar neutrinos: *"From an observational point of view, the ideal object is the Sun. If the oscillation length is smaller than the radius of the solar region effectively producing the neutrinos, direct oscillations will be smeared out and unobservable. The only effect on the Earth's surface would be that the flux of observable solar neutrinos must be two times smaller than the total (active and sterile) neutrino flux."* When the first results of the Davis solar neutrino experiment were obtained (1970), it occurred that the detected flux of the solar neutrinos was about 2-3 times smaller than the predicted flux. This observation became known as the Solar Neutrino Problem. It was anticipated by B. Pontecorvo. His explanation of the result of solar neutrino experiment by neutrino mixing and oscillations was widely accepted.

The next paper on neutrino oscillations was published by by Gribov and Pontecorvo

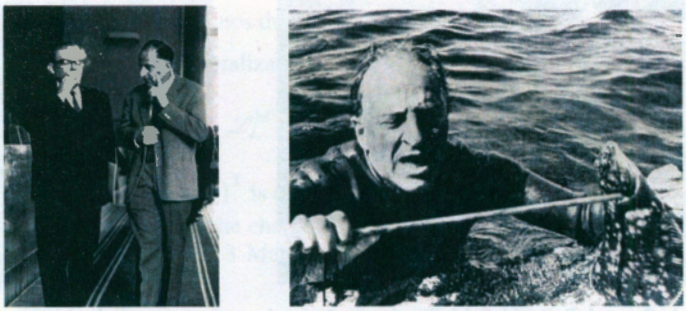

Figure 4. **Left panel**: B. P. with N. N. Bogoliubov (Dubna, 1970s).
Right panel: B. P. as a fisherman.

[7]. It was based on the assumption that only the left-handed neutrinos ν_e, ν_μ and right-handed antineutrinos $\overline{\nu}_e$, $\overline{\nu}_\mu$ exist in nature. The authors also assumed that in addition to V − A interaction, the full Lagrangian includes an effective interaction between the neutrinos which violates the lepton numbers L_e and L_μ. After the diagonalization of the effective interaction it was found that:

$$\nu_{eL} = \cos\theta\,\chi_{1L} + \sin\theta\,\chi_{2L},$$
$$\nu_{\mu L} = -\sin\theta\,\chi_{1L} + \cos\theta\,\chi_{2L},$$

where $\chi_{1,2}$ are the fields of Majorana neutrinos with masses $m_{1,2}$, respectively, and θ is the mixing angle. The neutrino masses and mixing angle are determined by three parameters of the effective interaction. For the $\nu_e \to \nu_e$ transition probability in vacuum it was obtained the following relation (in modern notations):

$$P(\nu_e \to \nu_e) = 1 - \frac{1}{2}\sin^2 2\theta\left(1 - \cos\frac{\Delta m^2 L}{2E}\right),$$

where $\Delta m^2 = |m_2^2 - m_1^2|$. The authors applied the developed formalism to the solar-neutrino oscillations. The maximal mixing ($\theta = \pi/4$) was considered as the most attractive possibility. In such a case, the averaged flux of the solar neutrinos is equal to $1/2$ of the predicted flux.

In 1975, B. Pontecorvo and myself started a long-term collaboration (about 15 years) on the study and development of the idea of neutrino masses, mixing and oscillations. Our first paper was based on the idea of quark-lepton analogy [8]. At that time, it was established that the quark charged current (CC) in case of four quarks has the form:

$$j_\alpha^{CC} = 2\left[\overline{u}_L\gamma_\alpha d_L^c + \overline{c}_L\gamma_\alpha s_L^c\right],$$

where $d_L^c = \cos\theta_C\, d_L + \sin\theta_C\, s_L$ and $s_L^c = -\sin\theta_C\, d_L + \cos\theta_C\, s_L$ are the Cabibbo–GIM mixed quark fields, and θ_C is the Cabibbo angle. It was known that the lepton CC has the same form as the quark one:

$$j_\alpha^{CC} = 2\left[\overline{\nu}_{eL}\gamma_\alpha e_L + \overline{\nu}_{\mu L}\gamma_\alpha \mu_L\right].$$

Figure 5. **Left panel**: B. P. with S. M. Bilenky at a "not so boring" seminar (Dubna, 1977). **Right panel**: B. P. with S. M. Bilenky (Dubna, 1983).

We believed in a deep analogy between the quarks and leptons and suggested that:

$$\nu_{eL} = \cos\theta\, \nu_{1L} + \sin\theta\, \nu_{2L},$$
$$\nu_{\mu L} = -\sin\theta\, \nu_{1L} + \cos\theta\, \nu_{2L},$$

where $\nu_{1,2}$ are the fields of neutrinos with definite masses $m_{1,2}$, respectively, and θ is the leptonic mixing angle. In such a scheme, all fundamental fermions have nonvanishing masses and are Dirac particles.

After the great success of the two-component neutrino theory, during many years there was a general belief that neutrinos are massless particles. Our arguments in favor of nonzero neutrino masses were the following:

- There is no principle (like gauge invariance in case of photons) which requires that the masses of neutrinos must be equal to zero.
- After the V – A theory, which is based on the assumption that the CC Lagrangian contains the L-components of all fields, it was natural to assume that the neutrinos are not special massless particles but—like quarks and charged leptons—have nonzero masses.

We also discussed the possible value of the mixing angle θ. We argued that:

- There is no reason for $\theta = \theta_C$.
- *"It seems to us that the special values of the mixing angles $\theta = 0$ and $\theta = \pi/4$ (maximum mixing) are of the greatest interest."* The probabilities of transitions $\nu_l \to \nu_{l'}$ are the same in the schemes involving the mixing of two Majorana and two Dirac neutrinos.

In our next paper we considered the most general neutrino mixing [9]. In 1977, we wrote the first review of the neutrino oscillations [10]. We characterized the neutrino mixing by neutrino mass terms, which is a common practice nowadays. In the general

case of three types of the neutrinos three types of mass terms are possible:

1. Majorana mass term (generalization of Gribov–B. P.):

$$\mathscr{L}_L^{\mathrm{M}} = -\frac{1}{2}\overline{\nu}_L M_L \nu_L^c + \mathrm{H.c.},$$

where $\nu_L = \left(\nu_{eL}, \nu_{\mu L}, \nu_{\tau L}\right)^{\mathrm{T}}$ is a three-component column of the left-handed neutrino fields, $\nu_L^c = C\overline{\nu}_L^{\mathrm{T}}$ is the charge conjugated field, and $M_L = M_L^{\mathrm{T}}$ stands for the (symmetric) complex 3×3 Majorana mass matrix. After diagonalization of the matrix M_L we obtain:

$$\nu_{lL} = \sum_{i=1}^{3} U_{li}\, \nu_{iL},$$

where U is the unitary 3×3 Pontecorvo–Maki–Nakagawa–Sakata (PMNS) matrix: $U^\dagger U = 1$, and $\nu_i = \nu_i^c$ is the field of a Majorana neutrino with mass m_i.

2. Dirac mass term:

$$\mathscr{L}^{\mathrm{D}} = -\overline{\nu}_L M^{\mathrm{D}} \nu_R + \mathrm{H.c.},$$

with $\nu_R = \left(\nu_{eR}, \nu_{\mu R}, \nu_{\tau R}\right)^{\mathrm{T}}$ being a three-component column of the right-handed neutrino fields and M^{D} the complex 3×3 Dirac mass matrix. In such scenario, the total lepton number L is conserved. Diagonalization of the matrix M^{D} again yields:

$$\nu_{lL} = \sum_{i=1}^{3} U_{li}\, \nu_{iL},$$

where ν_i is the field of a Dirac neutrino with mass m_i. The total lepton number of neutrino ν_i and antineutrino $\overline{\nu}_i$ is defined as $+1$ and -1, respectively.

3. Dirac–Majorana mass term:

$$\mathscr{L}^{\mathrm{D+M}} = \mathscr{L}_L^{\mathrm{M}} + \mathscr{L}^{\mathrm{D}} + \mathscr{L}_R^{\mathrm{M}}$$

with the right-handed Majorana mass term:

$$\mathscr{L}_R^{\mathrm{M}} = -\frac{1}{2}\overline{\nu_R^c} M_R \nu_R + \mathrm{H.c.}$$

In the case of such mass term there are no conserved lepton numbers. After the diagonalization, the neutrino mixing ($l = e, \mu, \tau$):

$$\nu_{lL} = \sum_{i=1}^{6} U_{li}\, \nu_{iL},$$

$$\nu_{\bar{l}R}^c = \sum_{i=1}^{6} U_{\bar{l}i}\, \nu_{iL}$$

is realized by a 6×6 generalization of the PMNS matrix U, while $\nu_i = \nu_i^c$ is the Majorana-neutrino fields with masses m_i ($i = 1, \ldots, 6$).

In case of the Dirac and Majorana mass terms, only the transitions between the active flavor neutrinos $\nu_l \rightleftarrows \nu_{l'}$ are possible. On the other hand, the Dirac–Majorana mass term also allows the transitions $\nu_l \rightleftarrows \overline{\nu}_{l'L}$ involving sterile neutrinos.

Our approach to the neutrino oscillations in vacuum is described below. What are the states of flavor neutrinos ν_e, ν_μ and ν_τ produced in the weak decays, captured in the neutrino processes, etc.? For example, a flavor muon neutrino ν_μ is a particle which is produced together with μ^+ in the decay: $\pi^+ \longrightarrow \mu^+ + \nu_\mu$, etc. We suggested that the states of flavor neutrinos are given by:

$$|\nu_l\rangle = \sum_i U_{li}^* |\nu_i\rangle ,$$

with $l = e, \mu, \tau$, while $|\nu_i\rangle$ are the states of neutrinos with definite momentum $\vec{p}$ and energy $E_i = \sqrt{\vec{p}^2 + m_i^2} \simeq E + \frac{m_i^2}{2E}$. In accordance with QFT, we assumed that the evolution of states is determined by the Schrödinger equation $i\partial_t |\Psi(t)\rangle = H |\Psi(t)\rangle$. If at a time $t = 0$ a flavor neutrino ν_l is produced, at a later instant t we have:

$$|\nu_l(t)\rangle = e^{-iHt} |\nu_l\rangle = \sum_i |\nu_i\rangle \, e^{-iE_i t} \, U_{li}^* .$$

Thus, in case of mixing the neutrino state at a time t is a superposition of states with different energies, i.e., a non-stationary state. From our point of view, this is a basis of neutrino oscillations. The neutrinos are detected via observation of weak-interaction processes in which the flavor neutrinos are participating ($\nu_{l'} + N \longrightarrow l' + X$, etc.). We have:

$$|\nu_l(t)\rangle = \sum_{l'} |\nu_{l'}\rangle \left(\sum_i U_{l'i} \, e^{-iE_i t} \, U_{li}^* \right) .$$

The probability of the transition $\nu_l \to \nu_{l'}$ reads:

$$P(\nu_l \to \nu_{l'}) = \left| \sum_i U_{l'i} \, e^{-iE_i t} \, U_{li}^* \right|^2 = \left| \delta_{l'l} + \sum_{i \neq k} U_{l'i} \left(e^{-i \frac{\Delta m_{ik}^2 L}{2E}} - 1 \right) U_{li}^* \right|^2 ,$$

where L is the distance source-detector and $\Delta m_{ik}^2 = m_k^2 - m_i^2$ is a mass-squared difference. This expression for the transition probability became a standard.

For many years, the idea of massless strictly two-component neutrinos prevailed. The situation changed drastically after the appearance of Grand Unified Theories and the seesaw mechanism of neutrino mass generation (by the end of the 1970s). Neutrino masses and mixing started to be considered a signature of new, beyond the Standard Model physics. However, there was (and still is) no theory which could predict the values of neutrino masses and mixing angles. Our approach was the following:

- It is plausible that the neutrinos are massive and mixed.
- Search for neutrino oscillations, which is an interference phenomenon, is the most sensitive way to search for small neutrino masses.

Figure 6. **Left panel**: B. P. with his secretary I. G. Pokrovskaya (Dubna, 1983).
Right panel: B. P. with H. Langevin-Joliot, daughter of Irène and Frédéric Joliot-Curie (Dubna, 1984).

- Neutrino oscillations must be searched for in experiments with neutrinos from all sources (reactor, accelerator, cosmic rays, the Sun, etc.), which have sensitivity to different values of Δm^2_{ik}.

This strategy brought success. At present, there is a proof that the neutrinos are massive and mixed particles. This proof was first obtained in the Super-Kamiokande atmospheric neutrino experiment, and later in the SNO solar neutrino experiment and the KamLAND reactor experiment. It was first verified in the K2K and MINOS accelerator experiments, and later in other neutrino oscillation experiments.

Starting from 1957, B. Pontecorvo became a great enthusiast of the idea of neutrino oscillations. For the rest of his life, the neutrino masses and oscillations remained his beloved research subject. The discovery of neutrino oscillations was a great triumph of B. Pontecorvo who came to the idea of neutrino oscillations at a time when the common opinion favored massless neutrinos and no neutrino oscillations. From my point of view, the history of neutrino oscillations is an illustration of the importance of analogy in physics. It is also an illustration of the importance of new courageous ideas which are not always in agreement with the general opinion.

B. Pontecorvo was a big fan of underwater fishing. In autumn, he usually went to some place about 100 km from Dubna next to a small, very clear river Nerl. Frequently, he invited my wife and myself for such trips. While he was in the river trying to catch fish, we usually made fire (to cook fish, if available) and picked up mushrooms. After about two hours in the river, Bruno returned happy, frozen, but often without fish... Yet, the fire and mushrooms were there. I remember that only once during a very hot and dry summer, when fires were forbidden, he caught a lot of fish... Alas, we could not prepare it and gave it to the local people.

We started our collaboration on neutrino oscillations in the car during one of such trip. The Cabibbo–GIM mechanism of quarks was firmly established at that time. I asked B. P.: *"Why neutrinos do not do the same?"* It seemed that this approach to neutrino masses and mixing was interesting to him. It concerned a symmetry between the quarks

Figure 7. B. P. (right) with L. B. Okun (left).

and leptons. After many days of work, we wrote our first paper on neutrino oscillations. It was only five pages long, but I remember that it took a lot of efforts and we were completely exhausted after writing it. Generally, it was always difficult to write papers with B. P. He would never admit any imprecise statements and always required very clear formulations of all assumptions and results. His English (as well as Russian) was perfect, and he always succeeded in finding apropriate phrases.

The years of work and friendship with Bruno Pontecorvo were the happiest and unforgettable years in my life. His wide and profound knowledge of physics, his love of physics, his ingenious intuition and his ability to understand complicated problems in a clear and simple way were his special gifts. He was a true scientist in the best, classical sense of the word. When he thought about some problem, he thought about it continuously from early morning till late evening. He devoted all his resources and great intellect to science, and although he was not indifferent to the recognition of his contribution to physics, his main stimulus was the search for truth.

More than 10 last years of his life were for Bruno the years of a courageous struggle against the Parkinson's disease. His love of physics and of the neutrino helped him to overcome the difficult problems related to the illness. He never ceased to work, to think about neutrinos and to continue his active life. Two days before his death, Bruno came to his office at the second floor of the Laboratory of Nuclear Problems in JINR Dubna, where he had been working for 43 years. When he was leaving the laboratory, he looked into the window upon the golden and yellow birches and said to his secretary, Ms. Irina Pokrovskaya: *"Look how beautiful these colors are..."* It was a nice Russian Golden Autumn, September 22, 1993.

Bruno Pontecorvo was one of the first men who understood the importance of neutrinos in elementary particle physics and astrophysics. He felt and understood neutrinos probably better than anybody else in the world. Starting from his time in Canada, he had been thinking about the neutrino for his whole life. He was never confined by narrow theoretical frameworks. He was completely open-minded, without any prejudices, very courageous and with very good intuition and scientific taste. He was also a very bright, wise, exceptionally interesting and very friendly personality. People liked him and he

had many friends in Italy, Russia, France, Canada and many other countries. The name of Bruno Pontecorvo will be forever connected to the neutrino as the name of the founding father of modern neutrino physics. He will remain with us in our memory and our hearts as a great and outstanding physicist, as a man of a great impact and humanity.

REFERENCES

1. B. Pontecorvo, *Inverse β-process,* Report PD-205, Chalk River Laboratory, 1946.
2. B. Pontecorvo, *Nuclear capture of mesons and the meson decay,* Phys. Rev. **72** (1947) 246.
3. B. Pontecorvo, *Electron and muon neutrinos,* Sov. Phys. JETP **10** (1960) 1236.
4. B. Pontecorvo, *Mesonium and anti-mesonium,* Sov. Phys. JETP **6** (1957) 429 [Zh. Eksp. Teor. Fiz. **33** (1957) 549].
5. B. Pontecorvo, *Inverse β-processes and non conservation of lepton charge,* Sov. Phys. JETP **7** (1958) 172 [Zh. Eksp. Teor. Fiz. **34** (1958) 247].
6. B. Pontecorvo, *Neutrino experiments and the question of the lepton charge conservation,* Sov. Phys. JETP **26** (1968) 984 [Zh. Eksp. Teor. Fiz. **53** (1967) 1717].
7. V. N. Gribov and B. Pontecorvo, *Neutrino astronomy and lepton charge,* Phys. Lett. *B28* (1969) 493.
8. S. M. Bilenky and B. Pontecorvo, *Quark-lepton analogy and neutrino oscillations,* Phys. Lett. **B61** (1976) 248.
9. S. M. Bilenky and B. Pontecorvo, *Again on neutrino oscillations,* Nuovo Cim. Lett. **17** (1976) 569.
10. S. M. Bilenky and B. Pontecorvo, *Lepton Mixing and Neutrino Oscillations,* Phys. Rept. **41** (1978) 225.

PHOTO GALLERY

Lecturers and organizers 1/5

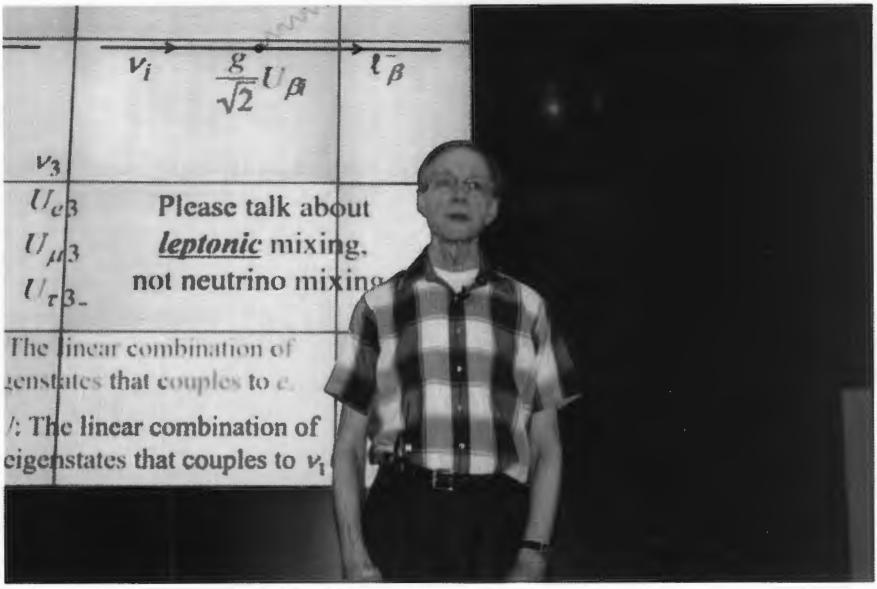

Lecturers and organizers 2/5

Lecturers and organizers 3/5

Lecturers and organizers 4/5

Lecturers and organizers 5/5

Lecture hall 1/7

Lecture hall 2/7

Lecture hall 3/7

Lecture hall 4/7

Lecture hall 5/7

Lecture hall 6/7

Lecture hall 7/7






Poster session

Excursion 1/3

Excursion 2/3

Excursion 3/3

POSTER SESSION

STUDENT POSTER PRESENTATIONS

(9 September 2019, Sinaia, Romania)

1. Aker, Max (KIT, Karlsruhe): "Development of a Metal Hydride Tritium Source to Search for keV Sterile Neutrinos Using Magnetic Micro Calorimeters"
2. Antonova, Maria (Inst. de Física Corpuscular, Paterna): "Proposal for Joint Neutrino Oscillation Analysis Using Data from the T2K and Reactor Experiments"
3. Benso, Cristina (MPI, Heidelberg): "Sterile Neutrino Dark Matter and Laboratory Possible Signals"
4. Chiriacescu, Ana and Parvu, Mihaela (Univ. of Bucharest): "Background Studies for Rare Events Physics Using LAr Detectors"
5. Dmitrievsky, Sergey (JINR, Dubna): "Monitoring of the Top Tracker Detector for the JUNO Experiment"
6. Dvornicky, Rastislav (JINR, Dubna): "Optical Noise Monitoring Systems of Lake Baikal Environment for the Baikal-GVD Telescope"
7. Ershova, Anna (MIPT, Moscow): "Technical Part of the Secondary Neutron Background from Cosmic Muons Simulation in the DANSS Experiment"
8. Ghinescu, Stefan-Alexandru (CIFRA, Bucharest): "Lorentz Violation Effects on Angular Correlations in $2\nu\beta\beta$ Decay"
9. Helis, Dounia (CEA, Saclay): "Neutrinoless Double Beta Decay Searches with Enriched $^{116}CdWO_4$ Scintillating Bolometers"
10. Huang, Guihong (IHEP, Beijing): "Energy and Vertex Reconstruction with Charge Info in JUNO"
11. Hussain, Hamzah (Univ. College London): "Investigating the Influence of Different Magnetic Fields on the Detection Efficiency for Neutrinoless Double Beta Decays in ^{82}Se"
12. Jokiniemi, Lotta Maria (Univ. of Jyväskylä): "Ordinary Muon Capture as a Probe of $0\nu\beta\beta$ Decays"
13. Kalitkina, Anastasiia (JINR, Dubna): "The Global Neutrino Analysis Package Development for Simulation of the NOvA Experiment"
14. Karl, Christian (MPP, Munich): "Analysis of First KATRIN Neutrino Mass Data"
15. Kasperovych, Dmytro (INR, Kyiv): "Experimental Study of 2β Decay of ^{150}Nd to the First 0^+ Excited Level of ^{150}Sm"
16. Klavdiienko, Volodymyr (INR, Kyiv): "^{50}V Decay Scheme"
17. Lebert, Manuel (MPP, Munich): "Characterization of the TRISTAN SDD Prototypes with Krypton"
18. Macko, Miroslav (Czech Technical Univ., Prague): "Neutrinoless Double Beta Decay: The Key to the Secrets of Mysterious Neutrinos?"
19. Marsteller, Alexander (KIT, Karlsruhe): "Performance of the Beta Electron Source of the KATRIN Experiment"

20. Niewczas, Kajetan (Univ. of Wrocław): "Modeling Neutrino-Nucleus Interactions in the Few-GeV Region"
21. Nitescu, Ovidiu-Vasile (CIFRA, Bucharest): "Lorentz Violation Effects on $2\nu\beta\beta$ Decay Electron Spectra"
22. Nosek, Tomas (Charles Univ., Prague): "Neutrino + Antineutrino Oscillations in NOvA"
23. Nugmanov, Radik (Kurchatov Inst., Moscow): "FADC DAQ System in Borexino: Doing Science while Waiting for Supernova"
24. Paun, Alice-Mihaela (INFLPR, Măgurele): "Neutrino Capture on Beta-Decaying Nuclei as Method to Detect Relic Neutrinos – General Considerations"
25. Petropavlova, Maria (JINR, Dubna): "Simulation of the Supernova Neutrino Signal in NOvA Detectors"
26. Picciau, Emmanuele (Univ. of Cagliari): "The Role of Coherent Elastic Neutrino Nucleus Scattering in Direct Dark Matter Detection"
27. Romanyuk, Maria (INR, Kyiv): "Investigation of the Double Beta Decay of ^{106}Cd with Help of $^{106}CdWO_4$ Crystal Scintillator"
28. Schweizer, Konstantin (TUM, Munich): "Determination of the Nonlinear Light Response Function of Liquid Scintillators"
29. Shelepov, Mark (INR, Moscow): "A Search for Cascade Events with Baikal Gigaton Volume Detector"
30. Sorokovikov, Maksim (JINR, Dubna): "Multicluster Events in the Baikal-GVD Telescope"
31. Sorokovikov, Maksim (JINR, Dubna): "The Atmospheric Neutrino Flux from Decays of Charmed Particles"
32. Spatafora, Alessandro (INFN, Catania): "Study of $^{20}\mathrm{Ne} + {}^{76}\mathrm{Ge}$ Elastic Scattering at 306 MeV: A Key Experiment for the NUMEN Project"
33. Sushenok, Evgenii (JINR, Dubna): "Baikal-GVD. Data Analysis: Monte-Carlo–Experiment Comparison"
34. Titov, Oleg (Kurchatov Inst., Moscow): "Recoil Force from Neutrino Radiation in Electron-Capture Decay"
35. Wang, Yakun (Peking Univ.): "Nuclear Matrix Element of $0\nu\beta\beta$ Decay Based on the Projected Shell Model"

Sterile Neutrinos, Dark Matter and Laboratory Signals

C. Benso, V. Brdar, M. Lindner, and W. Rodejohann

Max Planck Institute for Nuclear Physics, 69117 Heidelberg, Germany

Abstract. We consider keV-scale sterile-neutrino dark-matter detection prospects in terrestrial experiments. The present astrophysical and cosmological constraints disfavor the discovery of such a particle, produced through mixing with active neutrinos, in terrestrial experiments such as KATRIN. We propose several ideas how this can be solved, focusing on scenarios in which either X-rays limits are relaxed.

Keywords: keV sterile neutrino; dark matter; X-ray bounds; critical temperature
PACS: 14.60.St; 95.35.+d

INTRODUCTION

Sterile neutrinos can be defined as the right-handed components of the neutrino fields ψ_ν:

$$\nu_s = \nu_{\mathrm{RH}} = P_R \psi_\nu = \frac{1+\gamma^5}{2} \psi_\nu. \tag{1}$$

They appear to be singlets with respect to the symmetry group $\mathrm{SU}(3)_C \times \mathrm{SU}(2)_L \times \mathrm{U}(1)_Y$ that gives structure to the Standard Model (SM) of particle physics, since they have neither strong nor electromagnetic charge and they are not directly involved in weak interaction processes, contrary to the left-handed component of the neutrino field $\nu_{\mathrm{LH}} = \frac{1-\gamma^5}{2} \psi_\nu$. This peculiar combination of features earned them the epithet of *sterile* and made them (almost at all) invisible particles to our searches. However, even if they were not included in the SM content due to the fact that they have not been detected so far, our interest in them is well-motivated by three major problems (such as the active-ν-masses puzzle, the baryonic-asymmetry puzzle [1, 2, 3, 4], and the existence and nature of dark matter in our Universe) to which they could provide a compelling solution.

As for the dark-matter problem, we know that the major part of the matter content of our Universe is not constituted by ordinary baryonic matter [1] but by some element called dark matter (DM), of which we observe with good precision the large-scale gravitational effects but we still have not determined the particle nature. Based on the features that we know that a good DM candidate should have, we can say that sterile neutrinos with a keV-scale mass represent a possible well-fitting solution to this puzzle (see Table 1).

In our work, we consider the region of the parameter space to which the KATRIN experiment is sensitive, that corresponds to rather large values of ν_s mass and mixing angle. Despite the appeal characterizing the **Dodelson–Widrow mechanism** thanks to

Table 1. Comparison of the sterile neutrino with a general DM candidate.

General DM candidate	Sterile neutrino
No electromagnetic interaction	No electromagnetic interaction
No strong interaction	No strong interaction
Massive	Mass of $\mathcal{O}$(keV)
Perfectly stable or with $\tau_{\mathrm{DM}} > t_{\mathrm{U}}$	$\tau_{\nu_s} > t_{\mathrm{U}}$ if mixing small enough

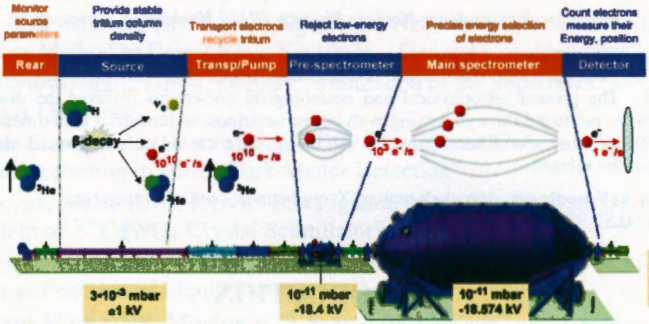

Figure 1. Scheme of the KATRIN experiment.

its extreme simplicity and naturalness, our region of interest is inaccessible by means of this mechanism due to two constraints for such values of the parameters m_s and θ:

- ν_s would have been overproduced in the early Universe, resulting today in a larger abundance of ν_s than the one of DM that we measured.
- We should observe a signal in the X-rays coming from the decay of our DM candidate into an active neutrino and a photon.

In the next sections, two ways of avoiding these constraints are presented and their implementation is shown in the final plot.

KATRIN AND THE ROLE OF CRITICAL TEMPERATURE

KATRIN is an experiment primary aim of which is to measure the mass of $\overline{\nu}_e$ with sub-eV precision, by examining the end of the spectrum of e^- emitted from the β decay of tritium. What characterizes this experiment, with respect to Mainz and Troitsk that performed similar research, is the high sensitivity reach thanks to the use of the 200 ton spectrometer that dominates Fig. 1, which allows for an extremely precise selection of the most energetic β electrons.

KATRIN can, in principle, also be used to get signals of sterile neutrinos with $m_s < Q_{^3\mathrm{H}\to{}^3\mathrm{He}+e^-+\overline{\nu}_e} \approx 18.6\,\mathrm{keV}$, if they have nonzero mixing with the active electron (anti)neutrinos, by looking at possible distortions of the entire decay spectrum, meaning

considering also less-energetic e^-. This kind of extended research requires modifications in the initial experimental apparatus as, for example, a modified detector able to handle the significantly enhanced electron rate of about $10^{11}\,\mathrm{s}^{-1}$. The sensitivity of this upgraded experiment is shown in the final plot and it would be clearly excluded by the X-ray bound in the full glory (the darkest-purple shaded region) and also unattainable in the simple Dodelson–Widrow scenario.

The constraint coming from the request of the abundance of sterile-neutrino DM not to exceed the content of DM measured today ($h^2\,\Omega_{\mathrm{DM}} = 0.1186$ [1]) can be evaded by introducing a critical temperature T_c such that the sterile-neutrino production is suppressed for $T > T_c$. In this way, the lower is the T_c, the larger are the values of sterile-neutrino m_s and θ needed to get $\Omega_{\nu_s} = \Omega_{\mathrm{DM}}$, as shown in the final plot. Concerning the possible origin of the critical temperature:

- It could be identified with the reheating temperature T_R if we consider $T_c \geq 5\,\mathrm{MeV}$, where this limit comes from the BBN observations [5].
- Alternatively, it could be related to a dynamical mechanism that made, at early times, the sterile-neutrino masses very small (for example, if they result from a symmetry breaking) or very large (for instance, in the case of a kind of misalignment mechanism) [6] in such a way that the term:

$$\sin^2(2\theta_M) = \frac{\left(\frac{m_s^2}{2p}\right)^2 \sin^2(2\theta)}{\left(\frac{m_s^2}{2p}\right)^2 \sin^2(2\theta) + \left(\frac{\Gamma_\alpha(p)}{2}\right)^2 + \left[\frac{m_s^2}{2p}\cos(2\theta) - V_T(p)\right]^2} \tag{2}$$

responsible for the active-sterile oscillation is suppressed for $T \geq T_c$. In this case, the critical temperature value can be lowered to $\sim 2\,\mathrm{MeV}$, roughly corresponding to the temperature at which the decoupling of the active neutrinos occurred with the effect that afterwards the conversion cannot happen anymore.

X-RAY BOUNDS AND CANCELLATION

For ν_s with mass below twice the electron mass, there are two possible decay channels:

1. $\nu_s \to \nu_i + \overline{\nu}_j + \nu_j$ is the dominant channel and happens at the tree level through Z-boson exchange, allowing us to set an upper limit on the value of the mixing angle by using the requirement of a SN mean lifetime larger than the age of the Universe, in order to have a stable DM candidate. From:

$$\Gamma_{\nu_s \to 3\nu} = \frac{G_{\mathrm{F}}^2 m_s^5}{96\pi^3} \sin^2(2\theta) = \frac{1}{4.7 \times 10^{10}\,\mathrm{s}} \left(\frac{m_s}{50\,\mathrm{keV}}\right)^5 \sin^2(2\theta) \tag{3}$$

we get [7, 8]:

$$\theta^2 < 1.1 \times 10^{-7} \left(\frac{50\,\mathrm{keV}}{m_s}\right)^5 . \tag{4}$$

2. $\nu_s \to \nu\gamma$ is the subdominant channel related to a decay amplitude $\mathcal{O}(10^{-2})$ times weaker than the dominant one:

$$\Gamma_{\nu_s\to\nu\gamma} = \frac{9\alpha G_F^2}{1024\pi^4}\sin^2(2\theta)m_s^5 \approx 5.5\times10^{-22}\theta^2\left(\frac{m_s}{\text{keV}}\right)^5 \text{s}^{-1}. \quad (5)$$

It is a radiative decay process occurring at 1-loop level and producing in the final state a photon, detectable as an almost monoenergetic line in the X-ray band due to the smallness of the mass of the active neutrino, that is produced together with the photon. The nonobservation of such a line in the spectra of DM-dominated objects led to a further constraint [7, 8]:

$$\theta^2 \leq 1.8\times10^{-5}\left(\frac{\text{keV}}{m_s}\right)^5. \quad (6)$$

The observable quantity related to the latter process is the flux of photons:

$$F_{\text{X-rays}} = \frac{\Gamma_{\nu_s\to\nu\gamma}M_{\text{DM,FoV}}}{4\pi D_L^2 m_s}, \quad (7)$$

where $M_{\text{DM,FoV}}$ is the mass of the DM within the telescope's field of view (FoV), D_L is the luminosity distance to the observed object, and $\Gamma_{\nu_s\to\nu\gamma} \propto \int \text{d}P_{\text{phasespace}}\,|\mathscr{M}|^2 \propto \sin^2(2\theta)m_s^5$.

Larger values of m_s and θ are allowed by the same value of the flux if $|\mathscr{M}|^2$ is globally reduced taking $\mathscr{M} = \mathscr{M}_1 + \mathscr{M}_2$, where $\mathscr{M}_1$ comes from the usual contribution of the diagram presented in Fig. 2(a) and $\mathscr{M}_2$ gives an opposite contribution related to the diagram in Fig. 2(b). Even if many different realizations are possible, the diagram (b) reflects a specific realization of the general idea such that the mediator of the decay process is a new scalar particle $\Sigma = (\sigma^0, \sigma^-)$, with quantum numbers $(1, 2, -1)$ under $\text{SU}(3)_C \times \text{SU}(2)_L \times \text{U}(1)_Y$, interacting with the leptonic sector according to:

$$\mathscr{L} \supset \lambda\,\overline{\nu}_s\Sigma^\dagger L_e + \lambda'\overline{e}_R\tilde{\Sigma}^\dagger L_e + \text{H.c.} \quad (8)$$

The suppression of the signal can in principle be partial or even complete if the parameters λ, λ' and m_Σ introduced together with the new scalar satisfy the relation:

$$\sin\theta = \frac{-4\lambda\lambda'}{3g^2}\frac{m_e}{m_s}\frac{m_W^2}{m_\Sigma^2}\left[\log\left(\frac{m_e^2}{m_\Sigma^2}\right)+1\right]. \quad (9)$$

GETTING TO THE SENSITIVE REGION OF THE PARAMETER SPACE

The plot in Fig. 3, taken from [9], shows the effects of the two combined methods allowing to get access to the usually excluded region of the parameter space in which

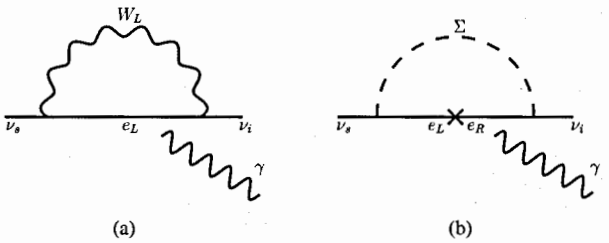

Figure 2. Contributions to the reduced decay amplitude.

KATRIN would be sensitive to the presence of sterile-neutrino DM (the white dashed line):

- The increasingly lighter shades of purple represent the relaxation of the X-ray bound that can be achieved assuming that the total flux of photons coming from the decay of sterile neutrinos gets contributions from both the usual Feynman diagram, where the mediator is the W_L boson, and the new-physics diagram that depends neither on m_s nor on θ.
- The colored thick lines are constituted by the points in the parameter space corresponding to the values of m_s and θ for which the entire content of DM of the Universe is accounted for by the sterile neutrinos ($h^2\,\Omega_{\nu_s} = h^2\,\Omega_{\rm DM} = 0.1186$) under the hypothesis of their production starting at different values of the critical temperature T_c.
- The sensitivity regions of KATRIN and other experiments, such as Troitsk and ECHo, are outlined by the dashed lines, while the gray shaded regions are excluded or at least disfavored by the request of the lifetime of our DM candidate to be larger than the age of the Universe and by the number of observed satellites of the Milky Way, respectively.

In conclusion, from the exclusion plot we see that an eventual signal of sterile-neutrino DM could be found by KATRIN in case of appropriate (by a factor of the order of 10^4 or more) cancellation of the X-ray bound if the production of sterile neutrinos started at temperatures around 20 MeV or lower and if we take into account also the limits on m_s coming from the phase-space arguments and the Milky-Way-satellite counts (gray shaded region). Otherwise, in the case of very large values of the mixing angle and very low critical temperatures, also the Troitsk experiment would be sensitive to such dark-matter candidates in the future.

ACKNOWLEDGMENTS

This work was supported by IMPRS-PTFS and also by DFG under Grant No. RO 2516/5-1.

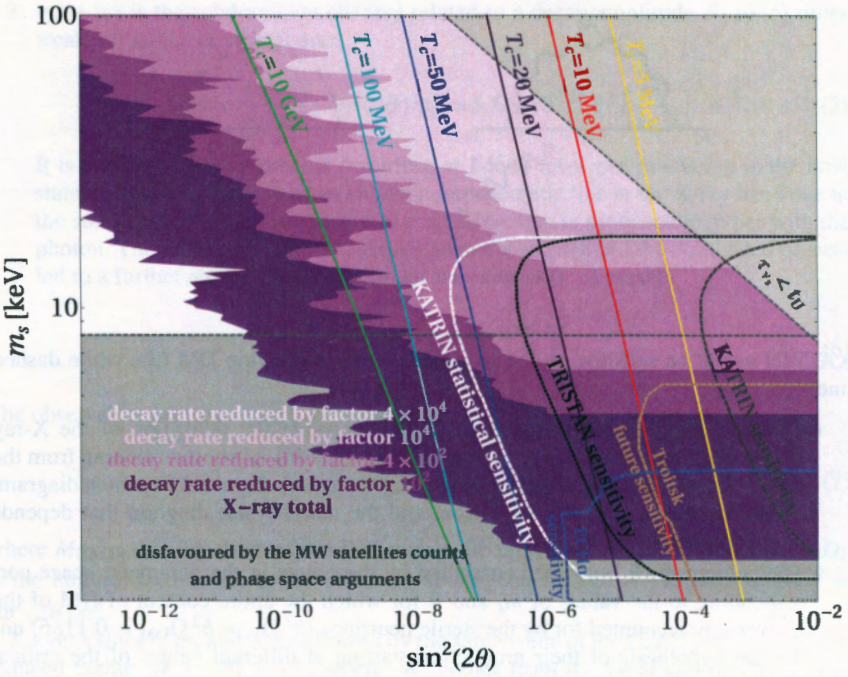

Figure 3. Sensitivity of the upgraded KATRIN experiment.

REFERENCES

1. M. Tanabashi et al. (Particle Data Group), "Review of Particle Physics," *Phys. Rev. D* **98**, 030001 (2018).
2. A. D. Sakharov, "Violation of CP Invariance, C Asymmetry, and Baryon Asymmetry of the Universe," *Pisma Zh. Eksp. Teor. Fiz.* **5**, 32–35 (1967).
3. P. Di Bari, "An Introduction to Leptogenesis and Neutrino Properties," *Contemp. Phys.* **53**, 315–338 (2012).
4. E. K. Akhmedov, V. A. Rubakov, and A. Yu. Smirnov, "Baryogenesis via Neutrino Oscillations," *Phys. Rev. Lett.* **81**, 1359–1362 (1998).
5. P. F. de Salas et al., "Bounds on Very Low Reheating Scenarios after Planck," *Phys. Rev. D* **92**, 123534 (2015).
6. F. Bezrukov, A. Chudaykin, and D. Gorbunov, "Hiding an Elephant: Heavy Sterile Neutrino with Large Mixing Angle Does Not Contradict Cosmology," *JCAP* **1706**, 051 (2017).
7. A. Boyarsky, O. Ruchayskiy, and M. Shaposhnikov, "The Role of Sterile Neutrinos in Cosmology and Astrophysics," *Ann. Rev. Nucl. Part. Sci.* **59**, 191–214 (2009).
8. M. Drewes et al., "A White Paper on keV Sterile Neutrino Dark Matter," *JCAP* **1701**, 025 (2017).
9. C. Benso, V. Brdar, M. Lindner, and W. Rodejohann, "Prospects for Finding Sterile Neutrino Dark Matter at KATRIN," *Phys. Rev. D* **100**, 115035 (2019).

Optical Noise of Luminescent Water in Lake Baikal Observed with the Baikal-GVD Telescope

A. D. Avrorin,[1] A. V. Avrorin,[1] V. M. Aynutdinov,[1] R. Bannash,[7] Z. Bardačová,[8] I. A. Belolaptikov,[2] V. B. Brudanin,[2] N. M. Budnev,[3] V. Y. Dik,[2] G. V. Domogatsky,[1] A. A. Doroshenko,[1] R. Dvornický,[2,8] A. N. Dyachok,[3] Zh.-A. M. Dzhilkibaev,[1] E. Eckerová,[8] L. Fajt,[9] S. V. Fialkovsky,[5] A. R. Gafarov,[3] K. V. Golubkov,[1] N. S. Gorshkov,[2] T. I. Gress,[3] R. A. Ivanov,[2] M. S. Katulin,[2] K. G. Kebkal,[7] O. G. Kebkal,[7] E. V. Khramov,[2] M. M. Kolbin,[2] S. O. Koligaev,[10] K. V. Konischev,[2] A. V. Korobchenko,[2] A. P. Koshechkin,[1] V. A. Kozhin,[4] M. V. Kruglov,[2] M. K. Kryukov,[1] V. F. Kulepov,[5] M. B. Milenin,[1] R. R. Mirgazov,[3] D. V. Naumov,[2] V. Nazari,[2] A. I. Panfilov,[1] D. P. Petukhov,[1] E. N. Pliskovsky,[2] M. I. Rozanov,[6] E. V. Ryabov,[3] V. D. Rushay,[2] G. B. Safronov,[1] B. A. Shaybonov,[2] M. D. Shelepov,[1] F. Šimkovic,[2,8,9] A. V. Skurikhin,[4] A. G. Soloviev,[2] M. N. Sorokovikov,[2] I. Štekl,[9] O. V. Suvorova,[1] E. O. Sushenok,[2] V. A. Tabolenko,[3] B. A. Tarashansky,[3] S. A. Yakovlev,[7] and D. N. Zaborov[1] (for the Baikal-GVD Collaboration)

[1] *Institute for Nuclear Research, Russian Academy of Sciences, 117312 Moscow, Russia*
[2] *Joint Institute for Nuclear Research, 141980 Dubna, Russia*
[3] *Irkutsk State University, 664003 Irkutsk, Russia*
[4] *Institute of Nuclear Physics, Moscow State University, 119991 Moscow, Russia*
[5] *Nizhny Novgorod State Technical University, 603950 Nizhny Novgorod, Russia*
[6] *St. Petersburg State Marine Technical University, 190008 St. Petersburg, Russia*
[7] *EvoLogics GmbH, 13355 Berlin, Germany*
[8] *Comenius University in Bratislava, 842 48 Bratislava, Slovakia*
[9] *Czech Technical University in Prague, 110 00 Prague, Czech Republic*
[10] *Dubna State University, 141982 Dubna, Russia*

Abstract. We present data on the luminescence of the Baikal water medium collected with the Baikal-GVD neutrino telescope. This three-dimensional array of light sensors allows for the observation of time and spatial variations of the ambient light field. We report on the observation of an increase of luminescence activity in 2016 and 2018. On the contrary, we observed a practically constant optical noise in 2017.

Keywords: Baikal-GVD experiment; neutrino astronomy; high-energy physics
PACS: 95.85.Ry; 95.55.Vj; 95.30.Cq

INTRODUCTION

The next-generation neutrino telescope Baikal-GVD is placed in the southern basin of Lake Baikal about 3.6 km from the shore at a depth of 1,366 m. The main goal of the experiment is the detection of high-energy astrophysical neutrinos, sources of which remain still unknown. In particular, the aim is the registration of Cherenkov radiation emitted when secondary charged particles, created in the reactions of neutrinos with the surrounding medium, are passing through the deep water in Lake Baikal. The detector itself is a three-dimensional array of photo-sensitive components called optical modules (OMs). A fully independent unit called cluster consists of 288 OMs attached on eight strings, seven peripheral strings surrounding the central one with a radius of 60 m. Each string carries 36 OMs with 15 m vertical spacing. The top and the bottom OMs are located at depths of 750 m and 1,275 m, respectively. In 2016, the first cluster "Dubna" has been deployed. In the two subsequent winter expeditions of 2017 and 2018, two more clusters have been deployed. Another two clusters have been deployed during the winter expedition of 2019. At the time of writing, the total number of deployed clusters is five [1].

Apart from the Cherenkov radiation, also the ambient background light is registered. The amount of registered background light is derived from the photomultiplier noise rates from each particular OM. There are two independent ways of collecting the data. The trigger system of every cluster is designed in such a way that signals from each OM in a time window of 5 μs are stored if a trigger condition is fulfilled [2]. In this way, we obtain the data on count rates of pulses registered by OMs. The origin of the background noise rates is mainly associated with the luminescence of the Baikal water. In this article, we present some selected results on luminescence in Lake Baikal.

OPTICAL ACTIVITY OF THE BAIKAL WATER

Baikal-GVD is designed to detect the Cherenkov light from charged particles. In open water, light not related to relativistic particles constitutes an unavoidable background to the Cherenkov light. Therefore, studies of the related light fields are of crucial importance. The photon flux from the sunlight below a depth of $\sim$ 700 m is negligible, as shown in the previous work [3].

In Fig. 1(a), we present data on the count rates for a selected OM for the period April 2016 – February 2017. There are two periods of relatively stable optical background noise, which are intermitted with increased optical activity. The charge distribution of the noise pulses is displayed in Fig. 1(b). We stress that the charge distribution remains unchanged in different periods of the optical activity. Our measurements are performed with a threshold of half a single photoelectron charge. In this way, the dark noise of the photomultiplier is significantly suppressed. We note that by setting the threshold to one photoelectron the background count rate is reduced by a factor of two. The one-photoelectron background is well correlated with the half-photoelectron background. The count rates in both cases exhibit the same modulation of the relative amplitude. We clearly see that the major contribution comes from the single-photoelectron pulses.

The depth dependence of the ambient light field is the same for all eight strings of

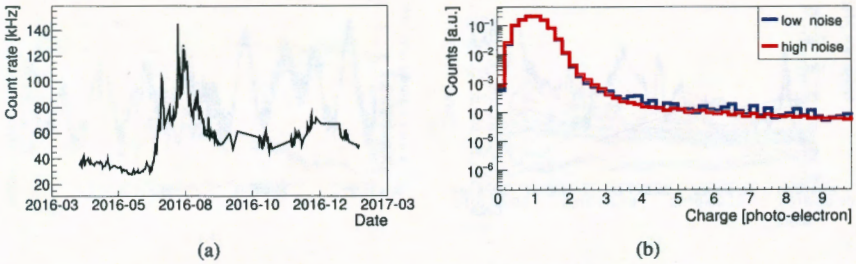

(a) (b)

Figure 1. (a) Count-rate evolution of a selected OM from April 2016 till February 2017. (b) Charge distribution of registered pulses in the units of photoelectrons.

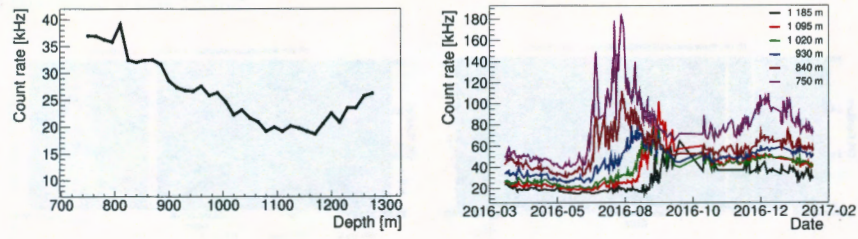

(a) (b)

Figure 2. (a) Count rates averaged for each depth over the OMs from different strings as a function of depth. The lake bed is at the 1,366 m depth. Data are taken from June 2016. (b) Count rates for the OMs of the same string at different depths. For simplicity, we show only six out of 36 OMs, placed at the depths of 750, 840, 930, 1,020, 1,095, and 1,185 meters.

a cluster. By averaging the count rates over the OMs at the same horizon, we obtain the depth dependence of the background light noise. The average count rates vs. depth are presented in Fig. 2(a). The analyzed data are from June 2016. This is the period of the lowest optical activity. We note that the pattern remains the same for other periods of stable noise activity. During the period of increased activity, the depth dependence is displayed in Fig. 2(b). The appearance of the outbreak maximum depends on time, starting with the top modules. Indeed, we observe a layer of highly luminescent water moving from the top to the bottom of the lake. By comparing the maxima for different depths, we obtain a velocity profile of the flows. In the beginning of August, the estimated speed reached its maximum value of $\sim 45\,\mathrm{m/d}$, while it remained almost constant ($\sim 8\,\mathrm{m/d}$) till the end of September, i.e., when the activity asymptotically reached the background plateau. The observed pattern is similar to previous investigations with the NT200 detector (see [4]).

The time evolution of the count rates, as shown in Fig. 2(b), exhibits sharp changes on top of relatively continuous smooth optical background. The effect is more visible in a particularly selected time window displayed in Fig. 3(a). The amplitude of these sudden changes reached almost 50 kHz. The duration of such variations which distort

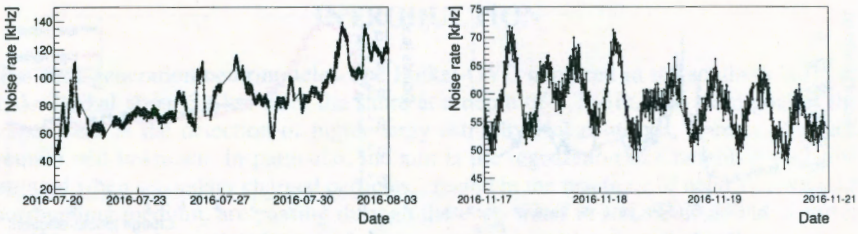

Figure 3. (a) Count rates for a particular OM during the optically highly-active period: from July till September 2016. A sudden outburst of the count rates is noticeable. (b) Example of a regular modulation of the noise rates. Data are taken from the period of a stable plateau: from October 2016 till February 2017.

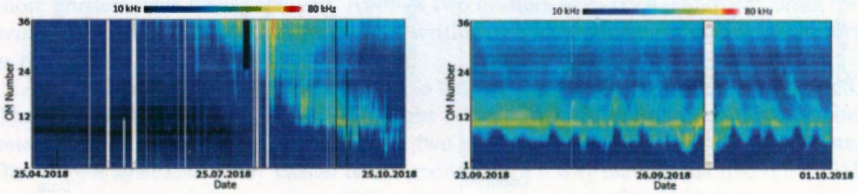

Figure 4. (a) Count rates for 36 OMs at the same string. The bottom and the top OMs are labeled No. 1 and No. 36, respectively. Data are collected from the year 2018. The high (low) noise rates are presented in red (blue). (b) The same as in (a) for a particularly selected time window, when the effect of a regular modulation is clearly manifest.

the smooth background ranges typically from several hours up to a few days. We note that the effect is present in July – September 2016, i.e., the period of increased luminescent activity. However, the period of a relatively stable plateau (October 2016 – February 2017) shows, in Fig. 3(b), a regular modulation of the noise rates. The period of these modulations is quite stable and varies from 10 to 12 hours. We stress that these waves are probably a manifestation of the internal waves in the lake. The end of these modulations cannot be determined as far as the measurement during the year is interrupted by the winter expedition (for further details, see [1]). On the other hand, we observed a practically constant background noise without a period of high luminescence activity in 2017.

However, the noise rates in 2018 exhibit a similar pattern to that already described above for the year 2016. In Fig. 4(a), we evidently see a luminescent layer moving from the top to the bottom of the lake. We again observed a regular modulation of the noise rates, as shown in Fig. 4(b). First, the modulations appeared on the top OMs in June 2018 and persisted till the end of October 2018. The maximal amplitude reached 70 kHz.

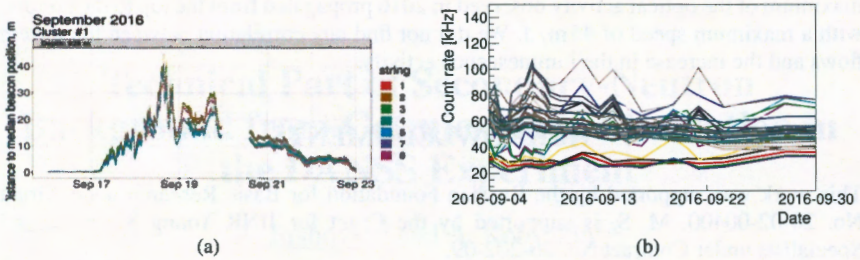

(a) (b)

Figure 5. (a) Deviations of the beacons from their median positions at different strings for the data of Fall 2016. In this period, the deviations of strings from their median positions were extreme. (b) Count rates of 36 OMs at the same string for data taken in the period when deviations of the string from its median position were extreme.

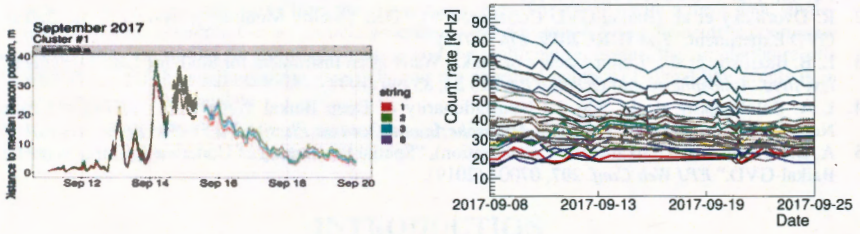

(a) (b)

Figure 6. The same as in Fig. 5 for the data collected in Fall 2017.

TORRENT CURRENTS IN LAKE BAIKAL

Due to the currents in Lake Baikal, the string geometry deviates from its vertical direction. To take these deviations into account, an acoustic positioning system for Baikal-GVD has been developed (for more details, see [5]). Our observations show two periods of extreme deviations of the strings in September 2016 and September 2017. Torrent flows in the lake may produce a remarkable tilt of the string from its vertical position, two examples of which are displayed in Fig. 5. For the same period, we present data on the count rates in Fig. 6. We did not find any correlation between the torrent flows of the deep water and the luminescence activity of the lake.

CONCLUSIONS

We presented the data on the luminescence in Lake Baikal which were collected by the Baikal-GVD neutrino telescope. We found an increase in the luminescence activity intermitting the periods of a relatively stable optical background in the years 2016 and 2018. In contrast, we observed a practically constant background noise without any period of high luminescence activity in the year 2017. Moreover, we found that the

maximum of the optical activity observed in 2016 propagated from the top to the bottom, with a maximum speed of 45 m/d. We did not find any correlation between the torrent flows and the increase in the luminescence activity.

ACKNOWLEDGMENTS

This work was supported by the Russian Foundation for Basic Research under Grant No. 20-02-00400. M. S. is supported by the Grant for JINR Young Scientists and Specialists under Contract No. 20-202-09.

REFERENCES

1. F. Šimkovic et al. (Baikal-GVD Collaboration), "Neutrino Telescope in Lake Baikal: Present and Future," *PoS* **ICRC2019**, 1011 (2019).
2. R. Dvornický et al. (Baikal-GVD Collaboration), "Data Quality Monitoring System in the Baikal-GVD Experiment," *PoS* **ICRC2019**, 874 (2019).
3. L. B. Bezrukov et al., "Luminescence of Baikal Water as an Instrument for Studying Lake Dynamics," *Izvestiya, Atmospheric and Oceanic Physics* **34**, 85–90 (1998).
4. I. A. Belolaptikov et al., "On the Nonstationarity of Deep Baikal Water Flows as Derived from Neutrino Telescope Data," *Izvestiya, Atmospheric and Oceanic Physics* **34**, 78–84 (1998).
5. A. D. Avrorin et al. (Baikal-GVD Collaboration), "Spatial Positioning of Underwater Components for Baikal-GVD," *EPJ Web Conf.* **207**, 07004 (2019).

Technical Part of Secondary-Neutron Background from Cosmic-Muon Simulation in the DANSS Experiment

A. Ershova[1,2] and A. Kobyakin[1,2]

[1] *Moscow Institute of Physics and Technology, 141701 Dolgoprudny, Russia*
[2] *Institute for Theoretical and Experimental Physics, 117218 Moscow, Russia*

Abstract. In this work, the results of modeling of cosmic muons passing through the muon veto of the DANSS experiment are presented. The simulated data were used to examine the background induced by neutrons originating from the muon interactions. Specifically within these data, single-neutron and multineutron Geant4 particle generators were developed. Since the neutron coordinate distributions are similar for the single-neutron and the multineutron events, the simulation results were tested for the single-neutron case only and the expected number of signal-like events is in agreement with the real data.

Keywords: DANSS; Geant4; neutron background; cosmic muons
PACS: 25.30.Mr

INTRODUCTION

The DANSS experiment [1] aims to search for sterile neutrinos. DANSS is placed on a movable platform under the core of a 3.1 GW industrial reactor at the Kalinin Nuclear Power Plant. The detector records 3,000–4,000 events per day after background subtraction at different distances from the reactor. A substantial contribution to the signal-like events is made by fast neutrons born in such materials as copper or lead (materials of the passive shielding) and concrete constructions of the floor and ceiling. The idea of reactor-antineutrino detection is based on the inverse beta-decay (IBD) reaction:

$$\overline{\nu}_e + p \rightarrow n + e^+. \tag{1}$$

The IBD process produces two time-separated signals. One signal, called "prompt," comes from the positron, while the other, called "delayed," comes from the neutron capture. The prompt signal is produced immediately and consists of the positron-track ionization and Compton scattering of two γ quanta coming from the positron annihilation. The neutron undergoes moderation and is subsequently captured by gadolinium included in the strip coating. The time difference between the prompt and the delayed signals is in the tens-of-microseconds range, which produces a very good reaction signature. Low-energy neutrons are captured by borated polyethylene contained in the passive shielding, but cosmic muons generate fast neutrons in materials of the passive shielding (such as copper and lead). A fast neutron produces a recoil proton during thermalization (a prompt-signal-like event) and is captured by ^{157}Gd or ^{155}Gd (a delayed-signal-like event). If more than one neutron is produced, two neutrons may be captured by the Gd

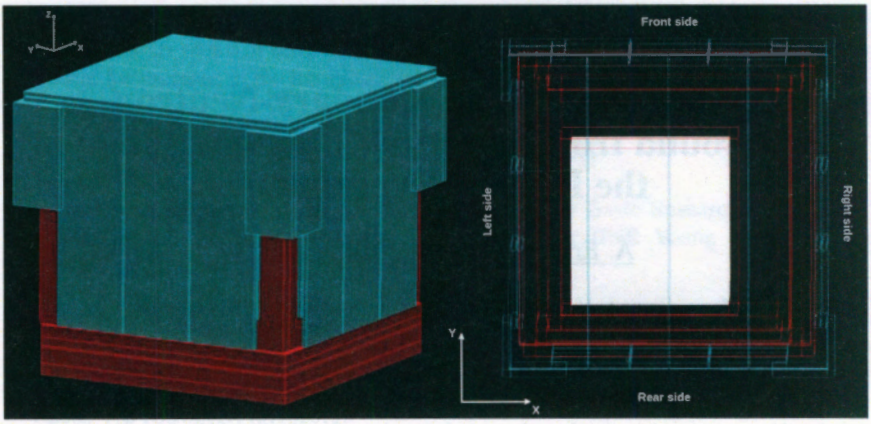

(a) (b)

Figure 1. Geant4 model of the DANSS detector: (a) Side view. (b) Top view. The muon-veto system is shown in blue, the passive shielding in red, and the sensitive volume in white. The origin of the coordinate system is located in the center of the sensitive volume. The Z axis is directed towards the reactor core. The plates parallel to the Z axis are the side plates, while the plates parallel to the X and Y axes and located in the regions with $Z > 0$ cm and $Z < 0$ cm are the top and bottom plates, respectively.

isotopes, where one of the captures may simulate a prompt signal and the other a delayed one.

The DANSS detector was simulated using the Geant4 simulation toolkit [2, 3] and the simulated data were processed using the ROOT package [4]. In order to estimate the energy threshold of the single-neutron-background mechanism, neutrons with uniform energy and isotropic angular distribution were generated near the sensitive volume without shielding and the energy of the neutrons which produced the signal was estimated. Here, the signal event is considered to be an event in which a capture by ^{157}Gd or ^{155}Gd occurred and the primary PMT signal exceeds 1 MeV. Our study showed that the fast neutrons are the neutrons with energies higher than 1.5 MeV.

VETO-SIGNAL CONSIDERATION: VETO-HIT CHECKER FUNCTION

The efficiency of the muon-veto system is very high ($\approx 97.5\%$). It consists of 40 plates, where each two plates form a sandwich operating in the coincidence mode. A geometrical checker was developed in order to take into account the veto signal without gaining it (the signal simulation takes a lot of time). During the generation of the primary muons, only those muons were simulated for which the combination of their point of birth (`X`, `Y`, `Z`) and direction of motion (`DirX`, `DirY`, `DirZ`) allowed them to pass through the gaps between the veto modules. Some of the muons are deflected while passing through materials of the detector and finally cross the veto, but the fraction of such

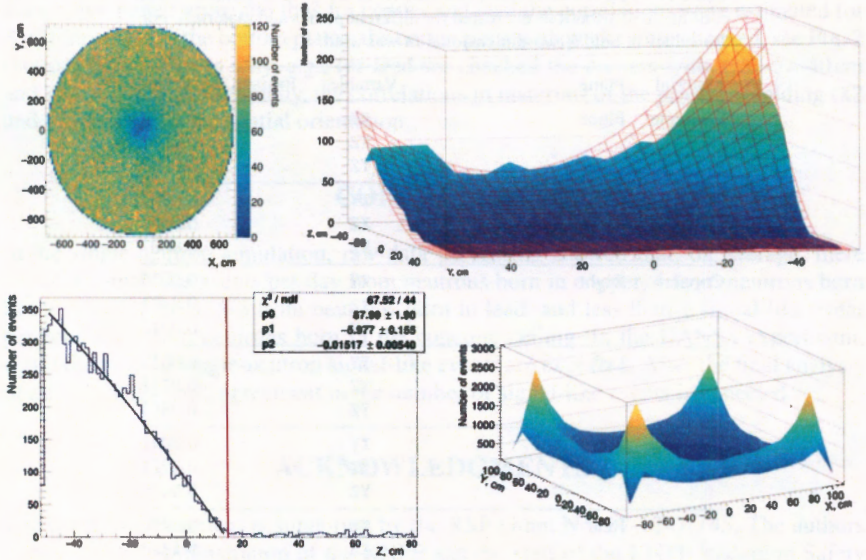

Figure 2. Top left: Example of a point-of-birth distribution in the concrete floor. The hole in the center is a consequence of the veto checker function. Top right: YZ point-of-birth distribution in copper (left plane). Fit: $(63 - 1.19\,\mathrm{Y} + 0.04\,\mathrm{Y}^2)(0.12 - 99.5 \times 10^{-4}\,\mathrm{Z} + 14.51 \times 10^{-5}\,\mathrm{Z}^2)$, where Y and Z are expressed in cm. Only the part with $\mathrm{Z} < 0$ cm was simulated. Bottom: Examples of point-of-birth distributions in lead. Bottom left: Z point-of-birth distribution in lead (rear plane). Fit: $p_0 + p_1\,\mathrm{Z} + p_2\,\mathrm{Z}^2$, with Z in cm. Bottom right: XY point-of-birth distribution in lead (bottom plane). The peak with $\mathrm{X}, \mathrm{Y} < 0$ cm was simulated as a two-dimensional distribution and the other peaks as one-dimensional distributions. This can be explained by the influence of the muon-veto shape on the point-of-birth distributions, see Fig. 1.

events is less than 1%. Since less than 1% of the neutrons are born in the top plates of copper and lead, they were not simulated. In the upper region (with $\mathrm{Z} > 0$ cm for copper and $\mathrm{Z} > 15$ cm for lead), significantly fewer neutrons are born, and thus this region was not simulated, either.

CORRELATIONS OF COORDINATE DISTRIBUTIONS

Some of the neutron point-of-birth distributions seem to be correlated. For estimation of the correlations, the Pearson correlation coefficient was used:

$$r_{xy} = \frac{\sum_{i=1}^{n}(x_i - \bar{x})(y_i - \bar{y})}{\sqrt{\sum_{i=1}^{n}(x_i - \bar{x})^2}\sqrt{\sum_{i=1}^{n}(y_i - \bar{y})^2}}, \tag{2}$$

where n is the sample size, x_i and y_i are the individual sample points labeled with the index i, and $\bar{x} = \frac{1}{n}\sum_{i=1}^{n} x_i$ (and analogously for $\bar{y}$) is the sample mean.

Table 1. Pearson correlation coefficients of the neutron point-of-birth coordinate distributions estimated for different planes and materials. For the values in bold a two-dimensional fit was used.

Material	Plane	Variables	Pearson coefficient
Concrete	Floor	XY	−0.0012
		XZ	0.0006
		YZ	0.0008
	Ceiling	XY	−0.0005
		XZ	0.0001
		YZ	0.0007
Copper	Right	XY	0.0036
		XZ	**0.0483**
		YZ	0.0017
	Left	XY	−0.0038
		XZ	−0.0211
		YZ	**−0.0853**
	Front	XY	−0.0041
		XZ	−0.0221
		YZ	**0.0440**
	Rear	XY	0.0216
		XZ	**−0.1228**
		YZ	−0.0197
	Bottom (X, Y < −20 cm)	XY	**0.1102**
		XZ	−0.0253
		YZ	0.0034
Lead	Front	XY	0.0177
		XZ	0.0268
		YZ	0.0139
	Rear	XY	0.0143
		XZ	**−0.0440**
		YZ	0.0124
	Bottom (X, Y < −40 cm)	XY	**−0.0740**
		XZ	−0.0159
		YZ	−0.0167
	Bottom (X, Y > 60 cm)	XY	0.0068
		XZ	0.0264
		YZ	0.0045

We assumed the correlated distributions to be the ones with the Pearson coefficient larger than 0.04. For the correlated distributions a two-dimensional fit was used, while for the uncorrelated distributions the fit was one-dimensional, see Fig. 2. The correlations were checked for neutrons born in the concrete floor and ceiling, as well as copper and lead of the passive shielding. Table 1 shows the correlations estimated for different planes and materials. The point-of-birth distributions in the floor and ceiling are uncorrelated. In the region with $Z > 0$ cm, the veto corner modules offer high protection

from muon penetration, and thus for copper and lead the correlations were estimated for $Z < 0$ cm only. For the bottom plates, the corner parts with peaks were checked, see Fig. 2 (bottom right). This is why, e.g., for lead we checked the corners with $X, Y < -40$ cm and $X, Y > 60$ cm. Additionally, the correlations in materials of the passive shielding (XZ and YZ) depend on the spatial orientation.

CONCLUSION

In the single-neutron simulation, raw-data processing showed that, on average, there are 14.4 signal-like events per day from neutrons born in copper, 4 from neutrons born in the concrete floor, 5.6 from neutrons born in lead, and less than 1 signal-like event per four days from neutrons born in the concrete ceiling. In the DANSS experiment, approximately 13 single-neutron signal-like events are expected. After the final analysis of the simulated data, agreement in the number of signal-like events is expected.

ACKNOWLEDGMENTS

The DANSS experiment is supported by the RSF Grant No. 17-12-01145. The authors appreciate the administration of the KNPP and the staff of the KNPP Radiation Safety Department for permanent assistance with the experiment, as well as the members of the DANSS Collaboration.

REFERENCES

1. I. G. Alekseev et al. (DANSS Collaboration), "DANSS: Detector of the Reactor AntiNeutrino Based on Solid Scintillator," *J. Instrum.* **11**, P11011 (2016).
2. S. Agostinelli et al. (GEANT4 Collaboration), "GEANT4—A Simulation Toolkit," *Nucl. Instrum. Methods Phys. Res. A* **506**, 250–303 (2003).
3. J. Allison et al., "Geant4 Developments and Applications," *IEEE Trans. Nucl. Sci.* **53**, 270–278 (2006).
4. R. Brun and F. Rademakers, "ROOT – An Object Oriented Data Analysis Framework," *Nucl. Instrum. Methods Phys. Res. A* **389**, 81–86 (1997).

Energy and Vertex Reconstruction with Charge Information in JUNO

G. Huang (for the JUNO Collaboration)

Institute of High Energy Physics, Chinese Academy of Sciences, 100049 Beijing, China

Abstract. Jiangmen Underground Neutrino Observatory (JUNO) is a medium-baseline reactor-neutrino experiment primarily designed to determine the neutrino-mass ordering by studying the disappearance of reactor neutrinos from the Yangjiang and Taishan nuclear power plants. Its central detector is a 35.4 m acrylic ball filled with 20 kton of liquid scintillator and mounted with around 18,000 20-inch PMTs and around 25,000 3-inch PMTs. Its energy resolution needs to achieve unprecedented 3% at 1 MeV, which is challenging for the reconstruction work. In this work, we studied the relationship between the vertex resolution and the energy resolution with the JUNO Monte Carlo simulation and found that the energy resolution is insensitive to the angular resolutions of vertex but is partially sensitive to the radial resolution of vertex in the total-reflection (TR) area. We proposed a method of energy and vertex reconstruction with charge information only. The algorithm can achieve a radial resolution $\sigma_r < 10$ cm at 1 MeV in the total-reflection area and the impact of vertex resolution on energy resolution is less than 3%.

Keywords: energy resolution; vertex resolution; charge information; total reflection
PACS: 29.40.Mc; 02.50.Ng

INTRODUCTION

JUNO [1] is under construction in the south of China and will be the largest liquid-scintillator (LS) detector in the world. Its total light level can reach $\sim 1{,}200$ p.e./MeV by achieving a large photocathode coverage of about 75%, doping the LS with a PPO concentration of ~ 2.5 g/l, aiming at an attenuation length larger than 20 m and a PMT detection efficiency higher than 27%. How to accurately position physical events and estimate their energy is the mission of the reconstruction work of the central detector (CD), which is important for the energy-resolution optimization, fiducial-volume cut and external-background control. Its challenges arise from the new detector structure and photon sensor [2, 3].

In this work, we propose an energy- and vertex-reconstruction method using charge information only, where energy and radius are free parameters in the maximizing process of likelihood while angular parameters are fixed to the values obtained from the charge-weighted-center method. The expected number of photoelectrons (NPE) of each PMT is calculated using a 3D NPE map derived from the Automated Calibration Unit (ACU) and the Cable Loop System (CLS) [4]. Its zenith resolution (σ_θ) can reach 0.03 rad, azimuth resolution (σ_ϕ) can reach 0.04 rad, radial resolution (σ_r) can reach less than 10 cm at 1 MeV in the $15.5\,\text{m} < r < 17.2\,\text{m}$ range and less than 30 cm at 1 MeV in the $r < 15.5$ m range. The impact of vertex resolution on energy resolution is less than 3%.

ENERGY-RESOLUTION COMPONENTS

We define the NPE energy estimator, which is the analytical solution of NPE-based maximum-likelihood estimation (PEMLE), to study the NPE-based energy-resolution components. The number of detected photoelectrons k_i is expected to follow a Poisson distribution with mean μ_i proportional to the visible energy E and the mean light level per unit visible energy $\mu_{i,0}$. The NPE-based likelihood function is constructed to describe the probability of k_i p.e. observed in the i^{th} channel when the event deposited energy E at position (r_s, θ_s, ϕ_s):

$$\mathscr{L}(k_1, k_2, \ldots, k_N \mid r_s, \theta_s, \phi_s, E) = \prod \mathscr{L}(k_i \mid r_s, \theta_s, \phi_s, E) = \prod \frac{e^{-\mu_i} \mu_i^{k_i}}{k_i!}, \quad (1)$$

where the product is over all PMTs and $\mu_i = E\,\mu_{i,0}$, with $\mu_{i,0}$ estimated using a 3D NPE map derived from the ACU + CLS calibration scheme.

Given a vertex, the energy solution of the maximum-likelihood function is given by the NPE energy estimator:

$$E_{\text{NPE}} = \frac{\sum k_i}{\sum \mu_{i,0}}. \quad (2)$$

The (single-point) energy resolution of the NPE energy estimator is given by:

$$\left(\frac{\sigma_{E_{\text{NPE}}}}{E_{\text{NPE}}}\right)^2 = \left(\frac{\sigma_{\sum k_i}}{\sum k_i}\right)^2 + \left(\frac{\sigma_{\sum \mu_{i,0}}}{\sum \mu_{i,0}}\right)^2, \quad (3)$$

where the first term comes from the scintillator and PMT-related fluctuation of NPE and is independent of vertex resolution, while the second term arises from nonuniformity of the detector and imperfect vertex resolution. The vertex-related term can be expanded as:

$$\left(\frac{\sigma_{\sum \mu_{i,0}}}{\sum \mu_{i,0}}\right)^2 = \left(\frac{\partial \sum \mu_{i,0}}{\partial r} \frac{\sigma_r}{\sum \mu_{i,0}}\right)^2 + \left(\frac{\partial \sum \mu_{i,0}}{\partial \theta} \frac{\sigma_\theta}{\sum \mu_{i,0}}\right)^2 + \left(\frac{\partial \sum \mu_{i,0}}{\partial \phi} \frac{\sigma_\phi}{\sum \mu_{i,0}}\right)^2 \quad (4)$$

and is determined by the total mean light level per unit visible energy $\sum \mu_{i,0}$, nonuniformity of $\sum \mu_{i,0}$, and vertex resolution. Here, the partial derivatives arise from nonuniformity of $\sum \mu_{i,0}$, while σ_r, σ_θ, σ_ϕ represent the vertex resolution. The distributions of $\sum \mu_{i,0}$ along r, θ, ϕ are shown in Fig. 1.

Combining Eq. (4) and Fig. 1, we can qualitatively infer that:

- Energy resolution is insensitive to the radial resolution of vertex in the $r < 15.5\,\text{m}$ range and is only partially sensitive to the radial resolution of vertex in the TR area.
- Energy resolution is insensitive to σ_ϕ while slightly sensitive to σ_θ.

These observations indicate that charge information may be of great use to fit radius in the TR area.

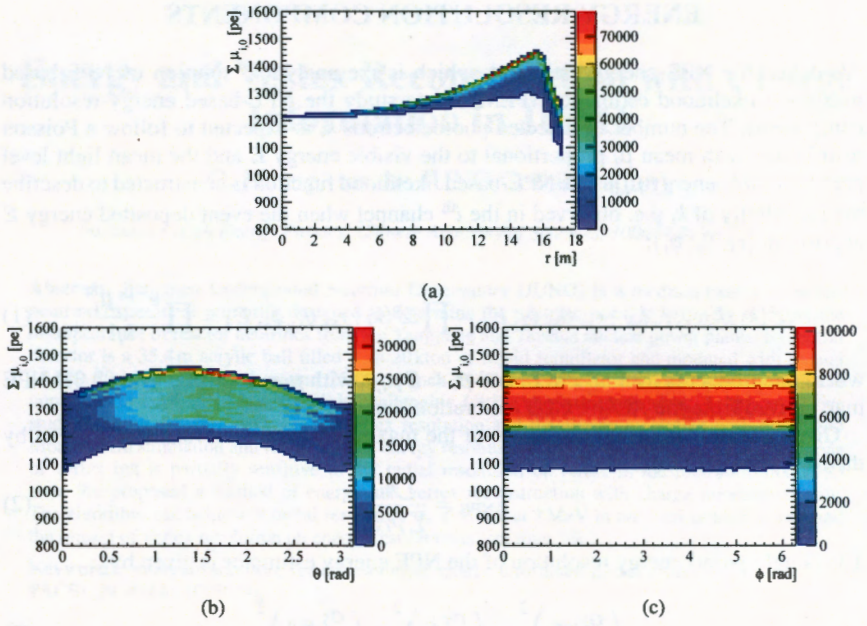

Figure 1. Distributions of $\sum \mu_{i,0}$ along: (a) r, (b) θ, (c) ϕ. Note that $\frac{\partial \sum \mu_{i,0}}{\partial r}$ becomes relatively large in the TR area.

EVENT RECONSTRUCTION WITH CHARGE INFORMATION

In order to handle the charge response of PMTs, the likelihood function of charge-based maximum-likelihood estimation (QMLE) is constructed as follows:

$$\mathscr{L}(q_1, q_2, \ldots, q_N \mid \mathbf{r}, E) = \prod_{\text{unhit}} e^{-\mu_j} \prod_{\text{hit}} \left(\sum_{k=1}^{+\infty} \frac{e^{-\mu_i} \mu_i^k}{k!} P(q_i \mid k) \right). \tag{5}$$

Here, q_i is the recorded charge of the i^{th} PMT, $P(q_i \mid k)$ is the probability of kPE resulting in the charge q_i that can be calculated by convolving the SPEs. In this study, preliminary models of the SPEs of the two types of large JUNO PMTs were constructed and are shown in Fig. 2.

Figure 1 shows that the detected light level is insensitive to the direction of the event. Since the time information is not included yet, the joint fitting of energy and vertex is challenging. This method usually needs vertex information as input, otherwise it will not converge. The analytical study in the previous Section also indicates that the angular resolutions of vertex may have little impact on the energy resolution, which simplifies the fitting without loss of energy-resolution performance. To confirm the hypothesis about the impact of vertex resolution on the energy resolution, we generated numerous

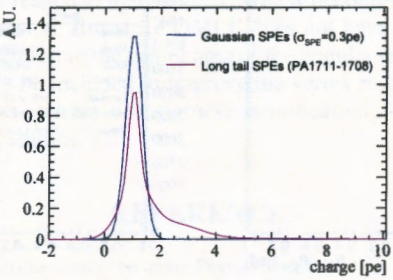

Figure 2. Single-photoelectron spectrum of a typical MCP PMT (long-tail SPEs) and dynode PMT (Gaussian SPEs).

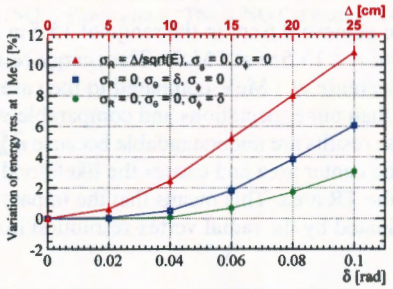

Figure 3. Impact of vertex resolution on energy resolution of QMLE at 1 MeV, where the energy resolution is defined as $\sqrt{a^2/E+b^2}$ [1] fitted from the reconstructed visible energy of 50,000 $P = \{0, 2, 5, 8, 10\}$ MeV e^+ events, Δ and δ are the radial and angular resolutions at 1 MeV, and fiducial-volume range is $r < 17.2$ m.

Monte Carlo events and then used QMLE to reconstruct their energy by fixing the vertex to the smearing vertex calculated from the true vertex to study the relationship between the energy resolution and the vertex resolution of JUNO in the JUNO Monte Carlo simulation. The energy reconstruction results, shown in Fig. 3, demonstrate that:

- 10 cm radial resolution lowers the energy resolution by 2.5% at 1 MeV, while 15 cm radial resolution lowers the energy resolution by 5.2% at 1 MeV.
- Energy resolution is slightly sensitive to σ_ϕ and σ_θ, but angular resolutions better than 0.04 rad are sufficient.

Angular resolutions of 0.04 rad are sufficient, and the angular resolutions of the charge-weighted-center method are better than 0.04 rad (see the next Section). Therefore, we can adopt θ and ϕ from the charge-weighted-center method and fix them. The free parameters of QMLE are radius and energy. In this way, we found that energy and vertex can be simultaneously estimated with charge information only.

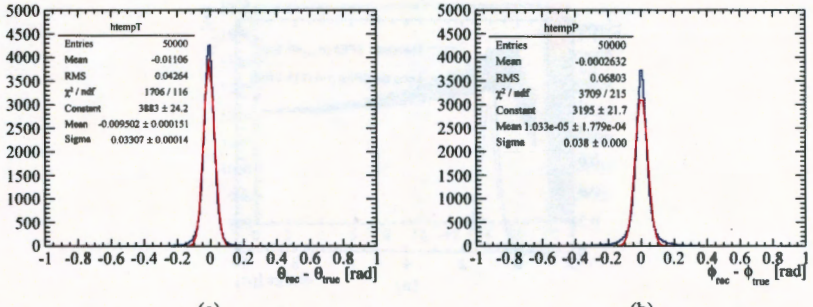

(a) (b)

Figure 4. (a) θ and (b) ϕ angular resolutions of the charge-weighted-center method.

Its radial resolution can achieve 9.6 cm in the range of 15.5 m $< r <$ 17.2 m at 1 MeV and 29.0 cm in the range of $r <$ 15.5 m at 1 MeV. The energy-resolution performance of QMLE exhibits a 2.7% decrease at 1 MeV compared to the case when the true vertices are known. This is better than our expectations and comparable with the performance of $\sigma_r = 10$ cm in Fig. 3. These results are understandable because $\partial \sum \mu_{i,0} / \partial r$ in the TR area is much sharper than in the center area and causes the likelihood to become much more sensitive to the radius in the TR area. This means that the impact of vertex resolution on energy resolution is dominated by the radial vertex resolution in the TR area.

CHARGE-WEIGHTED-CENTER METHOD

The initial vertex from the charge-weighted-center method is given by:

$$\mathbf{r}_{QC} = \alpha \frac{\sum q_i \mathbf{r}_i}{\sum q_i}, \tag{6}$$

where q_i is the recorded charge of the i^{th} PMT, $\mathbf{r}_i$ is the position of the center of photocathode of the i^{th} PMT, and $\alpha = 1.1$ was set in this study. The angular resolutions of the charge-weighted-center method are shown in Fig. 4.

CONCLUSION AND DISCUSSION

This study demonstrated that QMLE can achieve a radial resolution $\sigma_r <$ 10 cm at 1 MeV in the range of 15.5 m $< r <$ 17.2 m by using charge information only, while the impact of vertex resolution on energy resolution is less than 3%. The reason is that the symmetry and large scale of CD makes NPE insensitive to the event angle and small event radius, while the TR phenomenon leads to NPE partially sensitive to the event radius. For the energy resolution, this means that the radial resolution is much more important than the angular resolutions, especially in the TR range. For the vertex resolution, the derivative of NPE plays a role.

This method is time-response independent, which becomes an advantage regarding the feasibility and concision. But since QMLE does not have any significant ability to optimize the radial resolution in the center area or the angular resolutions, the time information must necessarily be included to improve the vertex resolution. This is important for the energy-resolution optimization, particle identification, further background reduction, and other relevant studies.

REFERENCES

1. F. P. An et al. (JUNO Collaboration), "Neutrino Physics with JUNO," *J. Phys. G: Nucl. Part. Phys.* **43**, 030401 (2016).
2. Q. Liu, M. He, X. Ding, W. Li, and H. Peng, "A Vertex Reconstruction Algorithm in the Central Detector of JUNO," *J. Instrum.* **13**, T09005 (2018).
3. W. Wu, M. He, X. Zhou, and H. Qiao, "A New Method of Energy Reconstruction for Large Spherical Liquid Scintillator Detectors," *J. Instrum.* **14**, P03009 (2019).
4. Q. Zhang and Y. Guo (JUNO Collaboration), "The JUNO Calibration System," *PoS* **ICHEP2018**, 811 (2019).

Ordinary Muon Capture as a Probe of $0\nu\beta\beta$ Decays

L. Jokiniemi,[1] J. Suhonen,[1] and H. Ejiri[2]

[1] *University of Jyväskylä, 40014 Jyväskylä, Finland*
[2] *Research Center for Nuclear Physics, Osaka University, 567-0047 Ibaraki, Japan*

Abstract. Existence of the neutrinoless double-beta ($0\nu\beta\beta$) decay is one of the most crucial open questions in neutrino physics. It has not yet been observed, even though numerous large-scale experiments have been trying to discover the process for decades. Thus, accurate theoretical calculations for the $0\nu\beta\beta$ decay are necessary in order to guide the experimentalists in planning of the experiments. In order to reliably describe the double-beta-decay processes one needs a possibility to test the involved virtual transitions against the experimental data. In this work, we investigate how to utilize the ordinary muon capture (OMC) in the study of the $0\nu\beta\beta$ decay.

Keywords: ordinary muon capture; double-beta decay; weak axial couplings
PACS: 21.60.Cs; 21.60.Jz; 23.40.Bw; 23.40.Hc

INTRODUCTION

The neutrinoless double-beta ($0\nu\beta\beta$) decay of atomic nuclei is a beyond-Standard-Model process that has not yet been observed, despite the fact that much effort has been made towards its detection (see Refs. [1, 2, 3]). The $0\nu\beta\beta$ decay is a lepton-number-violating process which would indicate that the neutrino is a Majorana particle, in conflict with the Standard Model of particle physics. Since the $0\nu\beta\beta$ decay is extremely challenging to study both experimentally and theoretically, we need some complementary tests in order to accurately assess the involved nuclear matrix elements and to design the large-scale experiments.

Double-beta ($\beta\beta$) decays take place between two even-even nuclei of an isobaric chain trough virtual states of the intermediate odd-odd nucleus. The $0\nu\beta\beta$ decay runs trough states of all possible multipolarities J^π of the intermediate nucleus, whereas the ordinary two-neutrino double-beta ($2\nu\beta\beta$) decay runs only trough the 1^+ virtual states. These intermediate J^π states of the $0\nu\beta\beta$ decay can be studied by utilizing the ordinary muon capture (OMC) on the daughter nucleus of the $\beta\beta$ triplet, which correspond to the right-branch virtual transitions of the $0\nu\beta\beta$ decay.

The large involved momentum transfer $q \approx 50$–$100\,\mathrm{MeV}$ in the OMC process corresponds to the momentum-exchange scale of the $0\nu\beta\beta$ decay, which makes it a promising tool to probe the $0\nu\beta\beta$ decay. Furthermore, due to the large mass of the muon, the OMC can populate the final nuclear states that are both highly excited and of high multipolarity J^π, quite like the $0\nu\beta\beta$ decay populates the intermediate virtual states.

In this study, we first tested our muon-capture approach on the OMC by ^{100}Mo, which has been measured at RCNP, Osaka [4]. We computed the muon-capture-rate spectrum in ^{100}Nb and compared it with the measured spectrum. Then, we applied the formalism

for computing the OMC spectra to the daughter nuclei of some $\beta\beta$ triplets.

FORMALISM OF ORDINARY MUON CAPTURE

The ordinary muon capture (OMC) is a weak-interaction process analogous to the electron capture. The main difference is the large mass of the captured muon—about 200 times the electron mass—which makes the process more promising as a probe of the $0\nu\beta\beta$ decay. The OMC process we are interested in can be written as follows:

$$\mu^- + {}^{A}_{Z}\mathrm{X}(0^+) \rightarrow \nu_\mu + {}^{A}_{Z-1}\mathrm{Y}(J^\pi), \tag{1}$$

where the muon (μ^-) is captured by the 0^+ ground state of the even-even nucleus X with atomic number Z and mass number A, leading to the J^π state of its odd-odd isobar Y with atomic number $Z-1$ and emission of a muon neutrino ν_μ. The energy release is about 100 MeV, of which the largest fraction is carried away by the emitted neutrino due to being the lightest object participating in the process. The large involved momentum exchange $q \approx 50$–100 MeV allows highly forbidden transitions as well as highly excited final states with high multipolarities J^π, which makes it a good probe of the $0\nu\beta\beta$ decay.

In our study, the ordinary-muon-capture rates are based on the Morita–Fujii formalism [5]. The partial muon-capture rate to a J^π final state can be written as follows:

$$W = 8\left(\frac{Z_{\mathrm{eff}}}{Z}\right)^4 P(\alpha Z m'_\mu)^3 \frac{2J_f+1}{2J_i+1}\left(1-\frac{q}{m_\mu + AM}\right)q^2, \tag{2}$$

where A denotes the mass number of the initial and final nuclei, J_i (J_f) is the angular momentum of the initial (final) nucleus, M is the average nucleon rest mass, m_μ is the bound-muon mass, m'_μ is the reduced mass of muon in the parent μ-mesonic atom, Z is the atomic number of the initial nucleus, α is the fine-structure constant, and q is the Q value of the OMC process [5]. For heavy nuclei, the atomic orbit of muon penetrates the nucleus, and hence the capture rate has to be corrected for the muon screening. Here, we follow the Primakoff procedure [6] in which the capture rate has been corrected by the factor of $(Z_{\mathrm{eff}}/Z)^4$, where the effective atomic number Z_{eff} is obtained from the work of Ford and Wills [7].

The factor P in Eq. (2) has a complex structure containing all the nuclear matrix elements, as well as weak couplings, some geometric factors, and Racah coefficients; its exact form can be found in [5]. P can be expanded in terms of a small quantity $1/M^2$ as $P = P_0 + P_1$, where P_0 is obtained by neglecting all terms containing $1/M^2$ (except for terms containing g_{P}^2, which is large compared to the other coupling constants) and P_1 contains all terms, including the terms of the order of $1/M^2$. The explicit form of the leading-order term P_0 can be found in [5]. The next-to-leading-order term P_1 is also introduced in our calculations, since it is found to be important for weak OMC transitions, usually to high-lying states [8].

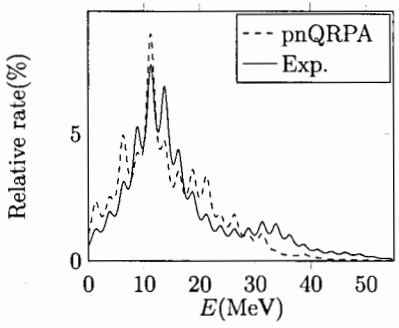

Figure 1. Comparison of the experimental and theoretical relative muon-capture-rate distributions in ^{100}Nb.

MUON-CAPTURE-RATE DISTRIBUTION FOR ^{100}Nb

For the first time, an OMC giant resonance was observed in ^{100}Nb at RCNP, Osaka [4]. Inspired by this observation, we computed the muon-capture-rate distribution in ^{100}Nb within the pnQRPA formalism with large no-core single-particle basis and compared the obtained spectrum with the experimental one [9]. Both the experimental OMC spectrum and the pnQRPA-computed one show a giant resonance at around 10–12.5 MeV and tails at higher energies (see Fig. 1).

However, the total capture rate $W_{\rm tot} = 17.7 \times 10^6\,{\rm s}^{-1}$ obtained using the coupling-constant values $g_{\rm A} = 0.8$ and $g_{\rm P} = 10$ is much larger than the corresponding Primakoff estimate $W_{\rm Prim.} = 7.7 \times 10^6$ (see Eq. (4.53) of the review article [10]). This suggests a strongly quenched axial-vector coupling constant $g_{\rm A} \approx 0.5$.

MUON-CAPTURE-RATE DISTRIBUTIONS FOR THE DAUGHTER NUCLEI OF $\beta\beta$-DECAY TRIPLETS

The ordinary muon captures by the daughter nuclei ^{76}Se, ^{82}Kr, ^{96}Mo, ^{100}Ru, ^{116}Sn, ^{128}Xe, ^{130}Xe, and ^{136}Ba of the key double-beta-decay triplets, leading to excited states of the corresponding intermediate nuclei, were computed within the pnQRPA framework using large no-core single-particle bases as in the case of ^{100}Mo. The corresponding OMC-rate functions were analyzed in terms of multipole decompositions (see Fig. 2 for examples).

The low-energy ($E < 1.1$ MeV) part of the computed spectrum for the transitions $^{76}{\rm Se}(0^+_{\rm g.s.}) + \mu^- \to {}^{76}{\rm As}(J^\pi) + \nu_\mu$ can be compared with the measured rates deduced from the recent results of Zinatulina et al. [11]. The capture rates for each J^π multipole below 1.1 MeV are summed, and the obtained experimental and pnQRPA-computed values are presented in Table 1 (for details, see Ref. [8]). In the pnQRPA calculations,

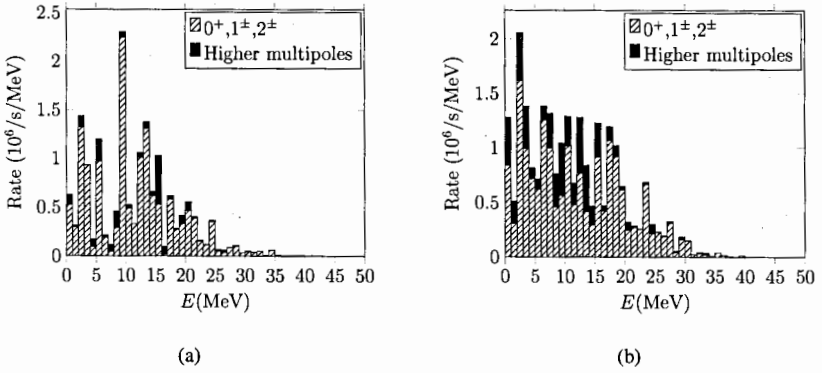

Figure 2. OMC-rate distributions for the transitions: (a) $^{76}\mathrm{Se}(0^+_{\mathrm{g.s.}}) + \mu^- \rightarrow {}^{76}\mathrm{As}(J^\pi) + \nu_\mu$ and (b) $^{130}\mathrm{Xe}(0^+_{\mathrm{g.s.}}) + \mu^- \rightarrow {}^{130}\mathrm{I}(J^\pi) + \nu_\mu$. Transitions to the lowest and higher multipole states are shown separately.

Table 1. The "most probable" experimental OMC-strength distribution below 1.1 MeV in ^{76}As [11] compared with the corresponding pnQRPA-computed distribution [8], where g.s. means transitions to the ground state that could not be measured.

	OMC rate [s^{-1}]			OMC rate [s^{-1}]	
J^π	Exp.	pnQRPA	J^π	Exp.	pnQRPA
0^+	5,120	414	3^+	60,160	55,355
1^+	218,240	236,595	3^-	53,120	34,836
1^-	31,360	28,991	4^+	–	2,797
2^+	120,960	114,016	4^-	30,080	23,897
2^-	g.s. + 145,920	177,802			

we used the parameter values $g_{\mathrm{A}} = 0.8$ and $g_{\mathrm{P}} = 7.0$. The obtained capture rates are generally surprisingly close to the experimental ones, but the pnQRPA method seems to underestimate the capture rates for transitions to the 0^+ states.

CONCLUSIONS

Neutrinoless double-beta decay has not yet been observed, despite substantial efforts made towards its detection. Thus, the $0\nu\beta\beta$ calculations are in need of some complementary tests in order to reliably describe the intermediate states and to finally probe the half-lives of $0\nu\beta\beta$ decays.

Ordinary muon capture by the daughter nuclei of $0\nu\beta\beta$ decays serve as a useful supplement to study the intermediate states in $0\nu\beta\beta$ decays. We studied a possibility to utilize these reactions in the study of $0\nu\beta\beta$ decay.

By extending the OMC experiments and calculations to other $0\nu\beta\beta$-decaying nuclei, we could shed light on the effective values of axial-vector (g_A) and induced pseudoscalar (g_P) couplings, as well as on the NMEs related to $0\nu\beta\beta$ decay and astro-(anti)neutrino interactions.

ACKNOWLEDGMENTS

This work was partially supported by the Academy of Finland under the Academy Project No. 318043.

REFERENCES

1. H. Ejiri, "Nuclear Spin Isospin Responses for Low-Energy Neutrinos," *Phys. Rep.* **338**, 265–351 (2000).
2. J. D. Vergados, H. Ejiri, and F. Šimkovic, "Neutrinoless Double Beta Decay and Neutrino Mass," *Int. J. Mod. Phys. E* **25**, 1630007 (2016).
3. H. Ejiri, J. Suhonen, and K. Zuber, "Neutrino–Nuclear Responses for Astro-Neutrinos, Single Beta Decays and Double Beta Decays," *Phys. Rep.* **797**, 1–102 (2019).
4. I. H. Hashim et al., "Muon Capture Reaction on ^{100}Mo to Study the Nuclear Response for Double-β Decay and Neutrinos of Astrophysics Origin," *Phys. Rev. C* **97**, 014617 (2018).
5. M. Morita and A. Fujii, "Theory of Allowed and Forbidden Transitions in Muon Capture Reactions," *Phys. Rev.* **118**, 606–618 (1960).
6. H. Primakoff, "Theory of Muon Capture," *Rev. Mod. Phys.* **31**, 802–822 (1959).
7. K. W. Ford and J. G. Wills, "Calculated Properties of μ-Mesonic Atoms," *Nucl. Phys.* **35**, 295–302 (1962).
8. L. Jokiniemi and J. Suhonen, "Muon-Capture Strength Functions in Intermediate Nuclei of $0\nu\beta\beta$ Decays," *Phys. Rev. C* **100**, 014619 (2019).
9. L. Jokiniemi, J. Suhonen, H. Ejiri, and I. H. Hashim, "Pinning Down the Strength Function for Ordinary Muon Capture on ^{100}Mo," *Phys. Lett. B* **794**, 143–147 (2019).
10. D. F. Measday, "The Nuclear Physics of Muon Capture," *Phys. Rep.* **354**, 243–409 (2001).
11. D. Zinatulina et al., "Ordinary Muon Capture Studies for the Matrix Elements in $\beta\beta$ Decay," *Phys. Rev. C* **99**, 024327 (2019).

Analysis of First KATRIN Neutrino-Mass Data

C. Karl,[1,2] S. Mertens,[1,2] and M. Slezák[1] (for the KATRIN Collaboration)

[1] *Max Planck Institute for Physics, 80805 Munich, Germany*
[2] *Technical University of Munich, 85748 Garching, Germany*

Abstract. The KATRIN experiment is designed to measure the effective electron-antineutrino mass m_ν by investigating the energy spectrum of tritium β decay. The first neutrino-mass measurement campaign took place between April 10 and May 13, 2019. This work presents one of the analysis strategies pursued which is based upon Monte Carlo propagation of uncertainties. A fit to the data including all dominant systematic effects leads to a best-fit value of $m_\nu^2 = -1.0^{+0.9}_{-1.1}\,\mathrm{eV}^2$. From this result, we derive an upper limit of $m_\nu < 1.1\,\mathrm{eV}$ at 90% C.L. using the sensitivity-limit method of Lokhov and Tkachov.

Keywords: KATRIN; neutrino; mass
PACS: 14.60.Pq; 14.60.Lm

INTRODUCTION

Various neutrino-oscillation experiments have proven that neutrinos are not massless particles [1, 2, 3] but, as the observables are the mass-squared differences, they cannot determine the absolute mass scale of neutrinos. Currently, three different approaches to measure the absolute mass scale are being pursued: 1. cosmological studies of large-scale structure (LSS) formations [4], 2. the search for neutrinoless double-β decay [5], and 3. the analysis of a spectral distortion near the endpoint in single-β decay.

The KArlsruhe TRItium Neutrino (KATRIN) experiment is designed to explore the absolute mass scale of neutrinos using the latter approach with an unprecedented sensitivity of 0.2 eV at 90% C.L. To achieve this goal, the following requirements must be fulfilled: a large number of counts in the region of interest close to the endpoint and an excellent energy resolution of the order of 1 eV. As only about 10^{-9} of the electrons emitted in β decay have an energy in the endpoint region, the first requirement demands a highly luminous source. KATRIN employs the Windowless Gaseous Tritium Source (WGTS), which can provide a column density of up to $5 \times 10^{21}\,\mathrm{m}^{-2}$ molecules corresponding to an activity of 10^{11} Bq [6]. The excellent energy resolution is realized using the same measurement principle as its predecessors in Mainz [7] and Troitsk [8]: magnetic adiabatic collimation with an electrostatic filter (MAC-E) [9, 10].

After the successful first tritium operation in 2018 [11], the first measurement campaign dedicated to neutrino-mass measurement was performed in Spring 2019. For this first period, the column density in the source was set to about 22% of the nominal value and the energy resolution was 2.8 eV. In the four weeks of β scans, around two million electrons in the region of interest were collected. This corresponds to an effective measurement time of about five days at full source activity. Nevertheless, this data can be used to improve the existing laboratory limits along with developing the analysis

strategies and tools for neutrino-mass determination.

NEUTRINO-MASS INFERENCE

As mentioned in the Introduction, the signature KATRIN searches for is a spectral distortion of the β spectrum near the endpoint as shown in Fig. 1(a). Two main ingredients make up the model used to describe the data. First, the Fermi theory of β decay describes the differential decay rate of tritium molecules in the source $R_\beta(E)$ as a function of the electron energy E. The second component is the experimental response function $f(qU, E)$ as a function of the retarding energy qU and E. It describes the transmission properties of the MAC-E filter as well as scattering effects in the source. Due to the high-pass-filter behavior of the MAC-E filter, KATRIN measures the differential decay rate integrated over the response function:

$$R(qU; \boldsymbol{\theta}) = A_S N_T \int_{qU}^{E_{0,\mathrm{eff}}} R_\beta(E; m_\nu^2, E_{0,\mathrm{eff}})\, f(qU, E)\, \mathrm{d}E + R_{\mathrm{bg}}, \tag{1}$$

where N_T absorbs any normalization components such as the total number of molecules in the source and the acceptance angle of the apparatus. We use $\boldsymbol{\theta}$ to denote the vector of free parameters that are inferred from the measured spectrum: the neutrino-mass squared m_ν^2, the effective endpoint $E_{0,\mathrm{eff}}$, the signal amplitude A_S, and the constant background rate R_{bg}. As the resolution of the KATRIN experiment is not sufficient to distinguish between the individual mass eigenvalues m_i, the observable m_ν^2 corresponds to an incoherent sum:

$$m_\nu^2 = \sum_i |U_{ei}|^2\, m_i^2, \tag{2}$$

where U_{ei} are the elements of the Pontecorvo–Maki–Nakagawa–Sakata mixing matrix.

To infer the best-fit values of $\boldsymbol{\theta}$, the standard procedure of maximizing the likelihood $\mathscr{L}$ or minimizing $-2\ln\mathscr{L}$ can be performed. A typical spectral fit to a two-hour scan of the β spectrum including statistical uncertainties only is shown in Fig. 1(b).

SYSTEMATICS TREATMENT: MONTE CARLO PROPAGATION OF UNCERTAINTY

This work focuses on one of the two analysis approaches pursued for analyzing the first neutrino-mass data [12], based on Monte Carlo propagation of uncertainty [13, 14, 15, 16]. The idea behind this method is to repeat the fit $\approx 10^4$ times with randomized but fixed input values for the systematic nuisance parameters $\boldsymbol{\eta}$. Compared to the well-known approach of free nuisance parameters constrained by pull terms, this method has two key advantages for the KATRIN analysis. First and foremost, the expensive response function does not have to be recomputed with varying $\boldsymbol{\eta}$ during the fit. Additionally, the minimization is technically simplified due to the reduced number of free parameters.

To retrieve an initial estimate of the best-fit values of $\hat{\boldsymbol{\theta}}_{\mathrm{data}}$, we fit the original data with the additional parameters $\boldsymbol{\eta}$ fixed to the best of our knowledge. We then generate Monte

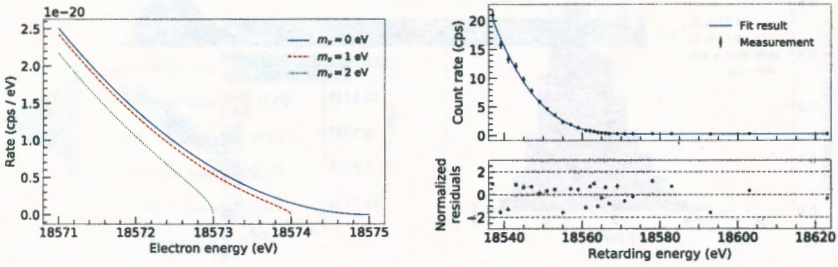

(a) (b)

Figure 1. (a) Impact of different neutrino-mass values on the differential β spectrum. (b) Spectral fit to a scan of two-hour measurement time including statistical uncertainties only. Due to the low statistics in an individual scan, m_ν^2 was fixed to zero. The residuals are normalized to the uncertainty. A p-value of 0.67 indicates an excellent goodness of fit.

Carlo (MC) spectra assuming the values $\hat{\boldsymbol{\theta}}_{\text{data}}$ for our model and a Poisson distribution of the counts. Each of these statistically randomized MC spectra is then fit to retrieve one sample of the values $\hat{\boldsymbol{\theta}}_{\text{sample}}$. The resulting distribution of $\{\hat{\boldsymbol{\theta}}_{\text{sample}}\}$ can be used to infer the statistical uncertainty of $\boldsymbol{\theta}$.

As a next step, we vary the values of $\boldsymbol{\eta}$ according to their uncertainty. The model is initialized with the values $\boldsymbol{\eta}_{\text{sample}}$ and fit to the data spectrum without statistical randomization. In principle, the resulting distribution of $\{\hat{\boldsymbol{\theta}}_{\text{sample}}\}$ reflects the systematical uncertainty taking into account only the external information on $\boldsymbol{\eta}$. However, the data also contains information to constrain $\boldsymbol{\eta}$. To take this into account, we weigh each sample $\hat{\boldsymbol{\theta}}_{\text{sample}}$ with the corresponding likelihood $\mathscr{L}(\hat{\boldsymbol{\theta}}_{\text{sample}})$. The resulting weighted distribution of $\{\hat{\boldsymbol{\theta}}_{\text{sample}}\}$ is then used to retrieve the systematic uncertainty of $\boldsymbol{\theta}$.

In the final step, we combine the statistics- and systematics-only steps described above. The model initialized with randomized $\boldsymbol{\eta}_{\text{sample}}$ is first fit to statistically randomized MC spectra to retrieve the values of $\hat{\boldsymbol{\theta}}_{\text{sample}}$. This model is then also fit to the unmodified data spectrum to retrieve the likelihood $\mathscr{L}(\hat{\boldsymbol{\theta}}_{\text{sample}})$. We infer the combined statistical and systematical uncertainty from the distribution of $\{\hat{\boldsymbol{\theta}}_{\text{sample}}\}$ weighted by these likelihood values.

APPLICATION TO FIRST NEUTRINO-MASS DATA

The method of Monte Carlo propagation of uncertainty was successfully applied to analyze the first KATRIN neutrino-mass data. The one-dimensional m_ν^2 distributions, shown in Fig. 2(a), are used to derive the best-fit value of $m_\nu^2 = -1.0^{+0.9}_{-1.1}\,\text{eV}^2$ (stat. + sys.). This best-fit value corresponds to a 1σ fluctuation to the negative values with a probability of 16% assuming $m_\nu = 0\,\text{eV}$. Figure 2(b) shows the two-dimensional distribution of m_ν^2 and $E_{0,\text{eff}}$ as well as the projection of the individual one-dimensional distributions. From

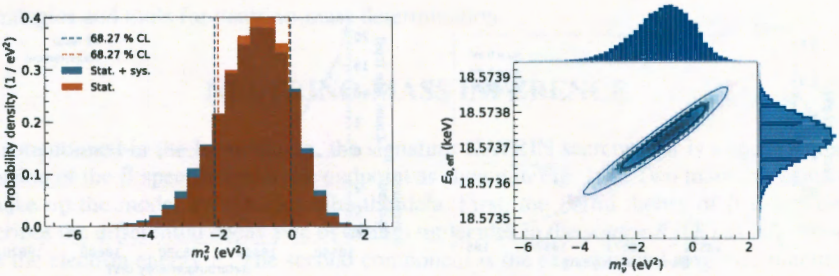

(a) (b)

Figure 2. Parameter distributions retrieved from Monte Carlo propagation with 50,000 samples: (a) One-dimensional distribution of m_ν^2 with statistical uncertainty only (orange) as well as statistical and systematical uncertainties combined (blue). The dashed lines indicate the 1σ confidence interval. (b) Two-dimensional distribution of m_ν^2 and $E_{0,\mathrm{eff}}$ including statistical and systematical uncertainties with one-dimensional projections. The ellipses indicate the 1σ and 2σ contours.

this result we derive a strong correlation of m_ν^2 and $E_{0,\mathrm{eff}}$ of 0.97.

Using the Monte Carlo propagation of uncertainty, it is possible to analyze the impact of individual systematic effects on the parameters of interest. As an application, we show the uncertainty budget of m_ν^2 from the first neutrino-mass campaign in Fig. 3. We can see that this first measurement phase is by far dominated by the statistical uncertainty (black). The next-largest components are related to the background. First of all, there is an enlarged uncertainty of the background rate from non-Poissonian effects (blue) [17]. Secondly, we constrain a possible slope of the background shape (orange). The uncertainty of the source properties (green) includes the imperfect knowledge of the gas density in the source as well as the energy-loss effects due to inelastic scattering. Furthermore, uncertainties of the magnetic-field values of the MAC-E filter are considered (red). Finally, uncertainties of the final-state distribution [18] of the daughter molecule have a small impact on the neutrino-mass result (brown).

CONFIDENCE INTERVAL

The final step of this analysis was to convert the best-fit value of m_ν^2 into a confidence interval for the value of m_ν. For this purpose, we followed two alternative approaches: the unified approach of Feldman and Cousins [19] as well as the so-called "sensitivity limit" by Lokhov and Tkachov [20]. The calculated confidence belts are shown in Figs. 4(a) and 4(b), respectively. In case of the unified approach of Feldman and Cousins, our best-fit value of $-1.0\,\mathrm{eV}^2$ corresponds to an upper limit of $m_\nu < 0.8\,\mathrm{eV}$ at 90% C.L. Using the method of Lokhov and Tkachov, we derive $m_\nu < 1.1\,\mathrm{eV}$ at 90% C.L., which coincides with the sensitivity of this measurement campaign.

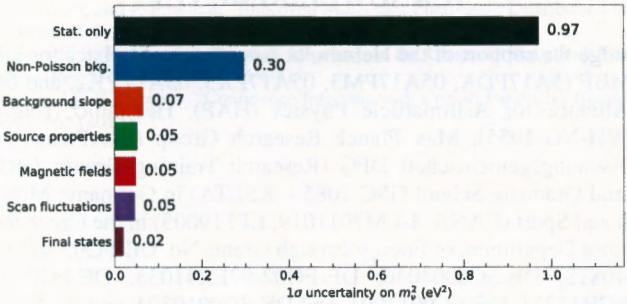

Figure 3. Breakdown of the impact of individual systematic uncertainties on the first neutrino-mass measurement using Monte Carlo propagation of uncertainty. Each bar represents the 1σ uncertainty of m_ν^2 introduced by the corresponding effect. The analysis is clearly dominated by statistical uncertainty, followed by systematics of the background rate and shape.

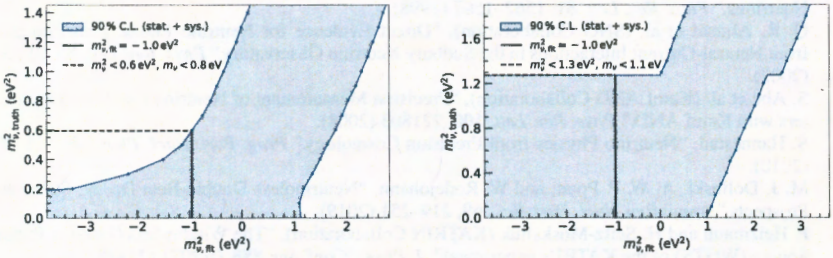

(a) (b)

Figure 4. Confidence belt of m_ν^2 for the first neutrino-mass measurement including statistical and systematical uncertainties at 90% C.L.: (a) Unified approach of Feldman and Cousins. (b) Sensitivity-limit method of Lokhov and Tkachov.

CONCLUSION

The first neutrino-mass data of the KATRIN experiment was taken in Spring 2019. We presented one analysis method based on Monte Carlo propagation of uncertainty and successfully applied it to this dataset. We retrieved a best-fit value of $m_\nu^2 = -1.0^{+0.9}_{-1.1}\,\mathrm{eV}^2$, from which we derived an upper limit of $m_\nu < 1.1\,\mathrm{eV}$ using the sensitivity-limit method by Lokhov and Tkachov at 90% C.L. This value coincides with the sensitivity of the measurement campaign and is an improvement to the existing laboratory limits by around a factor of two. It can be used as an input in cosmological studies of structure formation. We expect that the described techniques will provide a solid basis for the analysis of future measurement campaigns with a higher sensitivity to the neutrino mass.

ACKNOWLEDGMENTS

We acknowledge the support of the Helmholtz Association, Ministry for Education and Research BMBF (5A17PDA, 05A17PM3, 05A17PX3, 05A17VK2, and 05A17WO3), Helmholtz Alliance for Astroparticle Physics (HAP), Helmholtz Young Investigator Group (VH-NG-1055), Max Planck Research Group (MaxPlanck@TUM), and Deutsche Forschungsgemeinschaft DFG (Research Training Groups GRK 1694 and GRK 2149, and Graduate School GSC 1085 – KSETA) in Germany; Ministry of Education, Youth and Sport (CANAM-LM2011019, LTT19005) in the Czech Republic; and the United States Department of Energy through Grants No. DE-FG02-97ER41020, DE-FG02-94ER40818, DE-SC0004036, DE-FG02-97ER41033, DE-FG02-97ER41041, DE-AC02-05CH11231, DE-SC0011091, and DE-SC0019304, and the National Energy Research Scientific Computing Center.

REFERENCES

1. Y. Fukuda et al. (Super-Kamiokande Collaboration), "Evidence for Oscillation of Atmospheric Neutrinos," *Phys. Rev. Lett.* **81**, 1562–1567 (1998).
2. Q. R. Ahmad et al. (SNO Collaboration), "Direct Evidence for Neutrino Flavor Transformation from Neutral-Current Interactions in the Sudbury Neutrino Observatory," *Phys. Rev. Lett.* **89**, 011301 (2002).
3. S. Abe et al. (KamLAND Collaboration), "Precision Measurement of Neutrino Oscillation Parameters with KamLAND," *Phys. Rev. Lett.* **100**, 221803 (2008).
4. S. Hannestad, "Neutrino Physics from Precision Cosmology," *Prog. Part. Nucl. Phys.* **65**, 185–208 (2010).
5. M. J. Dolinski, A. W. P. Poon, and W. Rodejohann, "Neutrinoless Double-Beta Decay: Status and Prospects," *Annu. Rev. Nucl. Part. Sci.*, **69**, 219–251 (2019).
6. F. Heizmann and H. Seitz-Moskaliuk (KATRIN Collaboration), "The Windowless Gaseous Tritium Source (WGTS) of the KATRIN experiment," *J. Phys.: Conf. Ser.* **888**, 012071 (2017).
7. Ch. Kraus et al., "Final Results from Phase II of the Mainz Neutrino Mass Search in Tritium β Decay," *Eur. Phys. J. C* **40**, 447–468 (2005).
8. V. N. Aseev et al. (Troitsk Collaboration), "An Upper Limit on Electron Antineutrino Mass from Troitsk Experiment," *Phys. Rev. D* **84**, 112003 (2011).
9. V. M. Lobashev and P. E. Spivak, "A Method for Measuring the Electron Antineutrino Rest Mass," *Nucl. Instrum. Methods Phys. Res. A* **240**, 305–310 (1985).
10. A. Picard et al., "A Solenoid Retarding Spectrometer with High Resolution and Transmission for keV Electrons," *Nucl. Instrum. Methods Phys. Res. B* **63**, 345–358 (1992).
11. M. Aker et al. (KATRIN Collaboration), "First Operation of the KATRIN Experiment with Tritium," *arXiv:1909.06069 [physics.ins-det]* (2019).
12. M. Aker et al. (KATRIN Collaboration), "Improved Upper Limit on the Neutrino Mass from a Direct Kinematic Method by KATRIN," *Phys. Rev. Lett.* **123**, 221802 (2019).
13. R. D. Cousins and V. L. Highland, "Incorporating Systematic Uncertainties into an Upper Limit," *Nucl. Instrum. Methods Phys. Res. A* **320**, 331–335 (1992).
14. G. Cowan, K. Cranmer, E. Gross, and O. Vitells, "Asymptotic Formulae for Likelihood-Based Tests of New Physics," *Eur. Phys. J. C* **71**, 1554 (2011).
15. S. D. Biller and S. M. Oser, "Another Look at Confidence Intervals: Proposal for a More Relevant and Transparent Approach," *Nucl. Instrum. Methods Phys. Res. A* **774**, 103–119 (2015).
16. P. M. Harris and M. G. Cox, "On a Monte Carlo Method for Measurement Uncertainty Evaluation and Its Implementation," *Metrologia* **51**, 176–182 (2014).
17. S. Mertens et al., "Background Due to Stored Electrons following Nuclear Decays in the KATRIN Spectrometers and Its Impact on the Neutrino Mass Sensitivity," *Astropart. Phys.* **41**, 52–62 (2013).

18. A. Saenz, S. Jonsell, and P. Froelich, "Improved Molecular Final-State Distribution of HeT^+ for the β-Decay Process of T_2," *Phys. Rev. Lett.* **84**, 242–245 (2000).
19. G. J. Feldman and R. D. Cousins, "Unified Approach to the Classical Statistical Analysis of Small Signals," *Phys. Rev. D* **57**, 3873–3889 (1998).
20. A. V. Lokhov and F. V. Tkachov, "Confidence Intervals with a priori Parameter Bounds," *Phys. Part. Nucl.* **46**, 347–365 (2015).

Investigation of the Decay Scheme of ^{50}V

V. R. Klavdiienko,[1] F. A. Danevich,[1] M. Hult,[2] D. V. Kasperovych,[1] G. Lutter,[2] G. Marissens,[2] O. G. Polischuk,[1] and V. I. Tretyak[1]

[1] *Institute for Nuclear Research, 03028 Kyiv, Ukraine*
[2] *Joint Research Centre, European Commission, 2440 Geel, Belgium*

Abstract. Measurement of the ^{50}V electron-capture transition to the 2^+ 1553.8 keV level of ^{50}Ti and search for β^- decay of ^{50}V to the 2^+ 783.3 keV level of ^{50}Cr (both decays are four-fold forbidden with $\Delta I^{\Delta\pi} = 4^+$) were performed using a vanadium sample of natural isotopic abundance with a mass of 955 g. The experiment was conducted using an ultra-low-background HPGe-detector system located 225 m underground at the HADES laboratory (Belgium). Preliminarily, the measured partial half-life of the electron-capture (EC) transition was $T_{1/2}^{EC} = (2.64 \pm 0.20) \times 10^{17}$ yr. The β^- decay could not be detected, but a lower bound on the partial β^--decay half-life was set to $T_{1/2}^{\beta} \geq 8.1 \times 10^{18}$ yr at 90% C.L.

Keywords: electron capture; β decay; low-background experiment; radioactive contamination; ^{50}V; HPGe γ-ray spectrometry
PACS: 23.40.–s

INTRODUCTION

The isotope ^{50}V is present in the natural mixture of vanadium with a very low abundance of 0.250(10)% [1]. While the ^{50}V electron-capture transition to the 2^+ 1553.8 keV level of ^{50}Ti was observed in several experiments, a four-fold forbidden non-unique ($\Delta I^{\Delta\pi} = 4^+$, 4th-FNU) β^- decay of ^{50}V to the 2^+ 783.3 keV level of ^{50}Cr remains unobserved (the decay scheme of ^{50}V is shown in Fig. 1). Since in both channels the decays lead to excited levels of the daughter nuclei, the deexcitation γ quanta can be detected by means of γ-ray spectrometry of a vanadium sample. The decays are of special interest since the transition involves several different nuclear matrix elements with associated different phase-space factors (multiplied by the axial-vector coupling constant g_A) [2]. The value of g_A plays an important role in the search for rare processes. In particular, the neutrinoless double-beta decay half-life ($T_{1/2}^{0\nu\beta\beta}$) depends on g_A as follows [3]:

$$\left(T_{1/2}^{0\nu\beta\beta}\right)^{-1} = g_A^4 \, G^{0\nu\beta\beta} \left|M^{0\nu\beta\beta}\right|^2 m_{\beta\beta}^2, \qquad (1)$$

where $G^{0\nu\beta\beta}$ is the kinematic phase-space factor, $m_{\beta\beta}$ is the effective Majorana neutrino mass, and $M^{0\nu\beta\beta}$ is the nuclear matrix element. Calculations of the ^{50}V half-life using the nuclear shell model for different values of the constant g_A are presented in Table 1 [2].

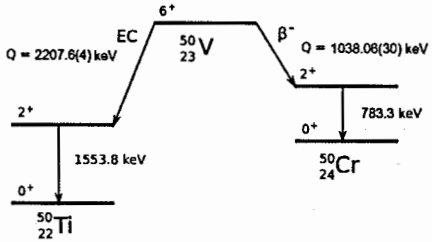

Figure 1. Decay scheme of ^{50}V.

Table 1. Computed partial half-lives for the 4th-FNU β and EC decays of ^{50}V [2].

	$T_{1/2}$ [10^{17} yr]	
Transition	$g_A = 1.00$	$g_A = 1.25$
$^{50}\text{V} \rightarrow {}^{50}\text{Ti}(2_1^+)$	5.13(7)	3.63(5)
$^{50}\text{V} \rightarrow {}^{50}\text{Cr}(2_1^+)$	234(2)	200(2)

EXPERIMENT

The experiment was conducted at the HADES underground laboratory in Belgium located at a depth of 225 m below the surface. We used a 955 g cylinder sample of pure vanadium. It was placed between two high-purity germanium (HPGe) detectors, here referred to as Ge10 and Ge11 with volumes 226 cm^3 and 330 cm^3, respectively. The two setups used in the measurements are shown in Fig. 2. Insertion of the additional plexiglass shielding reduced the background caused by radon 3–5 times. The background energy spectra were also measured in both setups. The majority of peaks in the energy spectra can be assigned to ^{40}K and nuclei of the ^{232}Th, ^{235}U, and ^{238}U decay chains. There are also clear peaks of ^{138}La and ^{176}Lu in the data taken with the vanadium sample as evidence of the sample contamination by La and Lu. The detection efficiency to γ quanta from ^{40}K, ^{138}La, and ^{176}Lu, as well as ^{232}Th, ^{235}U, and ^{238}U together with their daughter nuclei, in addition to γ quanta with the energies of 783.3 keV and 1553.8 keV, was calculated using the EGSnrc simulation package. The radioactive contamination of the vanadium sample was estimated through analysis of intense γ peaks in the experimental energy spectra; preliminary results of the analysis are presented in Table 2.

RESULTS AND DISCUSSION

The cumulative energy spectrum in the vicinity of the 1553.8 keV γ peak expected in the EC decay of ^{50}V accumulated from the vanadium sample over 144 d, together with the background spectrum measured without the sample over 59 d, is shown in Fig. 3. There is a clear peak with the energy of 1553.90(12) keV and the area of 654(28) counts in the

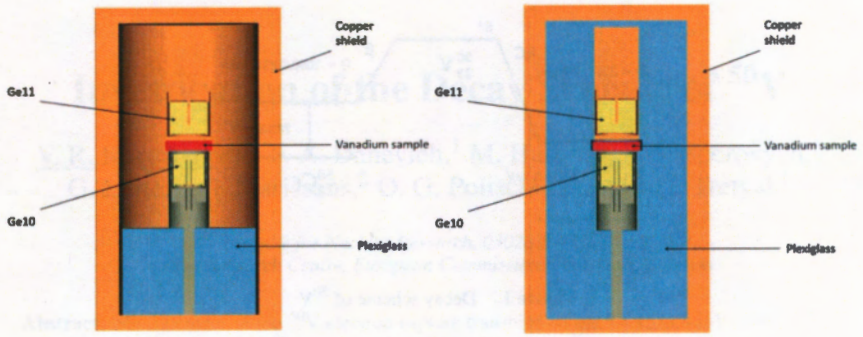

Figure 2. (a) The first and (b) second modifications of the experimental setup.

Table 2. Radioactive contamination of the vanadium sample.

Nuclide	Activity [mBq/kg]
^{238}U	45 ± 10
^{226}Ra	≤ 3.8
^{235}U	≤ 5.9
^{231}Pa	≤ 8.4
^{227}Ac	12.7 ± 0.6
^{228}Ra	17.8 ± 0.7
^{228}Th	14.5 ± 0.6
^{176}Lu	22.3 ± 0.2
^{138}La	20.1 ± 0.2
^{40}K	3.9 ± 0.3

spectrum that can be ascribed to the EC by ^{50}V with the half-life:

$$T_{1/2}^{\mathrm{EC}} = (2.64 \pm 0.11\ (\mathrm{stat.}) \pm 0.17\ (\mathrm{syst.})) \times 10^{17}\ \mathrm{yr}. \quad (2)$$

The systematic error consists of the Monte-Carlo-simulated detection-efficiency uncertainty, variation of the 1553.8 keV-peak area depending on the fit interval, and uncertainty in the number of ^{50}V nuclei in the sample due to inaccuracy in the representative isotopic abundance of the isotope. A careful analysis of the systematic error will be presented in the final publication of the result in preparation. The half-life value is consistent with the most accurate experiment described in Ref. [4] as well as with the latest theoretical calculations described in Ref. [2].

The peak expected from the β^- decay of ^{50}V to the 783.3 keV excited level of ^{50}Cr was not observed. Fit of the experimental spectrum by several peaks (which describe the γ peaks of the ^{138}La and U/Th daughters) plus the expected peak with the energy of 783.3 keV and by a straight line (which describes the continuous distribution) is shown

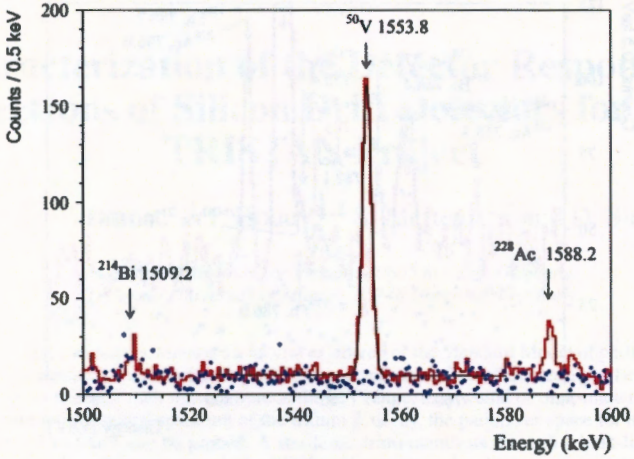

Figure 3. Part of the sum energy spectrum accumulated from the vanadium sample (with the exposure of $(2.25 \pm 0.08) \times 10^{22}$ yr of ^{50}V nuclei) in the vicinity of the 1553.8 keV γ peak from ^{50}V. Fit of the data by a sum of a Gaussian peak (effect) and a straight line (continuous distribution) is shown. The dotted histograms show the background data measured without the sample, normalized to the measurement time with the sample. Energy of the γ peaks is expressed in keV.

in Fig. 4. Fit of the data gives 3.3 ± 15.5 counts in the expected 783.3 keV peak, which means no evidence of the searched effect. Therefore, only an upper limit on the β^--decay half-life was set:

$$T^{\beta}_{1/2} > 8.1 \times 10^{18} \text{ yr at } 90\% \text{ C.L.} \quad (3)$$

CONCLUSIONS

The partial half-life of the electron-capture transition to the 2^+ 1553.8 keV level of ^{50}Ti was preliminarily measured: $T^{EC}_{1/2} = (2.64 \pm 0.20) \times 10^{17}$ yr. This value is in agreement with the result of a recent experiment [4] and theoretical predictions [2]. The β^- decay of ^{50}V to the 2^+ 783.3 keV level of ^{50}Cr could not be detected, but a lower bound on the partial β^--decay half-life was set to $T^{\beta}_{1/2} \geq 8.1 \times 10^{18}$ yr at 90% C.L. This limit is about two times weaker than the one set in Ref. [4]. Further improvement of the experiment sensitivity could be achieved by utilization of a deeply purified vanadium sample and an HPGe-detector system optimized to reach maximum detection efficiency/background ratio. One should keep in mind that in the case of a very pure V sample and suppression of the contributions from radioactive contamination, the background is expected to be mainly due to the unavoidable EC process in ^{50}V [4].

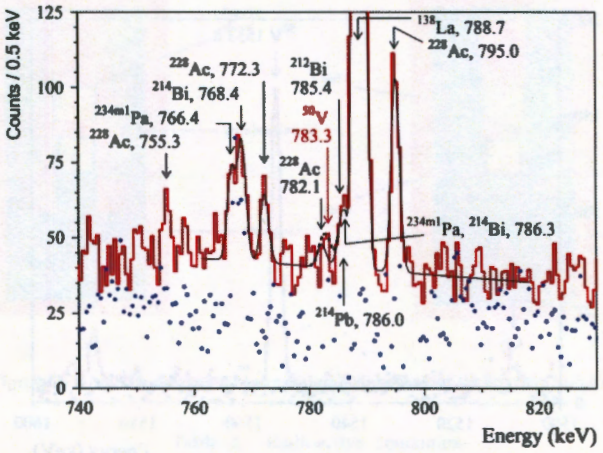

Figure 4. Part of the sum energy spectrum accumulated from the vanadium sample (with the exposure of $(2.25 \pm 0.08) \times 10^{22}$ yr of ^{50}V nuclei) in the vicinity of the expected β^--decay 783.3 keV γ peak from ^{50}V. Fit of the data by several γ peaks and by a straight line to describe the continuous distribution is shown by the solid curve, while the excluded peak expected from the β^- decay of ^{50}V is shown by the dashed curve. The dotted histograms show the background data measured without the sample, normalized to the measurement time with the sample. Energy of the γ peaks is expressed in keV.

ACKNOWLEDGMENTS

This project received support from the EC-JRC open access project EUFRAT under Horizon2020. The group from the Institute for Nuclear Research (Kyiv, Ukraine) was supported in part by the program of the National Academy of Sciences of Ukraine "Fundamental Research on High-Energy Physics and Nuclear Physics (International Cooperation)." D. V. K. and O. G. P. were supported in part by the project "Investigations of Rare Nuclear Processes" of the program of the National Academy of Sciences of Ukraine "Laboratory of Young Scientists" (Grant No. 0118U002328).

REFERENCES

1. J. Meija et al., "Isotopic Compositions of the Elements 2013 (IUPAC Technical Report)," *Pure Appl. Chem.* **88**, 293–306 (2016).
2. M. Haaranen, P. C. Srivastava, J. Suhonen, and K. Zuber, "β-Decay Half-Life of ^{50}V Calculated by the Shell Model," *Phys. Rev. C* **90**, 044314 (2014).
3. J. Suhonen, "Impact of the Quenching of g_A on the Sensitivity of $0\nu\beta\beta$ Experiments," *Phys. Rev. C* **96**, 055501 (2017).
4. M. Laubenstein, B. Lehnert, S. S. Nagorny, S. Nisi, and K. Zuber, "New Investigation of Half-Lives for the Decay Modes of ^{50}V," *Phys. Rev. C* **99**, 045501 (2019).

Characterization of the Detector Response to Electrons of Silicon Drift Detectors for the TRISTAN Project

M. Lebert,[1,2] T. Brunst,[1,2] T. Houdy,[1,2] S. Mertens,[1,2] and D. Siegmann[1,2]

[1] *Max Planck Institute for Physics, 80805 Munich, Germany*
[2] *Technical University of Munich, 85748 Garching, Germany*

Abstract. Right-handed neutrinos are a natural extension of the Standard Model of particle physics. Such particles would only interact through the mixing with the left-handed neutrinos, hence they are called sterile neutrinos. If their masses were in the keV range, they would be dark-matter candidates. By investigating the electron spectrum of the tritium β decay, the parameter space for masses up to the endpoint of 18.6keV can be probed. A sterile neutrino manifests through a kink-like structure in the spectrum. To achieve this goal, the TRISTAN project is developing a new detector system for the KATRIN experiment that can search for these new particles using the technology of silicon drift detectors. One major effect on the performance of the detectors is the so-called dead layer. In this work, a new characterization method for the prototype detectors is presented using the ^{83m}Kr-decay conversion electrons. By tilting the detector, its effective dead layer increases, leading to different peak positions. The difference of peak positions between two tilting angles is independent of source effects, and thus suitable for characterization. A dead layer is then extracted by comparing the measurements with Monte Carlo simulations. A dead layer of the order of 50nm was found.

Keywords: sterile neutrinos; detector characterization
PACS: 07.77.−n; 29.40.Wk

INTRODUCTION

In the Standard Model of particle physics, neutrinos are massless neutral leptons and the only particles that appear solely with left-handed chirality. The detection of neutrino oscillation by the SNO and Super-Kamiokande Collaborations [1, 2] showed that the neutrinos are in fact not massless, and therefore the Standard Model is incomplete. One possible natural extension would be the introduction of right-handed neutrinos, which would only interact through mixing with the known neutrinos and hence are called sterile neutrinos. Each sterile neutrino would introduce a new mass eigenstate mostly made of the sterile, and thus the mixing with the known neutrinos would be small. Depending on the mass scale of the additional mass eigenstate, the sterile neutrino could solve various open questions in particle physics. If the mass is large ($\mathcal{O}$(MeV)), the small masses of the active neutrinos could be explained by the seesaw mechanism. For smaller masses ($\mathcal{O}$(keV)), these new particles would be a viable dark-matter candidate [3].

To search for keV-scale sterile neutrinos, the electron spectrum of tritium β decay can be investigated. The neutrino reduces the maximum energy of the electron by mass of the mass eigenstate that was created. The β spectrum is a superposition of all mass eigenstates that can be created in the decay. Therefore, a heavy sterile mass eigenstate

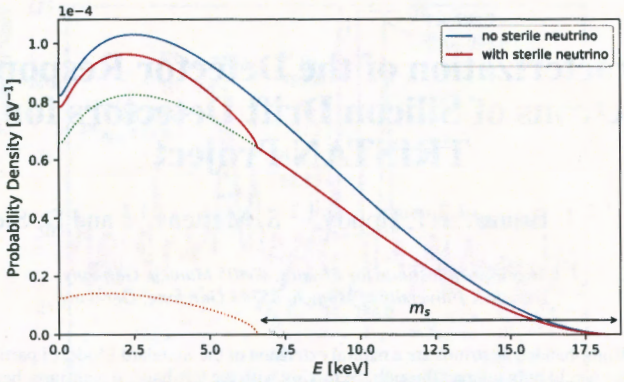

Figure 1. The effect of a sterile neutrino on the β spectrum, assuming a sterile-neutrino mass of 12 keV and a mixing angle of $\sin^2\Theta = 0.2$. A kink appears at the energy corresponding to the β-spectrum endpoint reduced by the mass of the sterile neutrino. Figure from Ref. [4].

would manifest itself through a kink-like structure deep in the spectrum (Fig. 1).

The amplitude of the kink and hence the mixing is extremely small ($\sin^2\Theta < 10^{-3}$). In order to find such a small structure, up to 10^{18} events are needed, and thus a source with high luminosity is required [4]. This makes the KArlsruhe TRItium Neutrino (KATRIN) experiment suitable for such a task. The Windowless Gaseous Tritium Source of KATRIN can provide up to 10^{11} decays per second [5]. Currently, the detector used for the neutrino-mass measurements cannot handle the high rates needed. Therefore, the TRitium Investigation on STerile to Active Neutrino mixing (TRISTAN) project will develop a new detector system using the technology of silicon drift detectors (SDDs). Count rates of up to $10^8\,\mathrm{s}^{-1}$ in the detector are a compromise between the data-collection time and the necessary development effort of the detector [4]. To handle these rates, the system will distribute them across $\approx 3,500$ pixels. In order not to wash out the kink, the energy resolution must not exceed 300 eV at 30 keV. Another important requirement is that the pixels need thin entrance windows. Electrons are charged particles, and therefore have a high interaction rate in matter through which they lose energy. In the entrance window of the detector, the energy collection of the detector is reduced, and therefore the energy deposited in this region is at least partially lost. This effect would shift the peak of monoenergetic electrons to lower energies and create a low-energy tail. This means that it also affects the overall β spectrum, and hence it must be minimized and understood very well.

The aim of this work is to investigate a characterization method of the entrance window of the TRISTAN prototype detectors. Different ion implantation techniques were implemented for the different prototype detectors. All prototype detectors have seven hexagonal pixels, see Fig. 2. A dead-layer model is assumed to describe the entrance window of the detectors. In this model, certain area at the entrance of the detector is completely insensitive, followed by an area of complete energy collection

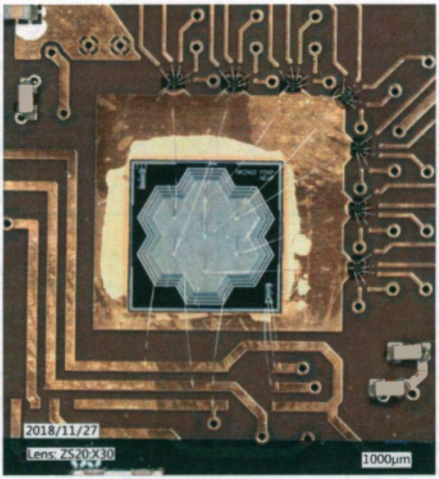

Figure 2. The back of a seven-pixel prototype detector of the TRISTAN project.

for the rest of the detector.

^{83}Rb/^{83m}Kr SOURCES

The monoenergetic electron source used in this characterization is ^{83m}Kr. This isomeric krypton is created via electron capture by ^{83}Rb with a half-life of 86.6 d. The metastable krypton state has an energy of about 41.6 keV and a half-life of 1.86 h [7], and decays into the ground state in two steps: the first decay releases 32.2 keV and the second one 9.4 keV [7]. Conversion electrons can be created in both transitions, but only from shells binding energies of which are lower than the provided transition energy. This also leads to emission of X-rays. If no electron is emitted, a γ photon is.

For our investigation, only the X-ray peaks of K_α and K_β and the conversion electrons of the K, L, M, and N shells from the 32.2 keV transition were of interest. The corresponding peaks are shown in Fig. 3. The conversion electrons from the 9.4 keV transition belong to the low-energy continuum, and therefore are unsuited for characterization. The energy differences within one shell are too small to be distinguished by the TRISTAN SDDs, and thus the L lines form one peak while the M and N lines form another one.

The calibration of the detector was done using the photon lines of ^{241}Am, since these are almost unaltered by the dead layer. One advantage of ^{83m}Kr is the occurrence of both the photon and electron lines, which makes an in-situ test of the calibration possible. In the setup of the calibration, no gaseous source could be used. For this reason, rubidium was vacuum-evaporated onto a backing of highly oriented pyrolytic graphite (HOPG) or rigid graphite at the Nuclear Physics Institute of the Czech Academy of Sciences, Řež,

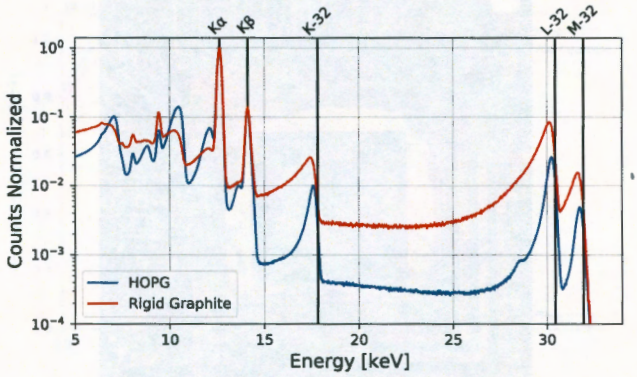

Figure 3. Comparison of the spectra obtained from the decay of ^{83m}Kr in the HOPG and rigid graphite sources, demonstrating that rigid graphite alters the electrons significantly.

Czech Republic, where roughly mono-layer ^{83}Rb was placed onto the graphite [8]. The energy losses of electrons traveling through this layer are negligible, which makes this kind of source acceptable for characterization.

MEASUREMENTS

The sources were placed approximately 1 cm below the detector in a vacuum chamber. The resulting spectra obtained from the HOPG and rigid graphite sources are shown in Fig. 3. The X-ray peaks are Gaussian with only a small asymmetry towards low energies. On the other hand, the electron peaks have a significant low-energy tail and are shifted to lower energies when compared to the theoretical values. Figure 3 also shows that the backing of the source has an influence on the conversion electrons. The electron peaks of the rigid graphite source have much more pronounced low-energy tails and are at slightly lower energies than the peaks from the HOPG source. The electron background in the region of 18–30 keV is again higher for the rigid graphite. HOPG has lower peak amplitudes, which comes from the different retention factors of the two sources. The retention factor states the probability that a bound ^{83}Rb will decay into the ^{83m}Kr noble gas which then stays in the original position of the rubidium. The noble gas is much more weakly bound and therefore can leave the source before decaying.

This comparison shows that the source can potentially disturb or alter the characterization. For this reason, a method is needed that is independent of any source effects. The electron-peak position $\overline{E}_i(\theta)$ depends on the tilting angle θ between the detector and the source. It can be described by:

$$\overline{E}_i(\theta) = \overline{E}_i^{\text{th}} - \Delta\text{DL}^i(\theta) - \delta_\Phi - \delta_{\text{source}}. \tag{1}$$

Table 1. Dead-layer shifts $\Delta\mathrm{DL}^i(\theta)$ for one prototype detector and the corresponding dead-layer thickness resulting from the comparison between measurement and simulation.

Peak	Energy [keV]	Shift	Shift [eV]	Dead layer [nm]
K-32	17.8	$\Delta\mathrm{DL}^{\mathrm{K}}$	45 ± 5	50 ± 6
L-32	30.4	$\Delta\mathrm{DL}^{\mathrm{L}}$	32 ± 5	55 ± 6
M-32	31.9	$\Delta\mathrm{DL}^{\mathrm{M}}$	29 ± 6	55 ± 9

Here, $\overline{E}_i^{\mathrm{th}}$ denotes the theoretical peak position, $\Delta\mathrm{DL}^i(\theta)$ is the energy of the electrons lost within the dead layer of the detector for the i^{th} peak, δ_Φ is the potential applied to the entrance-window side of the detector to deplete it, and δ_{source} represents the source effects. $\Delta\mathrm{DL}^i(\theta)$ increases with the tilting angle θ, because the effective dead layer, and thus also the energy loss, increases as well. Therefore, an energy difference Δ is observed if two measurements at different angles are compared. This shift is independent of any external effects and only depends on the dead layer:

$$\Delta = \overline{E}_i(\theta) - \overline{E}_i(\theta') = \Delta\mathrm{DL}^i(\theta') - \Delta\mathrm{DL}^i(\theta). \tag{2}$$

The measured shifts for the conversion-electron peaks from the 32.2 keV transition and the HOPG source are given in Table 1. A decreasing energy shift for higher electron energies appears due to the longer mean free path. Based on Monte Carlo simulations using the KATRIN simulation package KESS [9], we can relate the measured energy shift to a step-like dead layer with thickness of about 50 nm.

CONCLUSION

We have shown that the determined dead layers for each detector are constant for the different energies, as expected. Previous measurements with an electron microscope at 14 keV had energy shifts of (45 ± 1) eV and a dead layer of (46 ± 6) nm [10]. These values are compatible with the krypton measurements, which demonstrates that the tilt method can be used together with an electron microscope or conversion electrons from a $^{83\mathrm{m}}$Kr source as a cross-check. Therefore, this method is suitable for characterization of the TRISTAN detectors. Investigation of a more detailed depth-dependent charge-collection efficiency model and comparison with Geant4 [11] simulations are currently in progress.

REFERENCES

1. Q. R. Ahmad et al. (SNO Collaboration), "Direct Evidence for Neutrino Flavor Transformation from Neutral-Current Interactions in the Sudbury Neutrino Observatory," *Phys. Rev. Lett.* **89**, 011301 (2002).
2. Y. Fukuda et al. (Super-Kamiokande Collaboration), "Evidence for Oscillation of Atmospheric Neutrinos," *Phys. Rev. Lett.* **81**, 1562–1567 (1998).
3. R. Adhikari et al., "A White Paper on keV Sterile Neutrino Dark Matter," *J. Cosmol. Astropart. Phys.* **2017/01**, 025 (2017).

4. S. Mertens et al. (KATRIN Collaboration), "A Novel Detector System for KATRIN to Search for keV-Scale Sterile Neutrinos," *J. Phys. G: Nucl. Part. Phys.* **46**, 065203 (2019).
5. J. Angrik et al. (KATRIN Collaboration), "KATRIN Design Report 2004" (2005).
6. D. Vénos et al., "Properties of ^{83m}Kr Conversion Electrons and Their Use in the KATRIN Experiment," *J. Instrum.* **13**, T02012 (2018).
7. E. A. McCutchan, "Nuclear Data Sheets for $A = 83$," *Nucl. Data Sheets* **125**, 201–394 (2015).
8. D. Vénos et al., "The Development of a Super-Stable Standard for Monitoring the Energy Scale of Electron Spectrometers in the Energy Range up to 20keV" (erratum), *Meas. Tech.* **53**, 573–581 (2010).
9. P. Renschler, "KESS – A New Monte Carlo Simulation Code for Low-Energy Electron Interactions in Silicon Detectors" (doctoral dissertation), Karlsruhe Institute of Technology (2011).
10. D. Siegmann, "Investigation of the Detector Response to Electrons of the TRISTAN Prototype Detectors" (master's thesis), Technical University of Munich (2019).
11. J. Allison et al., "Recent Developments in Geant4," *Nucl. Instrum. Methods Phys. Res. A* **835**, 186–225 (2016).

Impact of Cross-Sectional Uncertainties on DUNE CPV Sensitivity due to Nuclear Effects

S. Nagu, Ja. Singh, Jy. Singh, and R. B. Singh

University of Lucknow, 226007 Lucknow, India

Abstract. The prerequisite for precise knowledge of neutrino-oscillation physics depends on many factors among which precise reconstruction of neutrino energy is of extreme importance. As we know that the neutrino-oscillation probability itself depends on the energy of the neutrinos, any incorrect measurement of neutrino energy will be propagated to the measurements of neutrino-oscillation parameters since it causes uncertainties in the cross-section measurement and event identification. Many important long-baseline neutrino-oscillation experiments use accelerator-generated neutrino beams. As these neutrino beams are not monoenergetic, for the reconstruction of neutrino energy complete information of final-state particles is required. The energy reconstruction of neutrinos from final-state particles needs careful examination since the identification of final-state particles in presence of nuclear effects is a challenging task. In this work we tried to impose constraints on systematic errors arising due to the presence of cross-sectional uncertainties.

Keywords: nuclear effects; cross-sectional uncertainties; CP-violation sensitivity
PACS: 13.15.+g; 21.60.−n

INTRODUCTION

Neutrino oscillation implies the change of neutrino flavor as they travel, i.e., a neutrino which is generated with a certain flavor after traveling a certain distance might end up having a different flavor. Much progress on the precise determination of neutrino-oscillation parameters has been made by achieving nearly precise determination of the mixing angles θ_{12}, θ_{23} and nonzero value of θ_{13} [1, 2, 3] and mass-squared differences Δm^2_{21}, $|\Delta m^2_{31}|$. The remaining unknown parameters on the canvas of neutrino-oscillation physics are: 1. the sign of Δm^2_{31} or the neutrino-mass ordering, 2. determination of the octant of θ_{23}, i.e., whether the value of θ_{23} lies in the lower octant (LO) $0 < \theta_{23} < \pi/4$ or higher octant (HO) $\pi/4 < \theta_{23} < \pi/2$, and 3. determination of the value of Dirac phase δ_{CP} which can lie in the range $-\pi < \delta_{CP} < \pi$. As we know, if the value of this parameter differs from 0 or π, it would indicate CP violation in the leptonic sector. This discovery can shed light on the origin of leptogenesis[4] and can be a tool to answer some of the intriguing questions like baryon asymmetry of the Universe[5]. Precise CP-phase value is also required for the exact absolute neutrino-mass measurement in double-beta-decay experiments and also for explaining the sterile-neutrino phenomenon [6]. The global analysis [7] shows two sets of best-fit values of neutrino-oscillation parameters in 1σ and 3σ ranges that correspond to the analysis done with and without Super-Kamiokande atmospheric-neutrino data.

Here, in an attempt to capture nuclear effects, we have selected two different simulation tools: GENIE [8] and GiBUU [9]. Both neutrino-event generators incorporate

nuclear effects in their simulation codes but differ in the selection of nuclear models and computation of various neutrino-nucleus interaction processes. The nucleus is a collection of nucleons and the study of the effect of all the nucleons in neutrino-nucleus interactions is not trivial. Different neutrino-event generators which include nuclear effects in their analysis program use different approximations to define nuclear effects. Since the result of an experiment must be model-independent, this motivated us to perform our analysis.

EVENT GENERATORS: GENIE AND GiBUU

The interaction cross section (ν-Ar) used in this work is computed with two neutrino event generators: GENIE (Generates Events for Neutrino Interaction Experiments) 2.12.06 [8] and GiBUU (Giessen Boltzmann–Uehling–Uhlenbeck) v-2019 [9]. We have considered the quasi-elastic (QE), resonance (RES) from Δ-resonant decay and contribution from higher resonances, two-particle–two-hole (2p2h/MEC) and deep-inelastic scattering (DIS) interaction processes. The estimated total cross section from the two generators is further converted into the format of the GLoBES package. Neutrino cross section as a function of neutrino energy is shown in Fig. 1. From both generators, we observe a difference in the values of cross sections for both ν_e and ν_μ. We observe that above 3 GeV, there is a nonnegligible difference in the cross sections for ν_e and ν_μ obtained from GiBUU while such a trend is not observed in GENIE. The difference in the distribution of events generated by the two generators arises due to a difference in the cross sections of the generators in use. The distribution of ν_μ and ν_e events as a function of reconstructed neutrino energy is illustrated in Fig. 2. The presented event rate is generated using GLoBES, by considering normal hierarchy as true hierarchy and $\delta_{CP} = -90°$.

SIMULATION AND EXPERIMENTAL DETAILS

For the simulation of the DUNE [10, 11, 12, 13] experiment, we have considered a far detector with a fiducial volume of 40 kton liquid argon ($A = 40$) placed at a distance of $L = 1300$ km from the wideband neutrino-beam source with a running time of 3.5 years, each in neutrino and antineutrino mode. The neutrino fluxes used here correspond to the 80 GeV beam configuration [14], with an assumed beam power of 1.07 MW for two beamline designs: 1. reference design and 2. optimized design. We perform the sensitivity analysis for DUNE with both the reference and optimized beams to explore the physics potential of DUNE. The main differences between the two beam designs include the geometry of the decay pipe and design of the horn. Further details regarding the potential beamline designs can be found in [11]. For performing the sensitivity analysis we have used the GLoBES (General Long Baseline Experiment Simulator) package [15, 16] which requires cross section, neutrino- and antineutrino-beam fluxes and detector parameterization values as input. The cross-section input format is: $\hat{\sigma}(E) = \sigma(E)/E\,[10^{-38}\,\mathrm{cm}^2/\mathrm{GeV}]$; one can find further details in [17]. The computation of binned event rates is performed by an energy-smearing algorithm which we have chosen

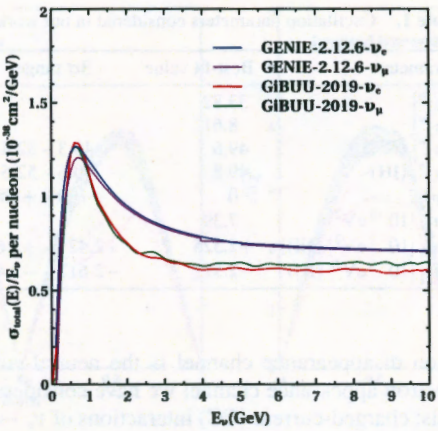

Figure 1. Total neutrino-argon interaction cross section per nucleon as a function of neutrino energy by GENIE and GiBUU in the energy regime 1–10GeV for different charged-current processes considered in our work.

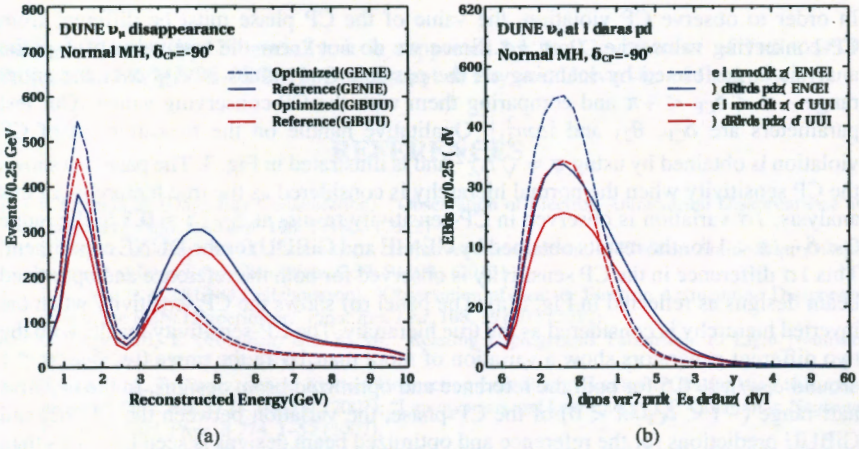

Figure 2. (a) ν_μ-disappearance and (b) ν_e-appearance event distributions as functions of reconstructed neutrino energy for both reference and optimized beamline designs in the energy regime 1–10GeV.

to be a Gaussian function of energy resolution [17]. The energy resolution for ν_e is $15\%/\sqrt{E\,[\mathrm{GeV}]}$ and for ν_μ is $20\%/\sqrt{E\,[\mathrm{GeV}]}$ [18]. The true values of the oscillation parameters [7] considered in this analysis are presented in Table 1. The numerical procedure carried out to study the sensitivities is done by calculating $\Delta\chi^2$ using the default definition present in GLoBES. The relevant background that is considered in

Table 1. Oscillation parameters considered in our work.

Parameter	Best-fit value	3σ range
θ_{12} [°]	33.82	
θ_{13} [°]	8.61	
θ_{23} [°] (NH)	49.6	40.3 – 52.4
θ_{23} [°] (IH)	49.8	40.6 – 52.5
δ_{CP} [°]	0	−180 – +180
Δm^2_{21} [10^{-5} eV^2]	7.39	
Δm^2_{31} [10^{-3} eV^2] (NH)	+2.525	+2.427 – +2.625
Δm^2_{31} [10^{-3} eV^2] (IH)	−2.512	−2.611 – −2.412

this work for the muon disappearance channel is the neutral-current interaction. For the background of electron appearance channel we have considered contributions from three different channels: charged-current (CC) interactions of $\nu_e \rightarrow \nu_e$, misidentified CC $\nu_\mu \rightarrow \nu_\mu$, and neutral-current (NC) backgrounds.

CP-VIOLATION SENSITIVITY FOR DUNE

In order to observe CP violation, the value of the CP phase must be different from CP-conserving values, i.e., 0 or $\pm\pi$. Since we do not know the true value of δ_{CP}, the analysis is performed by scanning all the possible true values of δ_{CP} over the entire range $-\pi < \delta_{CP} < +\pi$ and comparing them with the CP-conserving values. Our test parameters are δ_{CP}, θ_{23} and $|\Delta m^2_{31}|$. Qualitative handle on the measurement of CP violation is obtained by using $\sigma = \sqrt{\Delta\chi^2}$ and is illustrated in Fig. 3. The panel (a) shows the CP sensitivity when the normal hierarchy is considered as the true hierarchy. In this analysis, 1σ variation is observed in CP-sensitivity results at $\delta_{CP}/\pi \approx 0.5$ in the range $0 < \delta_{CP}/\pi < 1$ for the results obtained by GENIE and GiBUU for the DUNE experiment. This 1σ difference in the CP sensitivity is observed for both the reference and optimized beam designs as reflected in Fig. 3(a). The panel (b) shows the CP sensitivity when the inverted hierarchy is considered as the true hierarchy. The CP-sensitivity results with the two different generators show a variation of more than 1σ in the range $0 < \delta_{CP}/\pi < 1$ around $\delta_{CP}/\pi \approx 0.5$ for both the reference and optimized beam designs. In the negative half-range ($-1 < \delta_{CP}/\pi < 0$) of the CP phase, the variation between the GENIE and GiBUU predictions for the reference and optimized beam designs is seen to be less than 1σ for both the normal- and inverted-hierarchy cases.

ACKNOWLEDGMENTS

We would like to thank Prof. Raj Gandhi for various suggestions regarding this work. S. N. and J. D. would like to thank Prof. U. Mosel for many helpful discussions regarding GiBUU-related issues and to Newton Nath, Suprabh Prakash, and Debajyoti Dutta for their help with GLoBES. This work is supported by the Department of Physics,

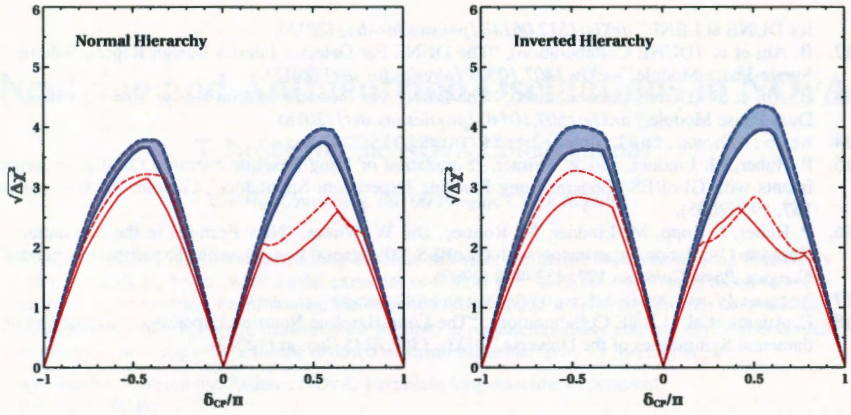

Figure 3. CP-sensitivity measurement as a function of the true value of δ_{CP} for (a) NH and (b) IH by GENIE (blue lines) and GiBUU (red lines). The reference and optimized designs are represented by the solid and dashed lines, respectively.

Lucknow University. Financially, it is supported by the Government of India, DST Project No. SR/MF/PS-02/2013, Department of Physics, University of Lucknow.

REFERENCES

1. F. P. An et al. (Daya Bay Collaboration), "Observation of Electron-Antineutrino Disappearance at Daya Bay," *Phys. Rev. Lett.* **108**, 171803 (2012)
2. F. P. An et al. (Daya Bay Collaboration), "Improved Measurement of Electron Antineutrino Disappearance at Daya Bay," *Chin. Phys. C* **37**, 011001 (2013)
3. J. K. Ahn et al. (RENO Collaboration), "Observation of Reactor Electron Antineutrino Disappearance in the RENO Experiment," *Phys. Rev. Lett.* **108**, 191802 (2012)
4. G. Engelhard, Y. Grossman, and Y. Nir, "Relating Leptogenesis Parameters to Light Neutrino Masses," *JHEP* **0707**, 029 (2007).
5. S. Pascoli, S. T. Petcov, and A. Riotto, "Connecting Low Energy Leptonic CP-Violation to Leptogenesis," *Phys. Rev. D* **75**, 083511 (2007); "Leptogenesis and Low Energy CP Violation in Neutrino Physics," *Nucl. Phys. B* **774**, 1–52 (2007).
6. J. Singh, "Constraining the Effective Mass of Majorana Neutrino with Sterile Neutrino Mass for Inverted Ordering Spectrum," *Adv. High Energy Phys.* **2019**, 4863620 (2019).
7. I. Esteban et al., "Global Analysis of Three–Flavour Neutrino Oscillations: Synergies and Tensions in the Determination of θ_{23}, δ_{CP}, and the Mass Ordering," *JHEP* **01**, 106 (2019).
8. C. Andreopoulos et al., "The GENIE Neutrino Monte Carlo Generator," *Nucl. Instrum. Meth. A* **614**, 87–104 (2010).
9. O. Buss et al., "Transport-Theoretical Description of Nuclear Reactions," *Phys. Rept.* **512**, 1–124 (2012).
10. B. Abi et al. (DUNE Collaboration), "The DUNE Far Detector Interim Design Report Volume 1: Physics, Technology and Strategies," *arXiv:1807.10334 [physics.ins-det]* (2018).
11. R. Acciarri et al. (DUNE Collaboration), "Long-Baseline Neutrino Facility (LBNF) and Deep Underground Neutrino Experiment (DUNE) Conceptual Design Report Volume 2: The Physics Program

for DUNE at LBNF," *arXiv:1512.06148 [physics.ins-det]* (2015).
12. B. Abi et al. (DUNE Collaboration), "The DUNE Far Detector Interim Design Report, Volume 2: Single-Phase Module," *arXiv:1807.10327 [physics.ins-det]* (2018).
13. B. Abi et al. (DUNE Collaboration), "The DUNE Far Detector Interim Design Report, Volume 3: Dual-Phase Module," *arXiv:1807.10340 [physics.ins-det]* (2018).
14. `http://home.fnal.gov/~ljf26/DUNE2015CDRFluxes`
15. P. Huber, M. Lindner, and W. Winter, "Simulation of Long-Baseline Neutrino Oscillation Experiments with GLoBES (General Long Baseline Experiment Simulator)," *Comput. Phys. Commun.* **167**, 195 (2005).
16. P. Huber, J. Kopp, M. Lindner, M. Rolinec, and W. Winter, "New Features in the Simulation of Neutrino Oscillation Experiments with GLoBES 3.0: General Long Baseline Experiment Simulator," *Comput. Phys. Commun* **177**, 432–438 (2007).
17. `https://www.mpi-hd.mpg.de/personalhomes/globes`
18. C. Adams et al. (LBNE Collaboration), "The Long-Baseline Neutrino Experiment: Exploring Fundamental Symmetries of the Universe," *arXiv:1307.7335 [hep-ex]* (2013).

Neutrino and Antineutrino Oscillations in NOvA

T. Nosek (for the NOvA Collaboration)

Charles University, 180 00 Prague, Czech Republic

Abstract. NOvA is a two-detector long-baseline neutrino-oscillation experiment using Fermilab's 700kW NuMI ν_μ beam. With a total exposure of $8.85 \times 10^{20} + 12.33 \times 10^{20}$ protons on target in neutrino + antineutrino beam modes, the experiment has made a 4.4σ-significant observation of $\overline{\nu}_e$ appearance in a $\overline{\nu}_\mu$ beam, measured the oscillation parameters Δm^2_{32} and $\sin^2\theta_{23}$, and excluded most values near $\delta_{CP} = \pi/2$ for the inverted neutrino-mass hierarchy by more than 3σ.

Keywords: neutrino oscillations; NOvA; Fermilab; long-baseline experiment
PACS: 14.60.Pq

INTRODUCTION

NOvA (NuMI Off-Axis ν_e Appearance) is a long-baseline neutrino-oscillation experiment designed to observe the disappearance of muon (anti)neutrinos ν_μ ($\overline{\nu}_\mu$) and the appearance of electron (anti)neutrinos ν_e ($\overline{\nu}_e$) in a ν_μ beam provided by the NuMI (Neutrinos at the Main Injector) facility at the Fermi National Accelerator Laboratory, USA. From these measurements, NOvA is able to address several concerns of neutrino oscillations in the standard three-active-neutrino-flavor paradigm: the mass splitting Δm^2_{32}, the mixing angle θ_{23}, the CP-violating phase δ_{CP}, and the question of neutrino-mass ordering (hierarchy). Recently, NOvA has published its first results using both neutrino- and antineutrino-dominated beams with a total exposure of 8.85×10^{20} protons on target (POT) for neutrinos and 12.33×10^{20} POT for antineutrinos [1].

THE NOvA EXPERIMENT

The neutrino beam is created by colliding 120GeV protons with a carbon target. The produced π and K mesons are focused by a pair of magnetic horns and subsequently decay into a neutrino and the associated lepton. By switching the polarity of the horns, oppositely charged mesons can be focused, and thus NOvA can effectively switch between both ν_μ- and $\overline{\nu}_\mu$-dominated beams. The beam is designed to run at a power of 700kW, which is roughly equivalent to 6×10^{20} POT per year. More details can be found in Ref. [2].

NOvA has two functionally identical detectors. The near detector (ND) has a mass of 300t and is located about 1km from the NuMI target. The far detector (FD) has a mass of 14kt and is located at a distance of 810km from ND. Both detectors sit at 14.6mrad off the axis of the neutrino beam in order to considerably narrow its energy spectrum around the 2GeV peak. This helps to suppress the high-energy-tail backgrounds and to reduce the uncertainty of the energy of incoming neutrinos.

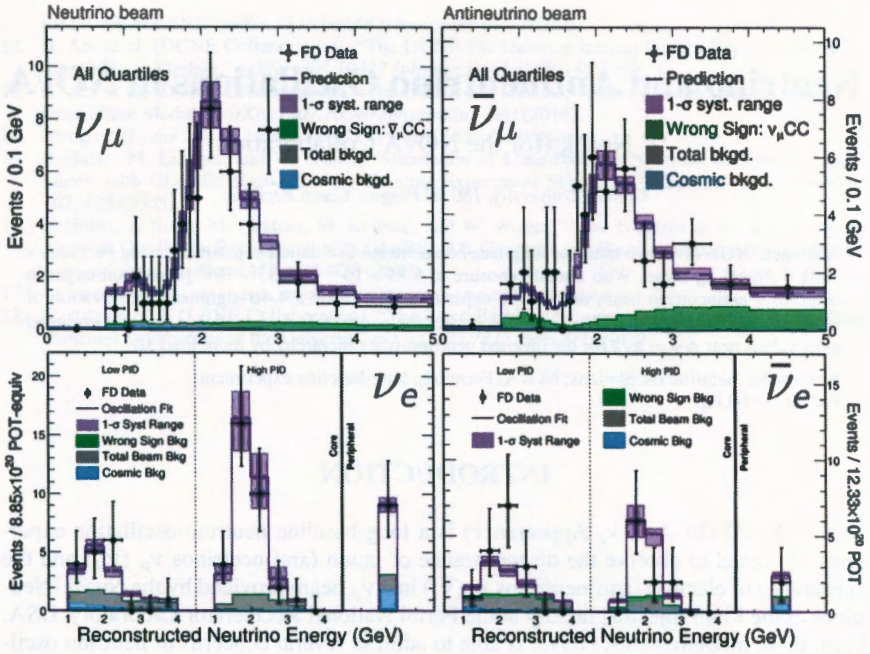

Figure 1. FD data (black points) vs. reconstructed energy of the selected (anti)neutrino candidates, compared with the best-fit prediction (purple line) including the 1σ systematic-uncertainty range (purple bands) and the expected wrong-sign-event background (green), other-beam background (gray), and cosmic background (blue). Top: $\nu_\mu \to \nu_\mu$ (left) and $\overline{\nu}_\mu \to \overline{\nu}_\mu$ (right) disappearance channels. Bottom: $\nu_\mu \to \nu_e$ (left) and $\overline{\nu}_\mu \to \overline{\nu}_e$ (right) appearance channels with additionally binned low and high PID bins and peripheral sample for energies up to 4.5 GeV.

The detectors are tracking calorimeters with excellent segmentation and $\sim 65\%$ of active mass. They consist of extruded PVC cells filled with liquid mineral-oil scintillator. A wavelength-shifting fiber loop connected to an avalanche photodiode collects light from the cells. The cells compose planes which alternate their vertical and horizontal directions to allow for a two-dimensional readout and reconstruction.

In order to identify and classify neutrino interactions, NOvA uses a convolutional visual network (CVN), which is a neural-network-based image-recognition technique using the maps of collected light in the detector cells (topological and structural image of the interactions) as an input. See Ref. [3] for more details.

The two similar detector designs allow for data-driven methods of signal and background predictions. Through an "extrapolation," ND data is used to correct the FD Monte Carlo simulations. This helps to substantially reduce the cross-section and flux uncertainties.

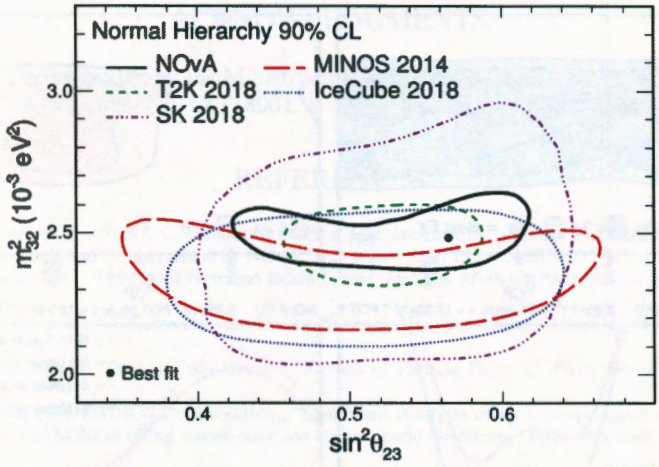

Figure 2. Comparison of the 90% C.L. allowed regions for Δm^2_{32} vs. $\sin^2\theta_{23}$ as obtained by the recent experiments: NOvA (black solid line) [1], MINOS (red long-dashed line) [5], T2K (green short-dashed line) [6], IceCube (blue dotted line) [7], and Super-Kamiokande (magenta dash-dotted line) [8].

OBSERVED $\nu_\mu/\overline{\nu}_\mu$ DISAPPEARANCE AND $\nu_e/\overline{\nu}_e$ APPEARANCE

There are two significant oscillation channels of ν_μ disappearance and ν_e appearance combined with two (ν and $\overline{\nu}$) beam modes at NOvA, which together result in four main analysis channels. In order to predict the FD neutrino signal spectra for both ν_μ and ν_e, the ND ν_μ sample is used, whereas the FD ν_e-beam background is predicted using the ND ν_e (i.e., ν_e-like) sample. The cosmic-background rate is estimated from data collected out-of-time with the NuMI beam.

In order to maximize the statistical power and to get the best effective use of the selected events, the samples are divided into specific populations later used in the analysis. The ν_μ ND reconstructed energy spectrum is split into four "quartiles" with different energy resolution ($\sim$ 6–11%). The ν_μ energy is estimated from the range of the produced muon and the remaining hadronic activity. The lower the fraction of hadronic energy, the better the overall energy resolution. The ν_e sample has two (low and high) particle-identification (PID) bins with different purity and background composition and a "peripheral" bin of not fully contained events with very strong PID constraints.

NOvA observed 113 (102) ν_μ ($\overline{\nu}_\mu$) CC candidates with an estimated background of $4.2^{+0.5}_{-0.6}$ (2.2 ± 0.4). There were 58 (27) ν_e ($\overline{\nu}_e$) CC candidates in the FD data with a total expected background of $15.0^{+0.8}_{-0.9}$ ($10.3^{+0.6}_{-0.5}$). This provides a 4.4σ evidence of $\overline{\nu}_e$ appearance in a $\overline{\nu}_\mu$ beam. All FD spectra along with best-fit predictions are shown in Fig. 1.

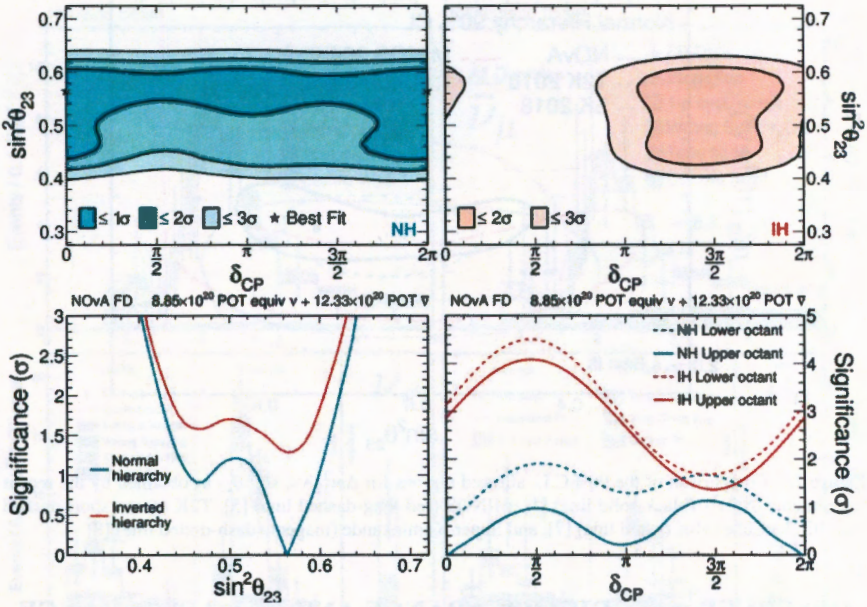

Figure 3. Top: 1σ, 2σ, and 3σ C.L. contours for $\sin^2\theta_{23}$ vs. δ_{CP} in the case of normal (left, blue) or inverted (right, red) neutrino-mass ordering including the best-fit points (black star markers). Bottom: exclusion significance for all values of $\sin^2\theta_{23}$ (left) and δ_{CP} (right) assuming the normal (blue) or inverted (red) neutrino-mass ordering and the upper (solid) or lower (dashed) θ_{23} octant.

CONSTRAINTS ON OSCILLATION PARAMETERS

The oscillation parameters Δm^2_{32}, θ_{23}, and δ_{CP} were obtained from a simultaneous fit of all spectra in Fig. 1. The mixing angle θ_{13} was taken from reactor-neutrino experiments while the solar parameters Δm^2_{21} and θ_{12} were fixed at their global-fit values, all presented in Ref. [4]. The analysis was based on the frequentist approach and used profiled systematics and penalty terms. We obtained the following best-fit values: $\Delta m^2_{32} = 2.48^{+0.11}_{-0.06} \times 10^{-3}\,\text{eV}^2$, $\sin^2\theta_{23} = 0.56^{+0.04}_{-0.03}$, and $\delta_{CP} = 0.0^{+1.3}_{-0.4}$.

The best fit corresponds to the normal mass ordering and the upper octant of θ_{23} (i.e., $\theta_{23} > 45°$). Although this result is consistent with the maximal θ_{23} mixing (i.e., $\theta_{23} = 45°$), the upper octant is preferred at 1.6σ C.L. The inverted mass ordering is disfavored at 1.9σ. The region of the parameter space around $\delta_{CP} = \pi/2$ for the inverted hierarchy is ruled out at more than 3σ C.L., while for the normal ordering and upper octant of θ_{23} all values of δ_{CP} are allowed at 1.1σ C.L. Regions for θ_{23} vs. Δm^2_{32} can be found in Fig. 2 and for θ_{23} vs. δ_{CP} plus mass ordering in Fig. 3.

ACKNOWLEDGMENTS

This work was supported by the Ministry of Education, Youth and Sports of the Czech Republic under Contract No. LTT18001.

REFERENCES

1. M. A. Acero et al. (NOvA Collaboration), "First Measurement of Neutrino Oscillation Parameters Using Neutrinos and Antineutrinos by NOvA," *Phys. Rev. Lett.* **123**, 151803 (2019).
2. P. Adamson et al., "The NuMI Neutrino Beam," *Nucl. Instrum. Methods Phys. Res. A* **806**, 279–306 (2016).
3. A. Aurisano et al., "A Convolutional Neural Network Neutrino Event Classifier," *J. Instrum.* **11**, P09001 (2016).
4. M. Tanabashi et al. (Particle Data Group), "Review of Particle Physics," *Phys. Rev. D* **98**, 030001 (2018).
5. P. Adamson et al. (MINOS Collaboration), "Combined Analysis of ν_μ Disappearance and $\nu_\mu \rightarrow \nu_e$ Appearance in MINOS Using Accelerator and Atmospheric Neutrinos," *Phys. Rev. Lett.* **112**, 191801 (2014).
6. K. Abe et al. (T2K Collaboration), "Search for CP Violation in Neutrino and Antineutrino Oscillations by the T2K Experiment with 2.2×10^{21} Protons on Target," *Phys. Rev. Lett.* **121**, 171802 (2018).
7. M. G. Aartsen et al. (IceCube Collaboration), "Measurement of Atmospheric Neutrino Oscillations at 6–56 GeV with IceCube DeepCore," *Phys. Rev. Lett.* **120**, 071801 (2018).
8. K. Abe et al. (Super-Kamiokande Collaboration), "Atmospheric Neutrino Oscillation Analysis with External Constraints in Super-Kamiokande I–IV," *Phys. Rev. D* **97**, 072001 (2018).

Trigger System of the NUCLEON Space Experiment

U. M. Nurtayeva,[1,3] V. M. Grebenyuk,[1] D. M. Karmanov,[4] A. Pan,[1,3]
D. M. Podorozhny,[4] S. Yu. Porokhovoy,[1] A. B. Sadovsky,[1]
A. V. Tkachenko,[1] and L. G. Tkachev[1,2]

[1] *Joint Institute for Nuclear Research, 141980 Dubna, Russia*
[2] *Dubna State University, 141982 Dubna, Russia*
[3] *The Institute of Nuclear Physics, 050032 Almaty, Kazakhstan*
[4] *Skobeltsyn Institute of Nuclear Physics, Moscow State University, 119991 Moscow, Russia*

Abstract. The NUCLEON satellite experiment is designed to directly investigate the energy spectra of galactic cosmic-ray (CR) nuclei and their charge composition before the "knee" in the energy interval from 100 GeV to 100 TeV and in the charge range of $Z = 1$–30, respectively. The "knee" energy range of 10^{11}–10^{16} eV is a crucial region for understanding of the cosmic-ray acceleration and propagation in the interstellar medium. The NUCLEON detector has been taking data since December 2014. The NUCLEON trigger system and CR-event selection are described, including the beam tests at SPS, CERN, flight tests in the orbit, and Monte Carlo simulation.

Keywords: high-energy physics; cosmic-ray experiments; direct measurement
PACS: 29.40.Gx; 95.55.Vj; 96.50.S−; 96.50.sb

INTRODUCTION

The "knee" area was discovered in 1958 in the spectrum of cosmic rays (CRs) at $E \sim 10^{15}$ eV. It remains an object of close attention, since it is unclear whether this phenomenon is a consequence of generation and acceleration of CRs in sources or a peculiarity of their propagation in the Galaxy. The uncertainty is largely due to lack of clear information about the spectrum and composition of the CRs in this area. The CR flux is mainly measured indirectly: by analysis of the extensive air showers (EASs) formed by CR particles in the atmosphere. For the EAS method, the signal is rather weak at the knee energy region and it cannot be unambiguously interpreted: measurement of neither the charge and mass nor the energy of the primary particle is possible. Recently, direct measurements on balloons have been made in the pre-knee region, but it was impossible to obtain sufficient statistics in these experiments. There is a hope for direct measurements of CRs using satellite detectors such as NUCLEON, launched into the orbit in December 2014, as well as the recently launched DAMPE [1], CALET [2], and ISS-CREAM [3] detectors.

The NUCLEON experiment aims to measure the spectrum and composition of CR in the pre-knee region in order to obtain the missing information about the sources of CR, and mechanisms of their acceleration and propagation in our Galaxy. During the flight, the data were obtained up to 5×10^{14} eV, which exceeds the existing statistics of the ATIC [4] and CREAM [5] balloon experiments.

THE NUCLEON DETECTOR

The NUCLEON experiment is based on the use of modern detectors. Strip and pad semiconductor silicon detectors are used to measure the charge of the primary particle and the tracks of the secondary particles. The NUCLEON is a stack of registering-plane detectors, a carbon target, and a calorimeter composed of silicon detectors and a tungsten converter of γ quanta. The initial CR particle interacts with the target nuclei to form a shower of secondary charged and neutral particles that pass through the secondary-particle detectors.

The detector consists of the following main systems (see Fig. 1):

1. Charge-measurement system (CMS) for the primary particles formed by four layers of pad silicon detectors.
2. 9 cm graphite target where the primary-interaction vertex should be located.
3. Tracker for the energy-measurement system (EMS) via the KLEM method, which comprises six layers: tungsten gamma converters and silicon microstrip-detector layers.
4. Fast STS for selection of useful and suppression of background events consisting of six layers of scintillators.
5. Tungsten-silicon ionization calorimeter of 12 radiation lengths for the KLEM calibration in flight and partially for direct energy measurement of the CR events.
6. Service electronics that performs the functions of DAQ and data-flow control with the satellite computer, and also controls the detector subsystems.

THE SCINTILLATION TRIGGER SYSTEM

The fast scintillation trigger system (STS) is one of the most important parts of the NUCLEON detector [6]. The purpose of the trigger system is to select useful events with the highest energy in the aperture of the detector and suppress the background events with low energy. The total particle flux through the apparatus is expected to be $2.5 \times 10^4\,\mathrm{s}^{-1}$ and the primary particle comes from arbitrary direction. The trajectory of the primary particle crosses some or all detecting layers, forming a shower of secondary particles after the interaction with the target nuclei, the converter, and other parts of the detector. The fast analysis of such events is a task for the STS. The aim of STS is to produce a trigger signal for the service electronics. STS has tunable trigger parameters: the registration threshold and the high voltage (HV) on the photomultiplier tubes (PMTs) from the softest (the lowest threshold) to the hardest (the highest threshold).

The STS consists of three modules and an electronic board PTS1. Each module consists of two planes, and each plane consists of 16 scintillation strips with a volume of $500 \times 31 \times 7.5\,\mathrm{mm}^3$. Strips of adjacent planes of a module are mutually perpendicular. The light signal is transmitted by using WLS fibers. The background events in the NUCLEON experiment are the CR particles with low energies. The events are considered useful if the primary CR interaction occurs in the carbon target and its axis lies in the

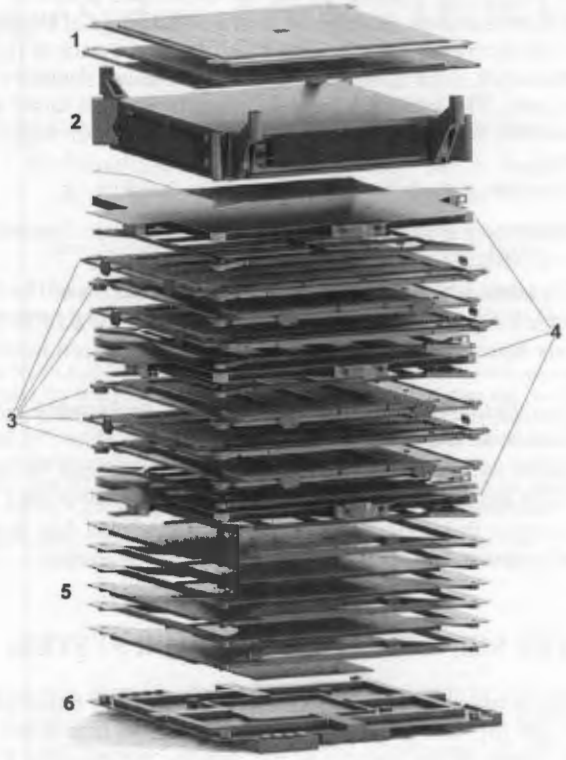

Figure 1. Schematic view of the NUCLEON device (stretched vertically).

detector aperture. The values of the actual threshold of the trigger modules were determined during the NUCLEON-detector tests at SPS, CERN.

CALIBRATION AND BEAM TESTS OF THE STS AT SPS, CERN

The NUCLEON scintillator and silicon detectors, readout, and data-taking electronics have been tested at SPS, CERN. The beam spot was $\sim 1.5\,\mathrm{cm}$ and the intensity was 10^3–10^4 particles per second. The beam tests of the NUCLEON-detector prototypes (see Fig. 2) were carried out with pions up to $350\,\mathrm{GeV}/c$.

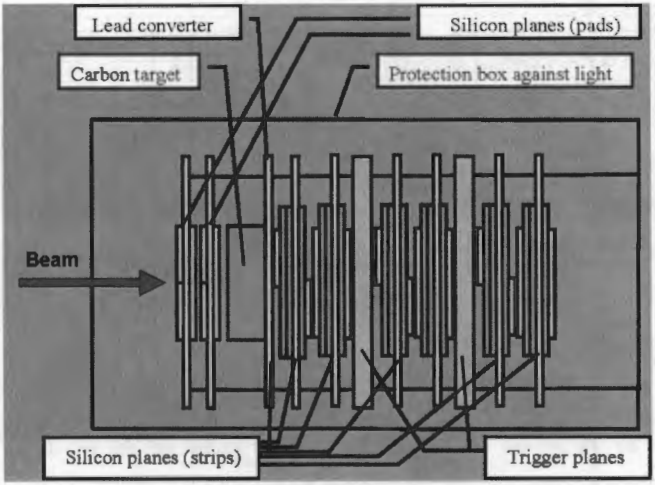

Figure 2. Scheme of the beam-test experiment at SPS, CERN.

Figure 3 shows the results of the trigger-efficiency measurements at different thresholds and HV on the PMTs. The rejection efficiency is defined as the ratio between the number of selected events and the total number of beam particles. Figure 3(a) shows the rejection-efficiency dependence of the HV value U2 on the PMT of the second trigger plane. The thresholds were fixed at T1 = 7 A.U. and T2 = 10 A.U. (expressed in arbitrary units) for the first and second planes, respectively. The HV on the second plane was changed from 900 V to 370 V. The HV on the first-plane PMT was fixed at U1 = 746 V. There was no event suppression at U2 = 900 V (the event-registration probability reached $\approx 100\%$). By reducing the value of U2 to 370 V, the suppression was ≈ 0.002, i.e., 99.8% of the events were suppressed. However, this is not enough for the cosmic experiment.

It is also necessary to vary the thresholds of the trigger electronics to increase the suppressing efficiency. The HV values were fixed at U1 = U2 = 413 V and the second threshold was increased from T2 = 10 A.U. to T2 = 20 A.U. at the fixed threshold T1 = 7 A.U. As a result, the suppressing efficiency was changed by a factor of ~ 3, from 0.041 to 0.014, see Fig. 3(b). Subsequently, the threshold on the second plane was raised to T2 = 30 A.U., while the threshold on the first plane was increased from T1 = 15 A.U. to T1 = 30 A.U. As seen in Fig. 3(c), the suppressing efficiency changed from 2.7×10^{-3} to 6×10^{-5}. According to the beam test, it is thus necessary to adjust the thresholds in the STS in addition to the HV on the 1-channel PMTs to achieve a suppression level of 10^{-5}–10^{-4} for the CR events with the energies of 100–300 GeV.

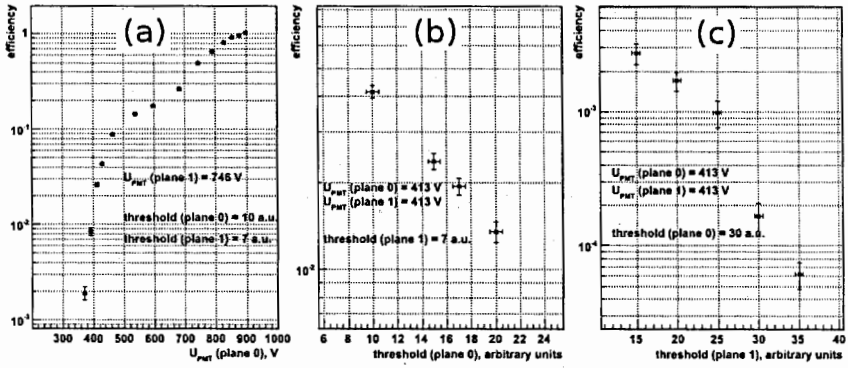

Figure 3. Suppressing efficiency of the beam particle for different thresholds and HV values.

COMBINED FLIGHT TESTS OF THE STS

The first few months of the NUCLEON flight were dedicated to the testing of the apparatus. During the flight tests of the NUCLEON detector, the STS selection criteria were established based on the results of the tests at SPS, CERN: to select events with the energy of the primary CR higher than 100 GeV and the trigger rate of $\sim 1\,\mathrm{s}^{-1}$ due to the bandwidth of the DAQ channel.

Distributions of the summarized amplitudes in the 16-channel PMTs of the STS planes are presented in Fig. 4. The systematic growth of the mean values sequentially in the modules No. 1, 2, and 3 characterizes the natural growth of the multiplicity of the secondary particles as the shower develops in accordance with the Monte Carlo simulation. Further investigation of the STS functionality is currently in progress with a purpose of increasing the NUCLEON energy range for the physical-data analysis.

CONCLUSION

The NUCLEON detector for the study of CR in the 10^{11}–5×10^{14} eV range was launched into the orbit in December 2014. The results obtained in the orbital-flight tests show that all the detectors and electronics of the STS operates reliably and stably, in accordance with the beam-test measurements at SPS, CERN. During the NUCLEON-detector operation in the orbit, a number of CR events were observed and preliminary physical results are being published.

ACKNOWLEDGMENTS

We acknowledge the support of the State Corporation for Space Activities (Roscosmos).

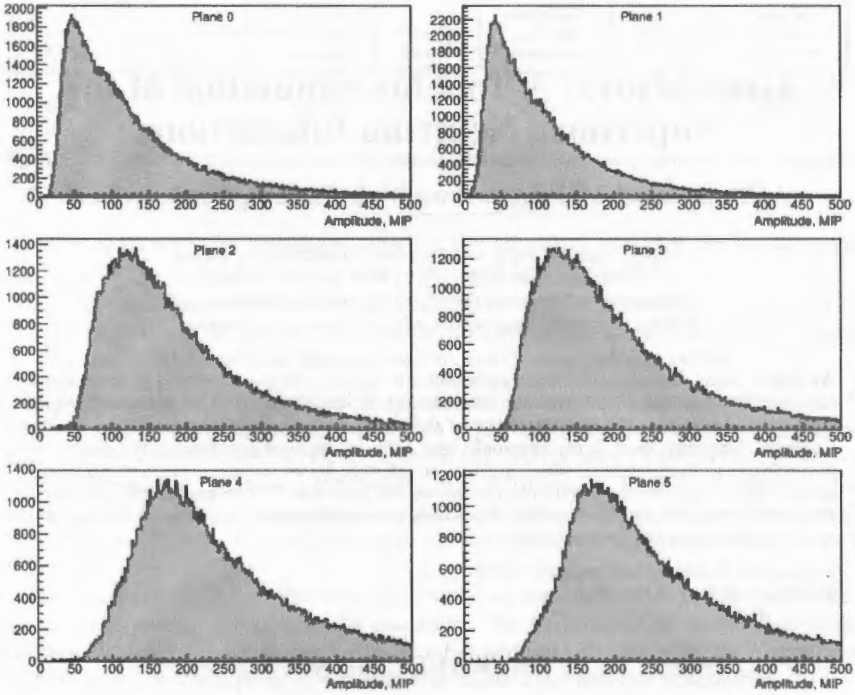

Figure 4. Distribution of the internal amplitudes in the STS planes.

REFERENCES

1. J. Chang, Y. Hu, and J. Wu, "Chinese High Energy Cosmic Particle Explorer (DAMPE)," *Proceedings of the 40th COSPAR Scientific Assembly* **40**, 484 (2014).
2. S. Torii, "CALET Mission for Exploring the High Energy Universe," *IEEJ Trans. Fundam. Mater.* **132**, 603–608 (2012).
3. E. S. Seo et al., "Cosmic Ray Energetics And Mass for the International Space Station (ISS-CREAM)," *Adv. Space Res.* **53**, 1451-1455 (2014).
4. J. Chang et al., "An Excess of Cosmic Ray Electrons at Energies of 300–800 GeV," *Nature* **456**, 362–365 (2008).
5. E. S. Seo et al., "Cosmic-Ray Energetics and Mass (CREAM) Balloon Project," *Adv. Space Res.* **33**, 1777–1785 (2004).
6. E. Atkin et al., "The NUCLEON Space Experiment for Direct High Energy Cosmic Rays Investigation in TeV–PeV Energy Range," *Nucl. Instrum. Methods Phys. Res. A* **770**, 189–196 (2015).

GenieSNova: A Tool for Simulation of the Supernova Neutrino Interactions

A. Sheshukov,[1] M. Petropavlova,[1,2] A. T. Habig,[3] and J. Vasel[4]

[1] *Joint Institute for Nuclear Research, 141980 Dubna, Russia*
[2] *Moscow State University, 119991 Moscow, Russia*
[3] *University of Minnesota Duluth, 55812 Duluth, Minnesota, USA*
[4] *Indiana University Bloomington, 47405 Bloomington, Indiana, USA*

Abstract. Many neutrino experiments are sensitive to the core-collapse supernova-neutrino signal. However, the development of detection methods and the evaluation of experiment sensitivity to such a signal requires a detailed simulation of the supernova-neutrino interactions in the detector geometry. Currently, there is no commonly used software for such simulations. We present the GenieSNova software package which provides an interface for the existing models of supernova-neutrino fluences within the GENIE neutrino-interaction generator. This package is being developed for the NOvA experiment, but is sufficiently general to be easily applied also to other detectors with different geometries and compositions.

Keywords: supernova; neutrino; simulation
PACS: 97.60.Bw; 14.60.Lm

INTRODUCTION

Neutrino emission plays a crucial role in the supernova-explosion mechanism. Neutrinos produced in the early phases of the collapse carry information from the core. A core-collapse supernova produces an enormous burst of neutrinos of all flavors in the few-tens-of-MeV range, taking away 99% of the gravitational binding energy of the resulting remnant. The signal has a timescale of a few tens of seconds [1].

Many neutrino experiments are sensitive to the core-collapse supernova-neutrino signal. The existing tool SNOwGLoBES [2] allows for an estimation of the number of events produced by the supernova neutrinos, as well as their spectra and distributions, taking into account the detector efficiencies and resolutions. However, in many cases a detailed simulation on the event-by-event basis is required, e.g., when developing the reconstruction and selection procedures for such methods.

Numerous neutrino experiments use a common pipeline for the simulation of the detector response to the neutrino interactions of interest. This pipeline can be divided into the following blocks:

1. Flux driver: an individual neutrino is sampled from the input neutrino distribution (flux model).
2. Neutrino-interaction generator: an interaction of the individual neutrino in the given detector geometry and material composition is simulated. The kinematic information about the interaction and the secondary particles are produced in this step.

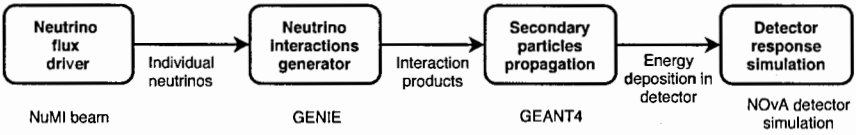

Figure 1. Standard simulation pipeline for the interactions of the beam neutrinos in the NOvA detectors.

3. Propagation of the secondary particles: the secondary particles are traced in the detector geometry, interacting with matter and depositing energy.
4. Detector-response simulation: the simulated energy deposition or interactions of the secondary particles in the sensitive volume of the detector are digitized and processed, emulating the detector readout and data-acquisition system.

Implementation of the individual blocks in this scheme is different for each experiment. Figure 1 shows the scheme of such a pipeline for the simulation of the beam-neutrino interactions in the NOvA experiment [3]. NOvA uses a custom flux driver for generating neutrinos following the NuMI-beam distributions, GENIE [4] package for generation of neutrino interactions, Geant4 [5] for propagation of the secondary particles, and detailed simulation of the optical and electronic readout systems of the NOvA detectors.

The default pipeline can also be used to simulate the interactions of supernova neutrinos, with minimal changes to the procedure. We introduce a dedicated flux-driver package GenieSNova, which produces the input neutrinos for the interaction generator GENIE, based on the supernova-neutrino-flux models and detector description.

THE GenieSNova PACKAGE

Since the real observations of supernova neutrinos are limited to the detection of SN 1987A [6, 7, 8, 9], the mechanism of stellar-core collapse and the inner processes are not yet precisely described. Predictions of the supernova-neutrino flux from detailed stellar-collapse simulations are varying with the progenitor-star parameters, simulation assumptions, and neutrino-mixing properties.

The supernova-neutrino flux $\Phi_\nu(E_\nu, t)$ is the input for the simulation package. GenieSNova is compatible with two input formats of the supernova-neutrino flux:

1. Table of neutrino fluxes for all neutrino flavors vs. time and energy bins:

$$\begin{aligned} & t_1, \frac{\mathrm{d}^2 N_\nu}{\mathrm{d}E_\nu\,\mathrm{d}t}(t_1, E_1), \ldots, \frac{\mathrm{d}^2 N_\nu}{\mathrm{d}E_\nu\,\mathrm{d}t}(t_1, E_M), \\ & \vdots \\ & t_N, \frac{\mathrm{d}^2 N_\nu}{\mathrm{d}E_\nu\,\mathrm{d}t}(t_N, E_1), \ldots, \frac{\mathrm{d}^2 N_\nu}{\mathrm{d}E_\nu\,\mathrm{d}t}(t_N, E_M). \end{aligned} \tag{1}$$

This input format is used in the models provided by the SND group [10] and is rather general. It can be used for neutrino spectra distorted by oscillations and collective effects or even for pre-supernova neutrino signals. The downside is that the effect of bin size is propagated into the simulation.

2. Table of neutrino energy luminosities for all flavors vs. time bins, and energy-spectrum parameters:

$$\begin{aligned} & t_1, \frac{\mathrm{d}L_\nu}{\mathrm{d}t}(t_1), \langle E_\nu(t_1)\rangle, \langle E_\nu^2(t_1)\rangle \\ & \vdots \\ & t_N, \frac{\mathrm{d}L_\nu}{\mathrm{d}t}(t_N), \langle E_\nu(t_N)\rangle, \langle E_\nu^2(t_N)\rangle. \end{aligned} \tag{2}$$

This input format is used in the models by the Garching group [11] and allows to get the neutrino energy spectrum using the parameterization:

$$f_\alpha(E) = \left(\frac{E}{\langle E\rangle}\right)^\alpha e^{-(\alpha+1)\frac{E}{\langle E\rangle}} \text{ with the shape parameter } \alpha = \frac{\langle E\rangle^2}{\langle E^2\rangle - \langle E\rangle^2}. \tag{3}$$

This parameterization of the distribution allows for sampling of the individual neutrino energies to be done faster and without any energy binning, but this parameterization may not be suitable in the case of distorted spectra.

In order to simulate the signal from a supernova in a detector, the neutrinos of all flavors which interacted in the detector need to be arranged by time and generated randomly according to a specified distribution. GenieSNova samples the individual supernova neutrinos, using the input information in the following steps:

- Neutrino position is generated uniformly in a rectangular window with a definite size, pointing towards the detector. The neutrino flux is scaled proportionally to the window area, divided by the squared distance to the supernova.
- Neutrino time is generated sequentially for each particle as if the neutrinos came from the supernova, using the neutrino-luminosity profile vs. time.
- Neutrino energy is sampled from the neutrino-flux distribution at the given time.

Figure 2 shows the abovementioned steps of a simulation as well as the input parameters from the configuration file, used at each step. The GenieSNova inputs are the supernova model, distance, and minimum energy- and flux-window sizes to produce the incoming neutrinos. Subsequently, in order to generate the neutrino interactions, a full description of the detector geometry (in the `.gdml` file format used by the Geant4, ROOT, and GENIE packages) and an interaction-channel list are needed. GENIE then calculates the cross-section splines and maximum path length for all materials in the detector. Finally, the user is required to define the name of the top volume in the geometry, in order to avoid generating neutrino interactions in the insensitive volume outside the detector.

Since GENIE is broadly used for beam-neutrino simulations, most of its models are tuned for $E_\nu \sim$ GeV neutrinos. The interaction processes in GENIE relevant to

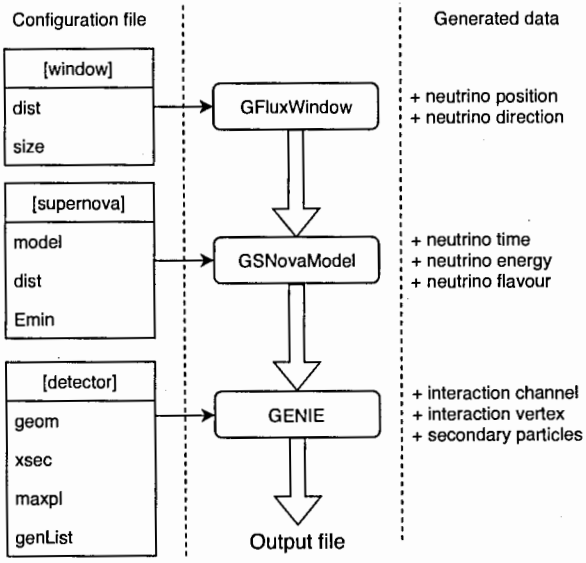

Figure 2. Scheme of the GenieSNova-simulation steps.

supernova neutrinos are currently limited to the inverse beta decay ($\overline{\nu}_e + p \rightarrow e^+ + n$) and elastic scattering of electron neutrinos ($\nu_e + e^- \rightarrow \nu_e + e^-$). These channels constitute more than 90% of the neutrino interactions expected in the liquid scintillator detectors. Other interaction channels, once they are incorporated into GENIE in the future, could be easily included in the GenieSNova simulations.

SIMULATION RESULTS FOR THE NOvA FAR DETECTOR

The far detector of the NOvA experiment [12] is a $16 \times 16 \times 60\,\mathrm{m}^3$ box-shaped volume constructed from extruded PVC tubes, filled with 14 kt of organic liquid scintillator. The dominant channel for supernova detection in this detector is the inverse beta decay (IBD).

Figure 3 shows the results of a simulation of the interactions of neutrinos from supernovae at a distance of 5 kpc using the Garching-group simulations of the core collapse of $9.6 M_\odot$ and $27 M_\odot$ progenitor stars. In order to validate the GenieSNova results, we compare them with the expected distribution of the IBD events, obtained by numerical calculations from the $\overline{\nu}_e$ flux $\Phi_{\overline{\nu}}(E,t)$, IBD cross section σ_{IBD} by [13], and total number N_{H} of hydrogen atoms in the detector:

$$N_{\mathrm{IBD}}(t) = N_{\mathrm{H}} \int_0^\infty \mathrm{d}E\, \Phi_{\overline{\nu}}(E,t)\, \sigma_{\mathrm{IBD}}(E). \tag{4}$$

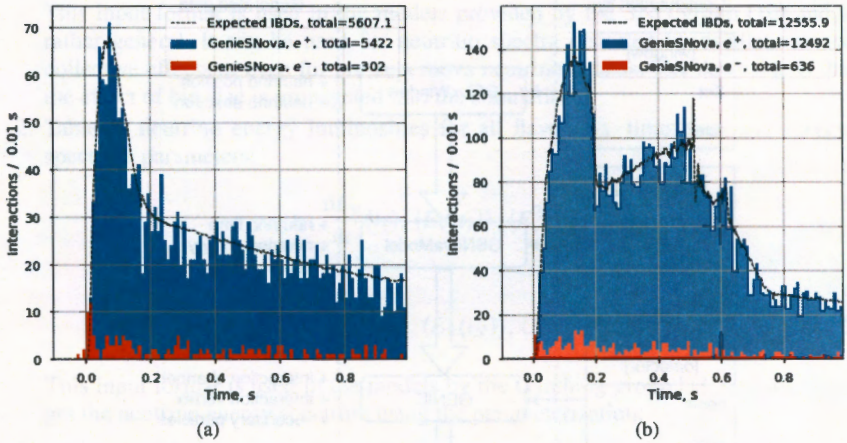

Figure 3. Time distribution of the secondary leptons produced by the supernova neutrinos from (a) $9.6M_\odot$ and (b) $27M_\odot$ progenitor stars. The dashed line shows the expected number of inverse-beta-decay positrons.

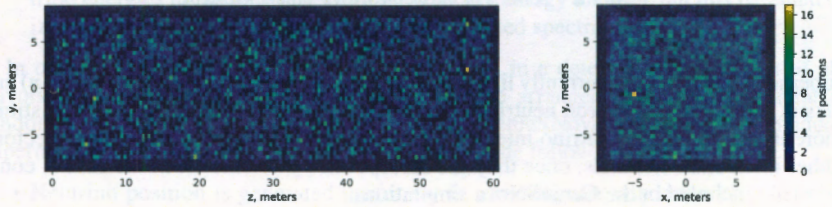

Figure 4. Spatial distributions of the IBD-interaction vertices in the volume of the NOvA far detector: (a) yz plane and (b) xy plane.

This calculation is shown by the dashed line in Fig. 3 and is consistent with the results of the GenieSNova simulation.

Figure 4 shows the spatial distribution of IBD interactions in the detector and surrounding materials. The vertices are distributed uniformly within the detector volume, as expected. The products of neutrino interactions, simulated at this step, are then passed to Geant4 and further down the default NOvA simulation chain in Fig. 1.

SUMMARY

The GenieSNova package provides an interface for the supernova-neutrino-flux models within the GENIE neutrino-interaction generator, serving as a tool for simulation of the

detector response to a supernova-neutrino signal for the given detector description. A simulation of neutrino interactions in the NOvA far detector showed an agreement with the expected distributions and normalization.

REFERENCES

1. K. Scholberg, "Supernova Neutrino Detection," *Annu. Rev. Nucl. Part. Sci.* **62**, 81–103 (2012).
2. `https://github.com/SNOwGLoBES`
3. M. A. Acero et al. (NOvA Collaboration), "New Constraints on Oscillation Parameters from ν_e Appearance and ν_μ Disappearance in the NOvA Experiment," *Phys. Rev. D* **98**, 032012 (2018).
4. C. Andreopoulos et al., "The GENIE Neutrino Monte Carlo Generator," *Nucl. Instrum. Methods Phys. Res. A* **614**, 87–104 (2010).
5. S. Agostinelli et al. (Geant4 Collaboration), "Geant4—A Simulation Toolkit," *Nucl. Instrum. Methods Phys. Res. A* **506**, 250–303 (2003).
6. K. Hirata et al. (Kamiokande-II Collaboration), "Observation of a Neutrino Burst from the Supernova SN1987A," *Phys. Rev. Lett.* **58**, 1490–1493 (1987).
7. E. N. Alekseev, L. N. Alekseeva, V. I. Volchenko, and I. V. Krivosheina, "Possible Detection of a Neutrino Signal on 23 February 1987 at the Baksan Underground Scintillation Telescope of the Institute of Nuclear Research," *J. Exp. Theor. Phys. Lett.* **45**, 589–592 (1987).
8. M. Aglietta et al., "On the Event Observed in the Mont Blanc Underground Neutrino Observatory during the Occurrence of Supernova 1987a," *EPL* **3**, 1315–1320 (1987).
9. R. M. Bionta et al., "Observation of a Neutrino Burst in Coincidence with Supernova 1987A in the Large Magellanic Cloud," *Phys. Rev. Lett.* **58**, 1494 (1987).
10. K. Nakazato et al., "Supernova Neutrino Light Curves and Spectra for Various Progenitor Stars: From Core Collapse to Proto-Neutron Star Cooling," *Astrophys. J., Suppl. Ser.* **205**, 2 (2013).
11. A. Mirizzi et al., "Supernova Neutrinos: Production, Oscillations and Detection," *Riv. del Nuovo Cim.* **39**, 1–112 (2016).
12. D. S. Ayres et al. (NOvA Collaboration), "The NOvA Technical Design Report" (technical report), Fermi National Accelerator Laboratory (2007).
13. A. Strumia and F. Vissani, "Precise Quasielastic Neutrino/Nucleon Cross-Section," *Phys. Lett. B* **564**, 42–54 (2003).

Role of CEνNS in Direct Dark-Matter Detection

E. Picciau[1,2,3] and M. Cadeddu[1]

[1] *National Institute for Nuclear Physics, 09042 Cagliari, Italy*
[2] *University of Cagliari, 09124 Cagliari, Italy*
[3] *University of Massachusetts Amherst, 01003 Amherst, Massachusetts, USA*

Abstract. The next-generation direct dark-matter detectors might have sufficient sensitivity to detect neutrinos from various sources, including atmospheric and diffuse supernova neutrinos, through the Standard-Model process called coherent elastic neutrino-nucleus scattering (CEνNS). This process constitutes irreducible background that the future detectors will have to deal with. In this work, we discuss the main ingredients for calculation of the neutrino-nucleus background for liquid argon (LAr) and liquid xenon (LXe) detectors. Finally, the impact of CEνNS on the sensitivity projections of different dark-matter detectors is shown and discussed.

Keywords: neutrinos; coherent scattering; dark matter; direct detection
PACS: 13.15.+g; 13.85.Dz; 95.35.+d

INTRODUCTION

The coherent elastic neutrino-nucleus scattering (CEνNS) plays a fundamental role in the detection of dark matter for high-exposure or low-threshold detectors. Indeed, the signal released by this type of neutrino interaction will be very difficult to distinguish from the signal induced by interactions of nuclei with weakly interacting massive particles (WIMPs).

So far, the dark-matter detectors have not seen any signal compatible with the WIMP hypothesis, which prompts the community to build new detectors with higher exposures to explore smaller dark-matter-interaction cross sections. In order to maximize the sensitivity of such experiments, reduction of the background abundance becomes crucial. The experimental challenge is to limit the effects of the CEνNS background, and thus increase the sensitivity to the WIMPs. The CEνNS process, recently observed by the COHERENT experiment [1] in CsI, is a process that, according to the Standard Model (SM), should be taken into account for large LAr and LXe dark-matter detectors.

In this work, we describe the sources of neutrinos important for the dark-matter searches and their uncertainties, as well as the theoretical framework of CEνNS and its consequences for the LAr and LXe experiments. Moreover, we determine the so-called single-neutrino-event curve for LAr in the WIMP cross-section vs. mass parameter plane. Finally, we provide a comparison between the exclusion limit at 90% C.L. and 5σ discovery limit for the future LAr and LXe experiments.

NEUTRINO SOURCES

In this section, we report on the neutrino background event rate starting from the description of individual neutrino-flux components. The main neutrino fluxes on the Earth can be divided into three categories: solar, diffuse supernova, and atmospheric neutrinos.

Solar neutrinos are produced in the nuclear-synthesis reactions inside the Sun, such as the proton-proton (*pp*) or carbon-nitrogen-oxygen (CNO) chains. These neutrino components are characterized by energies lower than $\sim 2\,\mathrm{MeV}$. A very important component of the *pp* chain consists of the ^{8}B and *hep* neutrinos. The former ones arise from the decay $^8\mathrm{B} \rightarrow {}^7\mathrm{Be}^* + e^+ + \nu_e$, which occurs in approximately 0.02% of the termination of the *pp* chain. The latter neutrinos come from the reaction $^3\mathrm{He} + p \rightarrow {}^4\mathrm{He} + e^+ + \nu_e$. The total flux produced in the *pp* chain is $5.94 \times 10^{10}\,\mathrm{cm}^{-2}\,\mathrm{s}^{-1}$. Following Ref. [2], the theoretical uncertainties of the solar-neutrino fluxes are of the order of 10%. In particular, the ^{8}B and *hep* neutrinos have an uncertainty of 16%.

Another important flux is represented by the diffuse supernova neutrino background (DSNB), which originates from all past supernova explosions in the Universe. The neutrino spectrum of a core-collapse supernova is assumed to be a Fermi–Dirac spectrum with temperature in the range of 3–8 MeV. The DSNB flux covers energies up to hundreds of MeV. Following Ref. [3], the DSNB flux strongly depends on the temperature spectrum, and for this reason the uncertainty is assumed to be 50%.

The last component is constituted by atmospheric neutrinos produced through cosmic-ray collisions with the Earth's atmosphere. The energy range is approximately 10–10^3 MeV. For these energies, the uncertainty of the predicted atmospheric-neutrino flux is approximately 20% [4]. Among the three described types of neutrino sources, the atmospheric-neutrino flux is the main ingredient responsible for the neutrino-nucleus background in the next-generation dark-matter experiments which aim to improve the limits in the heavy-WIMP region ($20\,\mathrm{GeV}/c^2 - 1\,\mathrm{TeV}/c^2$).

For the light-WIMP searches ($0.1\text{–}20\,\mathrm{GeV}/c^2$), the main background comes from the solar component, in particular the ^{8}B and *hep* reaction channels. In Fig. 1, the neutrino-flux components and neutrino background event rates are shown in detail.

COHERENT ELASTIC NEUTRINO-NUCLEUS SCATTERING

As predicted by the SM, neutrinos have the possibility to scatter coherently off a nucleus through a neutral-current process. The coherence of the scattering process is determined by the length scale of the interaction, which is related to the inverse of the momentum exchanged between the neutrino and nucleus.

The differential cross section depends on the neutrino energy E_ν, nuclear mass m_N, and nuclear-recoil energy E_R as follows:

$$\frac{\mathrm{d}\sigma^{\mathrm{CE}\nu\mathrm{NS}}(E_\nu, E_\mathrm{R})}{\mathrm{d}E_\mathrm{R}} = \frac{G_\mathrm{F}^2}{4\pi} Q_\mathrm{W}^2 m_\mathrm{N} \left(1 - \frac{m_\mathrm{N} E_\mathrm{R}}{2E_\nu^2}\right) |F(E_\mathrm{R})|^2, \tag{1}$$

where G_F is the Fermi coupling constant, $Q_\mathrm{W} = N - (1 - 4\sin^2\theta_\mathrm{W})Z$ is the weak

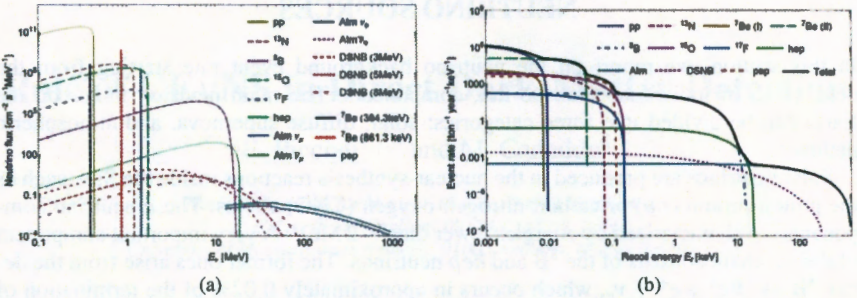

(a) (b)

Figure 1. (a) Neutrino fluxes on the Earth relevant for direct dark-matter detection at LNGS. From low to high energies: solar, diffuse supernova, and atmospheric neutrinos. (b) Rate of neutrino background events per tonne-year due to CEνNS as a function of the recoil energy considering an argon target (black solid line). Relative contributions of the partial neutrino fluxes are shown as well.

hypercharge, N is the number of neutrons, Z is the atomic number, θ_W is the weak mixing angle, m_N denotes the nuclear mass, and $|F(E_R)|$ is the nuclear form factor as a function of the nuclear-recoil energy E_R. Since the weak mixing angle has a running value depending on the energy scale, we used the value of $\sin^2\theta_W = 0.23857$ considering the process at energy scales below 300 MeV [5].

Usually, the nuclear form factor is constructed using Helm parameterization, which assumes that neutrinos couple equally to both neutrons and protons:

$$F(E_R) = 3\frac{j_1(qR_N)}{qR_N}e^{-\frac{1}{2}(qs)^2}, \tag{2}$$

where $q = \sqrt{2m_N E_R}$ is the momentum transfer, R_N is the nuclear-distribution radius, and s is the skin thickness of the nucleus that, in principle, is a parameter to be fitted. In this work, we set $s = 0.9$ fm as this value matches Helm form factor with different kinds of parameterization.

For a more detailed calculation, it is possible to separate the contributions of neutrons and protons in the form factor. Indeed, in Ref. [6] the CEνNS scattering was studied using the form factor:

$$F(E_R) = \frac{NF_N(E_R) + (1 - 4\sin^2\theta_W)ZF_Z(E_R)}{Q_W}, \tag{3}$$

in which the distributions of neutrons and protons were considered separately and weighted by different couplings. The effect and consequences of using such a form factor are discussed in Ref. [7]. The main problem with using this approach is that the neutron-distribution radius must be estimated through theoretical calculation since no experimental measurement has been performed so far. The proton-distribution radii are very well known [8], while the neutron ones have been measured only recently for CsI using data of the COHERENT experiment [6, 1]. For this reason, in this work all CEνNS calculations are made using Helm form factor from Eq. (2).

The neutrino differential rate is given by:

$$\frac{\mathrm{d}R^{\mathrm{CE}\nu\mathrm{NS}}}{\mathrm{d}E_{\mathrm{R}}} = \eta \int_{E_{\nu,\mathrm{min}}} \frac{\mathrm{d}N}{\mathrm{d}E_{\nu}} \frac{\mathrm{d}\sigma^{\mathrm{CE}\nu\mathrm{NS}}(E_{\nu}, E_{\mathrm{R}})}{\mathrm{d}E_{\mathrm{R}}} \mathrm{d}E_{\nu}, \tag{4}$$

where η is the number of nuclear targets per unit active detector mass and $\mathrm{d}N/\mathrm{d}E_{\nu}$ represents the total neutrino flux. The maximum recoil energy and the minimum neutrino energy (in the limit of $m_{\mathrm{N}} \gg E_{\nu}$) are determined by the kinematics:

$$E_{\mathrm{R,max}}^{\mathrm{CE}\nu\mathrm{NS}} = \frac{2m_{\mathrm{N}}E_{\nu}^2}{(m_{\mathrm{N}}+E_{\nu})^2}, \quad E_{\nu,\mathrm{min}}^{\mathrm{CE}\nu\mathrm{NS}} = \sqrt{\frac{m_{\mathrm{N}}E_{\mathrm{R}}}{2}}. \tag{5}$$

The rate of neutrino events per unit exposure as a function of E_{R} is shown in Fig. 1(b).

WIMP-NUCLEUS SCATTERING

In order to calculate the number of WIMP events expected in the detector of a given exposure, we assume equal couplings to protons and neutrons for the WIMP differential rate. Under this assumption, the rate R^{χ} per unit detector exposure as a function of the nuclear-recoil energy E_{R} reads:

$$\frac{\mathrm{d}R^{\chi}}{\mathrm{d}E_{\mathrm{R}}} = \frac{\rho_{\chi}}{2\mu_{\chi p}^2 m_{\chi}} \sigma_{\mathrm{SI}}^{\chi\mathrm{N}} A^2 |F(E_{\mathrm{R}})|^2 \int_{v_{\mathrm{min}}}^{\infty} \frac{f(v)}{v} \mathrm{d}v, \tag{6}$$

where ρ_{χ} is the WIMP number density, $\mu_{\chi p}$ is the WIMP–proton reduced mass, m_{χ} and $\sigma_{\mathrm{SI}}^{\chi\mathrm{N}}$ are the WIMP mass and cross section (treated as free parameters), A is the mass number of the target, and $f(v)$ is the distribution of the WIMP velocity v relative to the target. The shape of the differential event rate depends on a number of factors: the dark-matter and target-nucleus masses, which determine the kinematics of the process (such as the minimum WIMP velocity), the recoil energy, and the WIMP flux. A less trivial dependence is encoded in the nuclear form factor and in the shape of the dark-matter speed distribution $f(v)$ on the Earth.

Another difference between the neutrino and WIMP processes is in their kinematics. Indeed, the maximum recoil energy for a WIMP scattering is:

$$E_{\mathrm{R}}^{\mathrm{max}} = \frac{2\mu_{\chi\mathrm{N}}^2 v_{\mathrm{cutoff}}^2}{m_{\mathrm{N}}}, \tag{7}$$

in which $v_{\mathrm{cutoff}} = 776\mathrm{km/s}$ represents the escape velocity from the Milky Way in the reference frame of the Earth. In Fig. 2, we show comparison of the CEνNS and WIMP event rates for argon and xenon detectors and for different WIMP masses and cross sections.

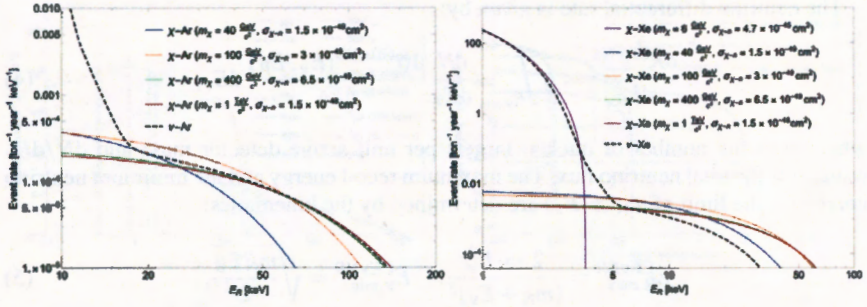

Figure 2. Comparison of CEνNS and WIMP event rates for: (a) argon detectors and (b) xenon detectors. The black dashed line represents the CEνNS rate, while the solid lines represent the WIMP rates for different masses and cross sections.

SINGLE-NEUTRINO-EVENT LIMIT AND FUTURE SENSITIVITY

Since neutrinos might become the dominant background in the future direct dark-matter detection, it could be interesting to set limits in the $\sigma^{\chi N}$ vs. m_χ parameter plane. The community typically refers to the discovery limit obtained for xenon by Billard et al. [9]. Another, more intuitive, neutrino curve is represented by the single-neutrino-event limit. This neutrino limit is obtained by generating a set of 200 background-free exclusion limits (defined as 2.3 WIMP events at 90% C.L.) with thresholds varying from 1 eV to 500 keV and adjusting the exposure of each curve such that a single neutrino event is expected. The minimum of these curves is what is defined as the single-neutrino limit.

In Fig. 3(a), we show the difference between the single-neutrino curve for Xe and Ar. In particular, above $m_\chi = 6\,\mathrm{GeV}/c^2$, the limit for Ar is higher by about a factor of 3 than the Xe curve. This is due to the higher event rate in the region above 10 keV of the recoil energy. The interpretation of this curve is the following: if in a background-free experiment the sensitivity curve is below this limit, the experiment should expect at least one event from the neutrino background during its data taking. Since this background is irreducible, in order to claim a discovery or to set an upper limit, the experiment would need to observe more WIMPs compared to the background-free case, and for this reason the sensitivity, including the neutrino events, will be worse. Moreover, considering that for a zero-background experiment the sensitivity increases in proportion to the exposure, once the single-event limit is reached, the sensitivity will increase as the square root of the exposure.

In this work, we calculated the sensitivity curves for the future LAr experiments through the statistical counting approach, comparing the obtained results with the LXe results for the future LZ [10] and DARWIN [11] detectors. Since the number of considered background events is sufficiently low, the counting approach should give results very similar to a more detailed analysis using, e.g., a profile likelihood ratio test. This statement will be studied more deeply in our future work. In Fig. 3(b), we show different upper limits at 90% C.L. and the 5σ discovery potential for the experiments listed

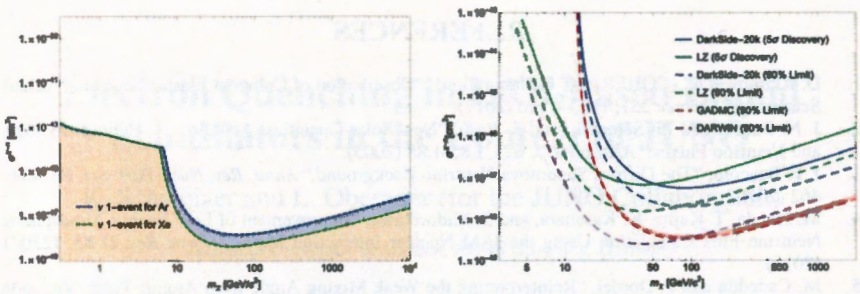

(a) (b)

Figure 3. (a) Single-neutrino-event limit for LAr and LXe in the WIMP parameter plane. (b) Sensitivity curves for the future direct-detection dark-matter experiments. The dashed curves represent the upper limits at 90% C.L., while the continuous ones indicate a 5σ discovery. The red band for GADMC represents a 20% uncertainty of the neutrino background.

Table 1. Future LAr and LXe direct-detection dark-matter experiments.

Experiment	Target	Threshold [keV]	Exposure [tyr]	Sensitivity
DarkSide-20k	LAr	30	100	Calculated
LZ	LXe	4–5	15	[10]
GADMC	LAr	30	1,500	Calculated
DARWIN	LXe	6.6	200	[11]

in Table 1. As one can see from the plot, for the large-scale experiments (GADMC and DARWIN) LAr provides a weaker upper limit above the masses of about $90\,\mathrm{GeV}/c^2$, while below this value the LXe experiments could reach a more significant detection of lighter WIMPs.

CONCLUSION

In this work, we evaluated and discussed the effects of CEνNS on the direct-detection dark-matter searches. The take-home message is that the future detectors will have to deal with the neutrino backgrounds induced by the coherent scattering that closely mimic the signal of a WIMP scattering off a nucleus. With the thresholds and exposures considered in this work, the DarkSide-20k and LZ detectors will be able to observe ~ 1 event, while the GADMC and DARWIN detectors will be able to reach ~ 10 events. This result opens a window to employ these devices as future neutrino detectors, allowing for measurement of the neutrino-flux components not directly observed so far and improvement of the current experimental results.

REFERENCES

1. D. Akimov et al. (COHERENT Collaboration), "Observation of Coherent Elastic Neutrino-Nucleus Scattering," *Science* **357**, 1123–1126 (2017).
2. J. N. Bahcall, A. M. Serenelli, and S. Basu, "New Solar Opacities, Abundances, Helioseismology, and Neutrino Fluxes," *Astrophys. J.* **621**, L85–L88 (2005).
3. J. F. Beacom, "The Diffuse Supernova Neutrino Background," *Annu. Rev. Nucl. Part. Sci.* **60**, 439–462 (2010).
4. M. Honda, T. Kajita, K. Kasahara, and S. Midorikawa, "Improvement of Low Energy Atmospheric Neutrino Flux Calculation Using the JAM Nuclear Interaction Model," *Phys. Rev. D* **83**, 123001 (2011).
5. M. Cadeddu and F. Dordei, "Reinterpreting the Weak Mixing Angle from Atomic Parity Violation in View of the Cs Neutron RMS Radius Measurement from COHERENT," *Phys. Rev. D* **99**, 033010 (2019).
6. M. Cadeddu, C. Giunti, Y. F. Li, and Y. Y. Zhang, "Average CsI Neutron Density Distribution from COHERENT Data," *Phys. Rev. Lett.* **120**, 072501 (2018).
7. M. Cadeddu and E. Picciau, "Impact of Neutrino Background Prediction for Next Generation Dark Matter Xenon Detector," *J. Phys.: Conf. Ser.* **956**, 012014 (2018).
8. G. Fricke et al., "Nuclear Ground State Charge Radii from Electromagnetic Interactions," *At. Data Nucl. Data Tables* **60**, 177–285 (1995).
9. J. Billard, E. Figueroa-Feliciano, and L. Strigari, "Implication of Neutrino Backgrounds on the Reach of Next Generation Dark Matter Direct Detection Experiments," *Phys. Rev. D* **89**, 023524 (2014).
10. D. S. Akerib et al. (LUX-ZEPLIN Collaboration), "Projected WIMP Sensitivity of the LUX-ZEPLIN (LZ) Dark Matter Experiment," *arXiv:1802.06039 [astro-ph.IM]* (2018).
11. J. Aalbers et al. (DARWIN Collaboration), "DARWIN: Towards the Ultimate Dark Matter Detector," *J. Cosmol. Astropart. Phys.* **2016/11**, 017 (2016).

Electron Quenching in LAB-Based Liquid Scintillators in the Context of JUNO

K. Schweizer and L. Oberauer (for the JUNO Collaboration)

Technical University of Munich, 85748 Garching, Germany

Abstract. We experimentally determine the energy-to-light conversion function of liquid scintillators in the context of the upcoming JUNO experiment.

Keywords: scintillator and semiconductor detectors; energy-scale calibration
PACS: 29.40.Mc

INTRODUCTION

The Jiangmen Underground Neutrino Observatory (JUNO) is a multipurpose neutrino experiment currently under construction in China [1]. It is designed to determine the neutrino-mass ordering (NMO) by detecting neutrinos emitted by two nuclear power plants at a distance of about 53 km as well as to improve on several neutrino-oscillation parameters. Additionally, questions regarding solar neutrinos, supernova neutrinos, and geoneutrinos, among others, are planned to be tackled.

The central detector consists of a spherical vessel 35.4 m in diameter filled with 20 kt of linear-alkylbenzene (LAB) liquid scintillator. Charged particles passing through the detector material deposit their energy, causing the LAB to emit scintillation light. The scintillation light is registered by $\sim 10,000$ of photomultiplier tubes (PMTs) directed towards the central detector [1]. The NMO can be determined in JUNO by precisely resolving the energy spectrum of the reactor antineutrinos. The oscillations induced by the squared-mass differences of the neutrino mass eigenstates are different for both NMOs, and as such the precise positions of these oscillations can be used to distinguish between the normal and inverted NMOs [2, 3, 4].

ENERGY-TO-LIGHT CONVERSION IN SCINTILLATORS

It is of utmost importance for the success of JUNO to be able to reconstruct the energy of the primary interacting particle with a resolution of 3% at 1 MeV. Therefore, the conversion function connecting the energy of an ionizing particle with the amount of light produced by the scintillator has to be known as precisely as possible. It has been known for a long time that scintillators exhibit a nonlinear behavior for small energy depositions. The empirical Birks' law describes the differential light yield [5]:

$$\frac{\mathrm{d}L}{\mathrm{d}x} = \frac{S\frac{\mathrm{d}E}{\mathrm{d}x}}{1 + k_{\mathrm{B}}\frac{\mathrm{d}E}{\mathrm{d}x}}, \tag{1}$$

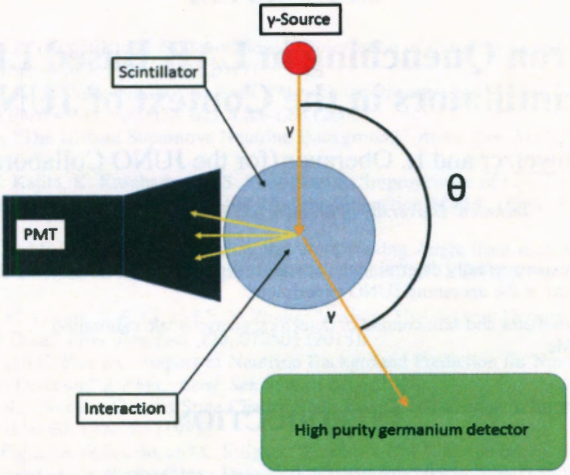

Figure 1. Scheme of the measurement principle. A radioactive source irradiates the scintillator sample with monoenergetic γ rays. The scintillation light is detected by the PMT and the scattered photon is detected by the HPGe detector.

where S is the absolute light yield, $\frac{dE}{dx}$ is the differential energy deposition per unit length and k_B is the Birks' factor. While S is an intrinsic property of each scintillator, k_B depends on the scintillator as well as on the properties of the incident ionizing particle.

Moreover, the nonlinearity parameter can have a significant distorting effect on the expected energy spectrum of the antineutrinos [6]. This can make the interpretation of the NMO very challenging. Hence, the determination of the parameter k_B is of great importance for the JUNO experiment.

MEASURING THE NONLINEARITY PARAMETER

In order to determine the energy-to-light conversion function and especially the Birks' parameter k_B, the amount of light produced per any given energy deposition has to be measured. Figure 1 shows the principle upon which the experiment is built. A monoenergetic γ source (shown in red) irradiates the scintillator sample (blue). When a γ particle from the source interacts with electrons in the target via Compton scattering, the electron produces scintillation light (yellow arrows). This light is detected by the PMT sensor (black) optically coupled to the sample. Depending on the scattering angle, the γ particle can then also reach the high-purity germanium (HPGe) detector (green) positioned near the scintillator. There, the γ particle might be absorbed and create a signal in the detector proportional to its remaining energy. Figure 2 shows a picture of the setup.

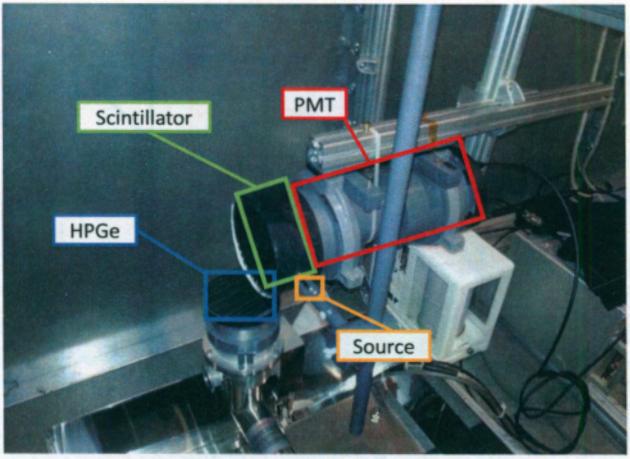

Figure 2. Picture of the experimental setup. The scintillator sample (green) and the PMT (red) which detects the scintillation light are contained in a plastic housing and constitute the light detector. Also visible are the top of the HPGe detector (blue) and the freely movable source holder (yellow).

Since the γ source emits monoenergetic photons, the amount of energy deposited in the scintillator can be easily calculated by subtracting the energy deposited in the HPGe detector from the initial energy value of the γ particle. The data-acquisition (DAQ) system employs a coincidence scheme to record only those events which produced signals in both detectors.[1] In this way, most of the registered events stem from the photon scattering as described above. We employed a ^{137}Cs source, which decays to ^{137}Ba through emission of a 661.7 keV γ particle.

We define the relative light yield (RLY) as follows:

$$\mathrm{RLY} = \frac{\text{charge of PMT signal}}{E_{\text{scintillator}}} = \frac{\text{charge of PMT signal}}{E_{\text{source}} - E_{\text{germanium}}}, \tag{2}$$

where the charge of the PMT is the integral over the PMT signal and a measure for the amount of light emitted by the scintillator, $E_{\text{scintillator}}$ is the energy deposited in the scintillator, E_{source} is the energy of photons emitted by the source, and $E_{\text{germanium}}$ is the energy measured by the HPGe detector. Therefore, the RLY is a measure of the light yield of the scintillator.

Figure 3 shows a typical spectrum obtained when the detectors are positioned as seen in Fig. 2 and the radioactive source above the scintillator cell is in a centered position. The charge of the PMT signal for each event is plotted against the energy measured by the HPGe detector. As the nonlinearity described by Eq. (1) is strongest for small

[1] Because the PMT signal is not calibrated, we could not impose cuts on the deposited energy. Therefore, we relied on Monte Carlo simulations to describe the background from accidental coincidences.

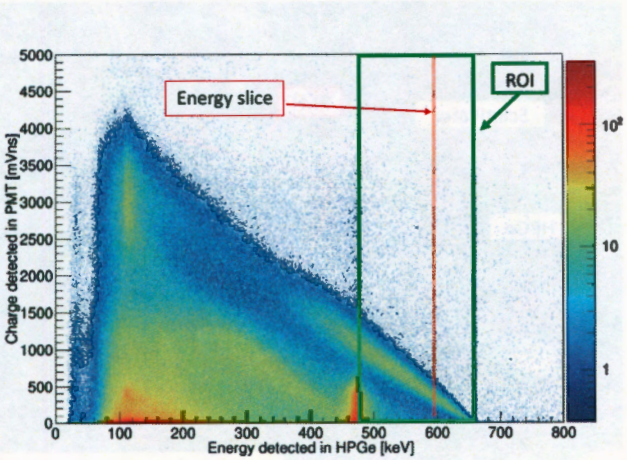

Figure 3. Two-dimensional spectrum of the measured PMT charge against the energy measured by the HPGe detector for the setup shown in Fig. 2 with the γ source located above the scintillator cell in a centered position. The nonlinearity of the scintillator is strongest for small energy depositions and approximately linear from 180 keV up, which corresponds to the ROI delimited by the green box. The RLY was fitted for each energy slice of the ROI. One of the energy slices is indicated by the red strip.

amounts of energy deposited in the scintillator, the region of interest (ROI) corresponds to large energy depositions in the HPGe detector. Following from Eq. (2), very small energy depositions correspond to energies of around 661 keV measured by the HPGe detector and all other values can be obtained by reading the horizontal axis from right to left starting from this value. The ROI was defined to include the energy depositions in the scintillator of up to 180 keV and is indicated by the green box.

Determination of the nonlinearity parameter k_B is based on fitting the RLY as a function of the energy deposited in the scintillator with the Birks' law from Eq. (1). Therefore, we divided the ROI into slices of 5 keV along the horizontal axis as illustrated by the red strip in Fig. 3. Then, we projected the events in each slice onto the RLY axis. The data in each slice were fitted with the sum of a Gaussian distribution and an appropriate model for the background. The mean of the Gaussian distribution corresponds to the RLY in the given energy range. The energy of the slice is defined as the average of the lower and upper limits of the slice.

Figure 4 shows the fitting parameters for the RLY as a function of the energy. The data were then fitted using Eq. (1), with the Birks' parameter k_B and the total scintillation efficiency S treated as free parameters. The uncertainty of the energy of each data point is given by the width of the RLY slice, whereas the uncertainty of the RLY is given by the variance of the Gaussian distribution. In the future, we plan to study full uncertainty propagation based on the determination of the charge and energy in the PMT and HPGe detector, respectively, as well as other possible sources of statistical and systematic uncertainties.

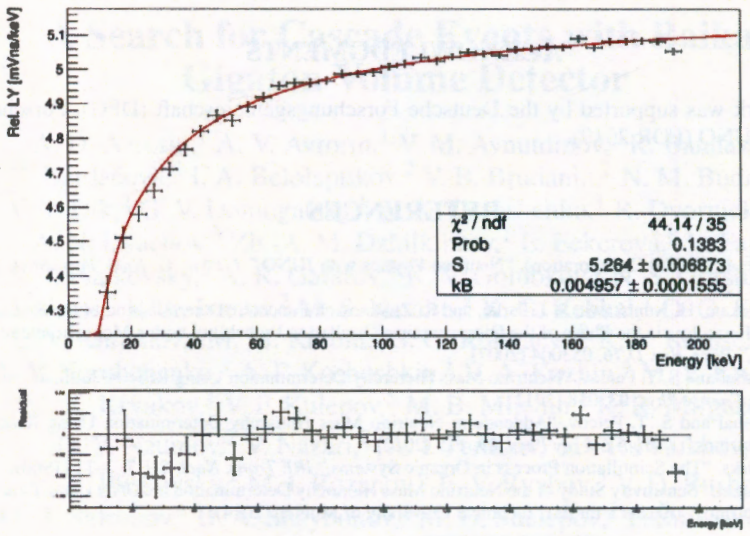

Figure 4. After fitting all the energies in the ROI from Fig. 3, the RLY of each slice was plotted against their corresponding energy. Then, Birks' law from Eq. (1) was fitted to the data with S and k_B treated as free parameters. Bottom: The residual, i.e., the difference between the data and the fitting function. In this case, the value of k_B was found to be $50\,\mu$m/MeV, whereas the preliminary result from repeated runs of the experiment was found to be $(98 \pm 8)\,\mu$m/MeV.

We characterized the experimental setup in order to exclude sources of nonlinear behavior or characterize them as systematic uncertainties. Additionally, possible gain variations of both detectors during a single measurement run have to be addressed. This is done by fitting prominent data features in all intervals of a few hours' run. By comparing the feature positions in each interval, a correction factor can be introduced and the gain drift eliminated.

CONCLUSION

We have built an experimental setup for the determination of the nonlinearity of the light yield of electrons in liquid scintillators. The primary goal of this setup is the measurement of the scintillator for the JUNO experiment to ensure a detailed knowledge of the light-to-energy conversion function, in particular to avoid a wrong interpretation of the neutrino-mass ordering. We demonstrated that our setup is capable of identifying the nonlinear behavior of our scintillator. In addition, we obtained a preliminary value of $(98 \pm 8)\,\mu$m/MeV for Birks' constant in a liquid scintillator similar to the proposed

scintillator of the JUNO experiment.

ACKNOWLEDGMENTS

This work was supported by the Deutsche Forschungsgemeinschaft (DFG), Forschergruppe JUNO (FOR 2319).

REFERENCES

1. F. An et al. (JUNO Collaboration), "Neutrino Physics with JUNO," *J. Phys. G: Nucl. Part. Phys.* **43**, 030401 (2016).
2. H. Minakata, H. Nunokawa, S. J. Parke, and R. Zukanovich Funchal, "Determination of the Neutrino Mass Hierarchy via the Phase of the Disappearance Oscillation Probability with a Monochromatic $\overline{\nu}_e$ Source," *Phys. Rev. D* **76**, 053004 (2007).
3. P. Ghoshal and S. T. Petcov, "Neutrino Mass Hierarchy Determination Using Reactor Antineutrinos," *J. High Energy Phys.* **03**, 058 (2011).
4. P. Ghoshal and S. T. Petcov, "Addendum: Neutrino Mass Hierarchy Determination Using Reactor Antineutrinos," *J. High Energy Phys.* **09**, 115 (2012).
5. J. B. Birks, "The Scintillation Process in Organic Systems," *IRE Trans. Nucl. Sci.* **7**, 2–11 (1960).
6. J. Sawatzki, "Sensitivity Study of the Neutrino Mass Hierarchy Determination in JUNO Using Reactor Antineutrinos" (master's thesis), Technical University of Munich (2014).

A Search for Cascade Events with Baikal Gigaton Volume Detector

A. D. Avrorin,[1] A. V. Avrorin,[1] V. M. Aynutdinov,[1] R. Bannash,[7] Z. Bardačová,[8] I. A. Belolaptikov,[2] V. B. Brudanin,[2] N. M. Budnev,[3] V. Y. Dik,[2] G. V. Domogatsky,[1] A. A. Doroshenko,[1] R. Dvornický,[2,8] A. N. Dyachok,[3] Zh.-A. M. Dzhilkibaev,[1] E. Eckerová,[8] L. Fajt,[9] S. V. Fialkovsky,[5] A. R. Gafarov,[3] K. V. Golubkov,[1] N. S. Gorshkov,[2] T. I. Gress,[3] R. A. Ivanov,[2] M. S. Katulin,[2] K. G. Kebkal,[7] O. G. Kebkal,[7] E. V. Khramov,[2] M. M. Kolbin,[2] S. O. Koligaev,[10] K. V. Konischev,[2] A. V. Korobchenko,[2] A. P. Koshechkin,[1] V. A. Kozhin,[4] M. V. Kruglov,[2] M. K. Kryukov,[1] V. F. Kulepov,[5] M. B. Milenin,[1] R. R. Mirgazov,[3] D. V. Naumov,[2] V. Nazari,[2] A. I. Panfilov,[1] D. P. Petukhov,[1] E. N. Pliskovsky,[2] M. I. Rozanov,[6] E. V. Ryabov,[3] V. D. Rushay,[2] G. B. Safronov,[1] B. A. Shaybonov,[2] M. D. Shelepov,[1] F. Šimkovic,[2,8,9] A. V. Skurikhin,[4] A. G. Soloviev,[2] M. N. Sorokovikov,[2] I. Štekl,[9] O. V. Suvorova,[1] E. O. Sushenok,[2] V. A. Tabolenko,[3] B. A. Tarashansky,[3] S. A. Yakovlev,[7] and D. N. Zaborov[1] (for the Baikal-GVD Collaboration)

[1] *Institute for Nuclear Research, Russian Academy of Sciences, 117312 Moscow, Russia*
[2] *Joint Institute for Nuclear Research, 141980 Dubna, Russia*
[3] *Irkutsk State University, 664003 Irkutsk, Russia*
[4] *Institute of Nuclear Physics, Moscow State University, 119991 Moscow, Russia*
[5] *Nizhny Novgorod State Technical University, 603950 Nizhny Novgorod, Russia*
[6] *St. Petersburg State Marine Technical University, 190008 St. Petersburg, Russia*
[7] *EvoLogics GmbH, 13355 Berlin, Germany*
[8] *Comenius University in Bratislava, 842 48 Bratislava, Slovakia*
[9] *Czech Technical University in Prague, 110 00 Prague, Czech Republic*
[10] *Dubna State University, 141982 Dubna, Russia*

Abstract. Baikal-GVD is a next-generation, kilometer-scale neutrino telescope currently under construction in Lake Baikal. The detector is formed by multi-megaton sub-arrays (clusters). The design of Baikal-GVD allows one to search for astrophysical neutrinos with flux values measured by IceCube already at early phases of the array construction. We present here results of the search for high-energy neutrinos via the cascade mode with data collected in the seasons 2016 and 2018.

Keywords: Baikal-GVD experiment; neutrino astronomy; high-energy physics
PACS: 95.85.Ry; 95.55.Vj; 95.30.Cq

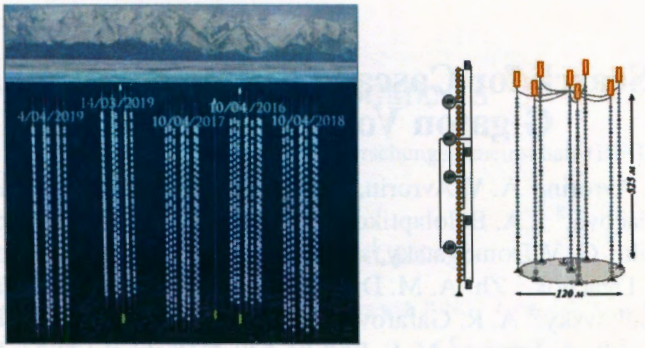

Figure 1. (a) Five Baikal-GVD clusters which are deployed and already taking data. (b) A schematic model of a cluster and a cluster string.

INTRODUCTION

The deep-underwater neutrino telescope Baikal Gigaton Volume Detector (GVD) is currently under construction in Lake Baikal [1]. The Baikal-GVD is formed by a three-dimensional array of optical modules (OMs), i.e., photomultiplier tubes located in transparent pressure spheres, arranged at vertical load-carrying cables to form strings. The telescope has a modular structure and consists of functionally independent clusters—sub-arrays comprising eight strings of optical modules, which are connected to the shore by individual electro-optical cables (Fig. 1). The first cluster named "Dubna" has been deployed and operated since 2015 in Lake Baikal. Since April 2019, the telescope has been successfully operated in a complex of five functionally independent clusters spaced at 300 m from the center of each other, where now are hosted 1440 OMs on 40 vertical strings. During Phase-1 of the Baikal-GVD implementation, an array consisting of eight clusters will be deployed by 2021. Since each GVD cluster represents a multi-megaton-scale Cherenkov detector, studies of neutrinos of different origins are allowed at early stage of the Baikal-GVD construction. Recently, a high-energy astrophysical neutrino signal has been reported by IceCube [2]. Data sample of high-energy events analysis comprises track and cascade events [3]. Baikal Collaboration has a long-term experience to search for diffuse neutrino flux with the NT200 array using cascade mode [4, 5]. The array Baikal-GVD has the potential to record astrophysical neutrinos with flux values measured by IceCube. A search for high-energy neutrinos with Baikal-GVD array is based on the selection of cascade events generated by neutrino interactions in the sensitive volume of array. Here we describe the cascade-event simulation and reconstruction procedures and discuss the first preliminary results obtained by analysis of data collected with the Baikal-GVD array in 2018.

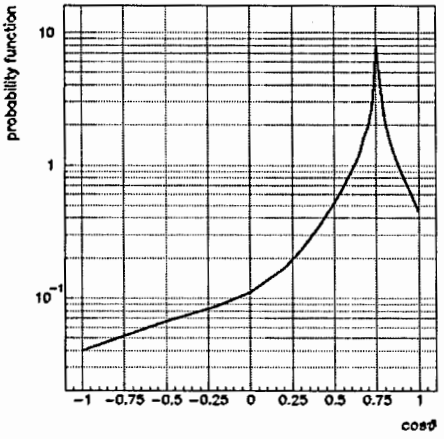

Figure 2. Angular distribution of the Cherenkov radiation from high-energy electromagnetic showers averaged over all charged-particle tracks.

CHERENKOV RADIATION OF CASCADES

The total number of Cherenkov photons from an electromagnetic or hardronic cascade is proportional to the cascade energy $E_{\rm sh}$:

$$N_{\rm ch}^{\rm tot} \approx 10^8 \frac{E_{\rm sh}}{\rm TeV}. \tag{1}$$

The number of Cherenkov photons $N_{\rm ch}(x, \vartheta, t)\,{\rm d}x\,{\rm d}\Omega\,{\rm d}t$ emitted at time t from an interval ${\rm d}x$ along the shower near point x in a spatial angle ${\rm d}\Omega$ at an angle ϑ to the shower axis can be represented as:

$$N_{\rm ch}(x, \vartheta, t) \approx N_{e^\pm}(x)\,\Psi(\vartheta)\,n_{\rm ch}\,\delta(t - x/c)\,{\rm d}x\,{\rm d}\Omega\,{\rm d}t, \tag{2}$$

where $N_{e^\pm}(x)$ is the linear density of electrons and positrons along the shower, $n_{\rm ch}$ is the linear density of Cherenkov radiation of electrons, and $\Psi(\vartheta)$ is the angular distribution of Cherenkov photons.

Photons emitted from vicinity of the shower-profile maximum dominate in the total Cherenkov radiation. It allows to use the angular distribution of Cherenkov photons in the shower maximum $\Psi(\vartheta)$ (Fig. 2) for every shower interval Δx. The longitudinal shower length is divided into intervals Δx and the shower is considered as a superposition of point sources of Cherenkov radiation located at the center of each interval Δx with the intensity $N_{\rm ch}(x, \Delta x, \vartheta, t)$.

LIGHT PROPAGATION AND OM RESPONSE

The response of OM on a shower Cherenkov radiation is simulated in two steps. In the first step, the propagation of Cherenkov radiation of a point-like shower from the source to the photosensor is simulated taking into account the angular distribution of radiation in the source and the spectral dependencies of absorption and scattering of light in the water, PMT quantum efficiency, as well as Cherenkov-light intensity and light velocity. A volume of about $10^8\,\mathrm{m}^3$ around the shower origin is filled with detection spheres with a size of the OM. When a simulated photon, moving in the direction $\Omega(\vartheta, \varphi)$, crosses the detection sphere located at the distance $r(\rho, z)$ from the shower vertex at a time t, the value in the corresponding cell of a table—which describes the spatial, directional, and temporal photon distribution—is increased by the value of PMT quantum efficiency corresponding to the photon wavelength. In the second step, a five-dimensional table for the expected average number of photoelectrons $n_{\mathrm{pe}}(\rho, z, \vartheta, \varphi, \tau)$ is generated by folding the photon flux obtained in the first step with the OM angular sensitivity. The variables ρ and z characterize the OM position relative to a point-like shower—the distance from the OM to the shower axis ρ and the coordinate along the z axis oriented in the direction opposite to that of the shower axis. The polar angle ϑ (measured from the direction coincident with the z direction) and the azimuth angle φ characterize the orientation of the OM with respect to the shower. The variable τ characterizes the time delay of the recorded photons relative to the arrival time of the direct photons.

RECONSTRUCTION METHOD

The procedure for reconstructing the parameters of high-energy showers—the shower energy, direction, and vertex—is performed in two steps. In the first step, the shower-vertex coordinates are reconstructed using the time information from the struck photosensors of the telescope. In this case, the shower is assumed to be a point-like source of light. The χ^2 minimization parameters are shower the coordinates ((x, y, z) in a Cartesian coordinate system or (r, ϑ, φ) in a spherical coordinate system):

$$\chi^2 = \frac{1}{(N_{\mathrm{hit}} - 4)} \sum_{i=1}^{N_{\mathrm{hit}}} \left(T_{\mathrm{th}_i}(\vec{r}_{\mathrm{sh}}, t_0) - T_{\mathrm{exp}_i}\right)^2 / \sigma^2, \tag{3}$$

where T_{exp_i} and T_{th_i} are the experimentally measured and theoretically expected trigger times of the i^{th} photosensor, t_0 is the shower generation time, σ is the uncertainty in measuring the time, and N_{hit} is the hit multiplicity.

In the second step, the shower energy and direction are reconstructed by applying the maximum-likelihood method and using the shower coordinates reconstructed in the first step. The values of the variables ϑ, φ, and E_{sh} corresponding to the minimum value of the following functional are chosen as the polar and azimuthal angles characterizing the shower direction and energy:

$$L_A = -\sum_{i=1}^{N_{\mathrm{hit}}} \log\left(p_i(A_i, E_{\mathrm{sh}}, \Omega_{\mathrm{sh}}(\vartheta, \varphi))\right). \tag{4}$$

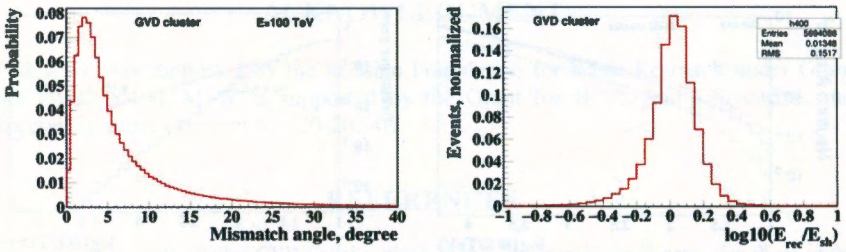

(a) (b)

Figure 3. (a) Accuracy of the cascade-direction reconstruction. (b) Accuracy of the cascade-energy reconstruction.

The functions $p_i(A_i, E_{\text{sh}}, \Omega_{\text{sh}}(\vartheta, \varphi))$ are the probabilities for a signal with amplitude A_i (measured in photoelectrons) from a shower with energy E_{sh} and direction Ω_{sh} to be recorded by the i^{th} triggered photosensor:

$$p_i = \sum_{i=1}^{N_{\text{hit}}} P(n \mid n_{\text{pe}}) \int_{A_i-\alpha/2}^{A_i+\alpha/2} \xi_i(A, n)\, \mathrm{d}A, \tag{5}$$

where $P(n \mid n_{\text{pe}})$ is the probability of detecting n photoelectrons at the mean n_{pe} of a Poisson distribution, $\xi(A, n)$ is the probability density function for recording the amplitude A at an exposure level of n photoelectrons, and α is the scale-division value of the amplitude in photoelectrons. The mean n_{pe} is determined by simulating the responses of the telescope's OMs to the Cherenkov radiation of a shower with energy E_{sh} and direction Ω_{sh} with allowance made for the light propagation in water, the relative positions and orientation of the OMs and the shower, and the effective OM sensitivity.

CASCADE DETECTION IN ONE CLUSTER

The search for high-energy neutrinos with a cluster array is based on the selection of cascade events generated by neutrino interactions in the sensitive volume of the array. Performances of event-selection and cascade-reconstruction procedures were tested by MC simulation of the signal and background events and reconstruction parameters of the cascades. The accuracy of cascade-energy reconstruction is about 30%, while the accuracy of direction reconstruction is about 4° (Fig. 3). The neutrino-effective areas for different flavors averaged over all arrival angles are shown in Fig. 4(a). The energy distributions of cascade events expected for one year of observation from astrophysical fluxes following a power-law $E^{-2.46}$ spectra and single-flavor normalizations $4.1 \times 10^{-6}\,\text{GeV}^{-1}\,\text{cm}^{-2}\,\text{s}^{-1}\,\text{sr}^{-1}$ [3] as well as the distribution of expected background shower events from atmospheric neutrinos are shown in Fig. 4(b). The expected number of background events from atmospheric neutrinos is strongly suppressed for energies higher than 100 TeV. About 0.4 cascade events per year with energies above 100 TeV

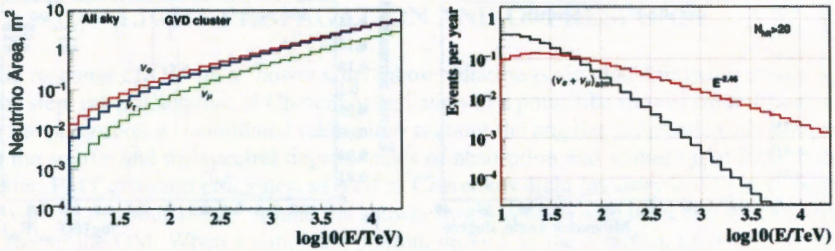

(a) (b)

Figure 4. (a) Neutrino-effective areas for different flavors. (b) Energy distributions of cascade events expected for one year observation.

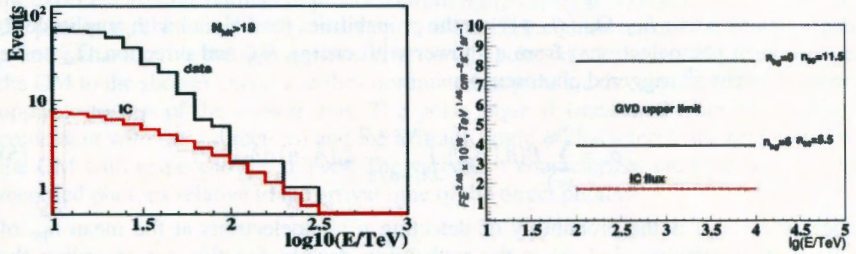

(a) (b)

Figure 5. (a) Energy distribution of the events with $N_{\text{hit}} > 19$. (b) Upper bound on the astrophysical flux from Baikal-GVD and IceCube.

and hit multiplicities $N_{\text{hit}} > 20$ from the astrophysical fluxes with $E^{-2.46}$ spectra, respectively, and 0.08 background events from the atmospheric neutrinos are expected.

RESULTS

For the search for a high-energy neutrino flux of astrophysical origin, the data collected in the seasons 2016 and 2018 were used. The data sample corresponds to 368 live days and to about 5×10^9 events for the subsequent analysis. After applying an iterative procedure of the cascade-vertex reconstruction for hits with charge higher than 1.5 photoelectrons, followed by a rejection of the hits contradicting the cascade hypothesis at each iteration stage, cascade-energy reconstruction and event-quality cuts applying, 2,704 cascade-like events have been selected with $N_{\text{hit}} > 10$ and $E > 10$ TeV. A total of six events from the final sample were reconstructed with energies above 100 TeV and $N_{\text{hit}} > 19$. Energy distribution of events with $N_{\text{hit}} > 19$ is shown in Fig. 5(a). In Fig. 5(b) is shown the astrophysical flux in the conservative case ($n_{\text{bg}} = 0$) and in the most stringent case ($n_{\text{bg}} = 6$). Upper limit on the flux is consistent with the IceCube results.

ACKNOWLEDGMENTS

This work was supported by the Russian Foundation for Basic Research under Grant No. 20-02-00400. M. S. is supported by the Grant for JINR Young Scientists and Specialists under Contract No. 20-202-09.

REFERENCES

1. A. D. Avrorin et al. (Baikal-GVD Collaboration), "The Prototyping/Early Construction Phase of the Baikal-GVD Project," *Nucl. Instrum. Meth. A* **742**, 82–88 (2014).
2. M. G. Aartsen et al. (IceCube Collaboration), "Evidence for High-Energy Extraterrestrial Neutrinos at the IceCube Detector," *Science* **342**, 1242856 (2013).
3. M. G. Aartsen et al. (IceCube Collaboration), "Observation of High-Energy Astrophysical Neutrinos in Three Years of IceCube Data," *Phys. Rev. Lett.* **113**, 101101 (2014).
4. V. M. Aynutdinov et al. (Baikal-GVD Collaboration), "Search for a Diffuse Flux of High-Energy Extraterrestrial Neutrinos with the NT200 Neutrino Telescope," *Astropart. Phys.* **25**, 140–150 (2006).
5. A. V. Avrorin et al. (Baikal-GVD Collaboration), "Search for high-energy neutrinos in the Baikal neutrino experiment," *Astron. Lett.* **35**, 651 (2009).

Multicluster Events in the Baikal-GVD Telescope

A. D. Avrorin,[1] A. V. Avrorin,[1] V. M. Aynutdinov,[1] R. Bannash,[7]
Z. Bardačová,[8] I. A. Belolaptikov,[2] V. B. Brudanin,[2] N. M. Budnev,[3]
V. Y. Dik,[2] G. V. Domogatsky,[1] A. A. Doroshenko,[1] R. Dvornický,[2,8]
A. N. Dyachok,[3] Zh.-A. M. Dzhilkibaev,[1] E. Eckerová,[8] L. Fajt,[9]
S. V. Fialkovsky,[5] A. R. Gafarov,[3] K. V. Golubkov,[1] N. S. Gorshkov,[2]
T. I. Gress,[3] R. A. Ivanov,[2] M. S. Katulin,[2] K. G. Kebkal,[7] O. G. Kebkal,[7]
E. V. Khramov,[2] M. M. Kolbin,[2] S. O. Koligaev,[10] K. V. Konischev,[2]
A. V. Korobchenko,[2] A. P. Koshechkin,[1] V. A. Kozhin,[4] M. V. Kruglov,[2]
M. K. Kryukov,[1] V. F. Kulepov,[5] M. B. Milenin,[1] R. R. Mirgazov,[3]
D. V. Naumov,[2] V. Nazari,[2] A. I. Panfilov,[1] D. P. Petukhov,[1]
E. N. Pliskovsky,[2] M. I. Rozanov,[6] E. V. Ryabov,[3] V. D. Rushay,[2]
G. B. Safronov,[1] B. A. Shaybonov,[2] M. D. Shelepov,[1] F. Šimkovic,[2,8,9]
A. V. Skurikhin,[4] A. G. Soloviev,[2] M. N. Sorokovikov,[2] I. Štekl,[9]
O. V. Suvorova,[1] E. O. Sushenok,[2] V. A. Tabolenko,[3] B. A. Tarashansky,[3]
S. A. Yakovlev,[7] and D. N. Zaborov[1] (for the Baikal-GVD Collaboration)

[1] *Institute for Nuclear Research, Russian Academy of Sciences, 117312 Moscow, Russia*
[2] *Joint Institute for Nuclear Research, 141980 Dubna, Russia*
[3] *Irkutsk State University, 664003 Irkutsk, Russia*
[4] *Institute of Nuclear Physics, Moscow State University, 119991 Moscow, Russia*
[5] *Nizhny Novgorod State Technical University, 603950 Nizhny Novgorod, Russia*
[6] *St. Petersburg State Marine Technical University, 190008 St. Petersburg, Russia*
[7] *EvoLogics GmbH, 13355 Berlin, Germany*
[8] *Comenius University in Bratislava, 842 48 Bratislava, Slovakia*
[9] *Czech Technical University in Prague, 110 00 Prague, Czech Republic*
[10] *Dubna State University, 141982 Dubna, Russia*

Abstract. Baikal-GVD is a cubic-kilometer-scale neutrino telescope which is currently under construction in Lake Baikal. In 2019, it consisted of five standalone telescope units, functionally complete smaller-scale detectors, the clusters, which can operate independently. The time synchronization system allows us to perform a search for causally related events detected on different clusters, the multicluster events. We present a preliminary analysis of the multicluster events in the Baikal-GVD telescope.

Keywords: Cherenkov detectors
PACS: 29.40.Ka; 95.55.Vj

INTRODUCTION

The neutrino telescope Baikal Gigaton Volume Detector (Baikal-GVD) is installed in Lake Baikal at a 1,366 m depth and 3.6 km from the shore [1]. In 2021, it will consist

of nine clusters—2,592 optical modules (OMs)—with sensitive volume $\sim 0.4\,\mathrm{km}^3$. Five clusters—1,440 OMs—have been already installed and they are currently running and taking data. The Baikal-GVD Collaboration consists of 52 physicists and engineers from nine institutions. Lake Baikal has very clear water (low absorption and scattering) and it also freezes for a few months each year which provides an ideal platform for detector installation and maintenance. Every clusters consists of eight strings (one central plus seven peripheral) of 525 m length wherein there are 36 OMs divided into three sections on every string. In every section, there is also a Central Module with 12-bit 12-channel 200 MHz FADC which processes all signals from the 12 OMs in the section. The basic detection unit is an OM which comprises a PMT R7080-100, a controller, calibration LEDs, and electronics. Every string also includes four acoustic modules for position measurements.

Currently, the data processing in the Baikal-GVD telescope is designed for a single-cluster events reconstruction, i.e., the analyzed data from the optical modules are from one cluster. In 2019, the five clusters operated—a collection of five sets of the single-cluster events is accumulated. Indeed, the time synchronization system allows us to perform further progress in the telescope data analysis, which is the production of multicluster events. Usage of the multicluster events in the reconstruction improves the energy and angular resolutions, and also allows to suppress the background significantly. Moreover, the OM responses on several clusters indicate high-energy neutrinos. Thus, the multi-cluster events are an appropriate tool for the alert-messages formation of Baikal-GVD. An important task for the development of data analysis is the procedure of creation of the multicluster events. In other words, a search for causally related single-cluster events and their joining to one databank.

TIME SYNCHRONIZATION SYSTEM

The Baikal-GVD telescope has two independent time synchronization systems (TSS) [2]. The first one is the Synchronization System of the Baikal Telescope (SSBT) that was developed especially for the detector. The second one, being more widely used, is the White Rabbit (WR). In this approach, it is assumed that both systems independently assign time marks to the trigger signals from different clusters. This allows to perform a mutual control of their operation. The SSBT is equipped with the high-precision rubidium oscillator with thermostabilization, which provides a time resolution of $\sim 10\,\mathrm{ns}$ for the system (with a possibility of improvement down to $\sim 5\,\mathrm{ns}$). The WR time synchronization system has a time resolution of $\sim 1\,\mathrm{ns}$ and is able to operate in two modes: using both the internal generator and the external high-precision GPS time server. It is worth mentioning that there is a possibility of time-marks connection from SSBT and WR with the pulse-per-second (PPS) signals generated by the WR system.

SEARCH FOR MULTICLUSTER EVENTS

Currently, the search for multicluster events is realized in pairs of clusters. In the 2018 season, the time synchronization systems operated only on the two clusters (clusters

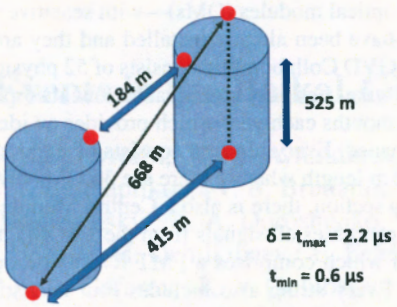

Figure 1. Time window δ for a track-like event between the clusters No. 2 and 3.

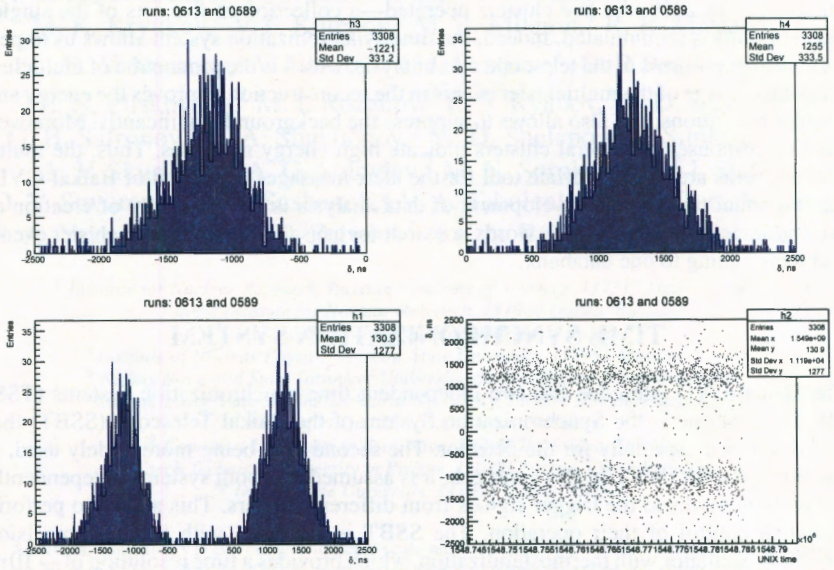

Figure 2. Distributions of multicluster events in the standard type of run.

No. 2 and 3). However, in the 2019 season, all five clusters were equipped with TSS and the recorder events have synchronized time stamps. In summary, the number of datasets for clusters paired with TSS is one in 2018 and ten in 2019. The selection condition for multicluster events is $|t_i - t_j| < \delta$, where t_i and t_j are the detection times of events in two different clusters. The time window δ is determined by the geometry of the telescope, $\delta = l_{\max}/c$, where $l_{\max}$ is the maximum distance between the OMs in the two clusters, and c is the speed of light (Fig. 1).

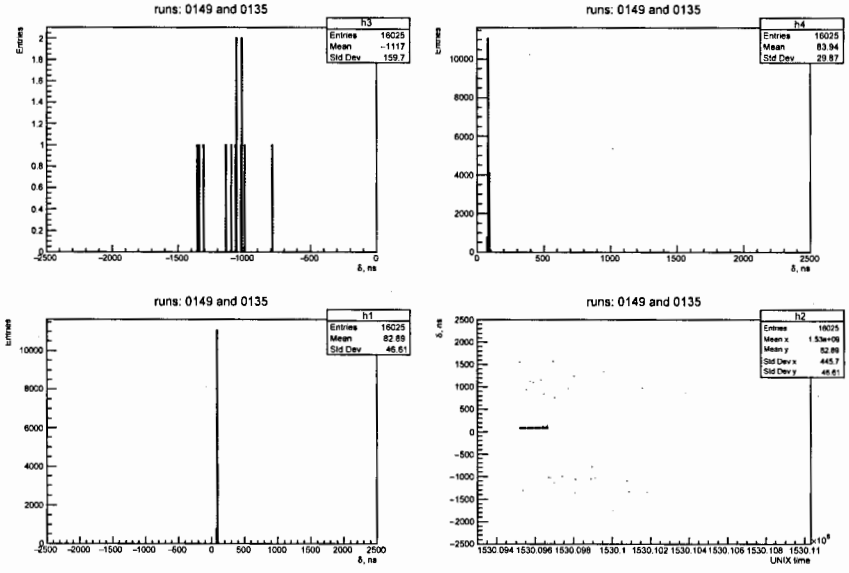

Figure 3. Distributions of multicluster events in the laser type of run.

Distributions of the multicluster events were obtained using the selection condition (Fig. 2). The two peaks correspond to the opposite directions of the muon propagation through the two clusters. There is a substrate of background light beyond the time borders for track-like event ($\pm 2.2\,\mu$s and $\pm 0.6\,\mu$s). The mean propagation time was $\sim 1.2\,\mu$s, which corresponds to an effective distance of ~ 360 m.

The string with laser calibration source was deployed near the cluster No. 2 and cluster No. 3, and it is 18.6 m closer to the cluster No. 2, which corresponds to a time difference of ~ 85 ns. Fig. 3 shows the multicluster event distributions obtained in the run with the laser calibration source (the laser run). The mean value of time differences of the multicluster events is consistent with the expected difference in the propagation times of a laser flash to the clusters. Small amount of the background light is due to a high trigger condition during the laser run.

RATE OF MULTICLUSTER EVENTS

In 2018, about 700 runs were launched on the clusters No. 2 and 3, most of which overlapped in time. In Fig. 4, we present the total amount of multicluster events and its rate in a $5\,\mu$s time window during the whole year. We found that the total amount of multicluster events for standard runs is about 5×10^3, while for laser sessions it lies in the range $(12\text{–}35) \times 10^3$, with the exception of the standard runs with a large

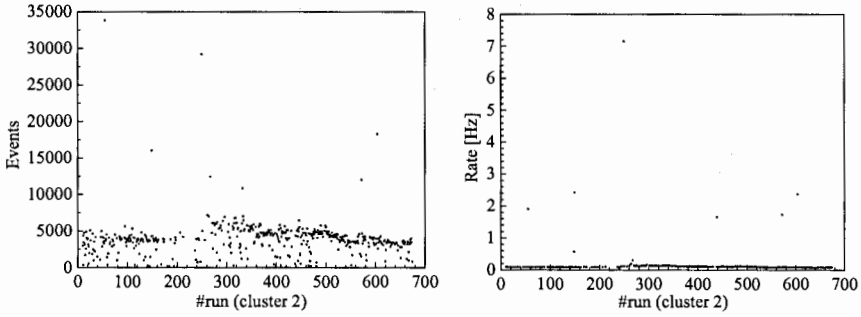

Figure 4. (a) Total amount and (b) rate of multicluster events during the 2018 season.

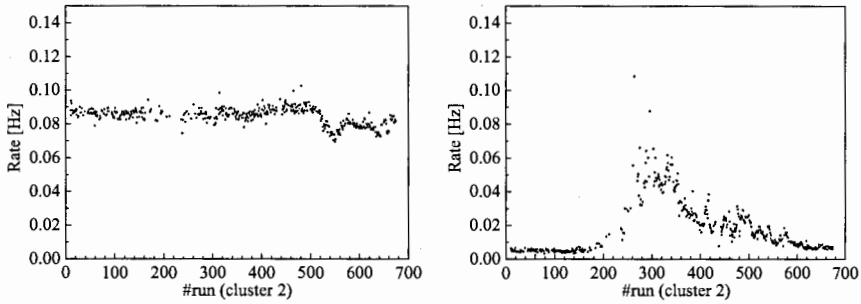

Figure 5. Rates of multicluster events during the 2018 season: (a) Allowable multicluster events. (b) Background light.

duration during the unstable period and the test laser runs (runs No. 267, 332, and 148, 439, respectively). The laser runs also stand out in terms of the rate (> 0.5 Hz), as the multicluster event rate in the standard sessions is suppressed.

Multicluster events in the 5 μs time window contain a contribution of the background light, which is partly excluded. The multicluster events that are in the allowed time borders for track-like events have a stable rate of ~ 0.1 Hz (Fig. 5). It is 10^2–10^3 times smaller than the rate of the single-cluster events. On the other hand, we see a dynamical behavior of the rate of the background light: there are two relatively stable periods which are intermitted with increased optical activity related to highly luminescent water [3].

In Fig. 6, we show the 2019 data for the new clusters No. 4 and 5. The rate of allowable multicluster events is practically constant and has the maximum value (0.2 Hz) among the cluster pairs. A beginning of the increased optical activity is seen, and the rate of the background light during the stable period is smaller by a factor of ~ 2 in comparison to the rate of the allowable multicluster events.

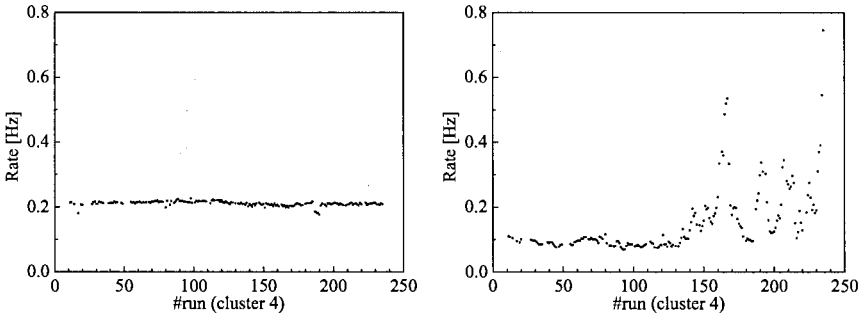

Figure 6. Rates of multicluster events between the clusters No. 4 and 5 during the 2019 season: (a) Allowable multicluster events. (b) Background light.

CONCLUSION

We presented the data on multicluster events in the Baikal-GVD neutrino telescope. We found that during the 2018 season, the rate of the multicluster events in the standard runs is about 0.1 Hz, and it is 10^2–10^3 times smaller than the rate of the single-cluster events. The mean propagation time through two clusters is $\sim 1.2\,\mu$s, which corresponds to an effective distance of ~ 360 m. In data from the 2019 season, the rate of the multicluster events was in the range 0.025–0.2 Hz, with a maximum value for the cluster No. 4–5 pair and a minimum one for the cluster No. 3–5 pair. We found an unstable period of the background light, namely, an increase in the optical noise activity associated with the luminescence of the Baikal water. At the time of writing, we also see the start of an unstable period in the current season.

ACKNOWLEDGMENTS

This work was supported by the Russian Foundation for Basic Research under Grant No. 20-02-00400. M. S. is supported by the Grant for JINR Young Scientists and Specialists under Contract No. 20-202-09.

REFERENCES

1. A. D. Avrorin et al. (Baikal-GVD Collaboration), "Status of the Baikal-GVD Neutrino Telescope," *EPJ Web Conf.* **207**, 01003 (2019).
2. A. D. Avrorin et al. (Baikal-GVD Collaboration), "The Inter-Cluster Time Synchronization Systems within the Baikal-GVD Detector," *arXiv:1908.05533 [physics.ins-det]* (2019).
3. A. D. Avrorin et al. (Baikal-GVD Collaboration), "Luminescence of Water in Lake Baikal Observed with the Baikal-GVD Neutrino Telescope," *EPJ Web Conf.* **207**, 09002 (2019).

Initial-State Interaction of the ^{20}Ne+^{76}Ge Nuclear Reaction at 306 MeV

A. Spatafora,[1,2] F. Cappuzzello,[1,2] D. Carbone,[1] M. Cavallaro,[1] J. A. Lay,[3,4] L. Acosta,[5] C. Agodi,[1] D. Bonanno,[6] D. Bongiovanni,[1] I. Boztosun,[7] G. A. Brischetto,[1,2,8] S. Burrello,[1] S. Calabrese,[1,2] D. Calvo,[9] E. R. Chávez Lomelí,[5] I. Ciraldo,[1,2] M. Colonna,[1] F. Delaunay,[9,10,11] N. Deshmukh,[1] J. L. Ferreira,[12] P. Finocchiaro,[1] M. Fisichella,[9] A. Foti,[6] G. Gallo,[1,2] A. Hacısalihoğlu,[1,13] F. Iazzi,[9,10] G. Lanzalone,[1,14] H. Lenske,[15] R. Linares,[12] D. Lo Presti,[2,6] J. Lubian,[12] M. Moralles,[16] A. Muoio,[1] J. R. B. Oliveira,[17] A. Pakou,[18] L. Pandola,[1] H. Petrascu,[19] F. Pinna,[9,10] S. Reito,[6] G. Russo,[2,6] G. Santagati,[1] O. Sgouros,[1] S. O. Solakci,[7] V. Soukeras,[1] G. Souliotis,[20] D. Torresi,[1] S. Tudisco,[1] A. Yildirim,[7] and V. A. B. Zagatto[17] (for the NUMEN Collaboration)

[1] *Laboratori Nazionali del Sud, 95123 Catania, Italy*
[2] *University of Catania, 95123 Catania, Italy*
[3] *University of Seville, 41012 Seville, Spain*
[4] *Carlos I Interuniversity Institute of Theoretical and Computational Physics, 41080 Seville, Spain*
[5] *National Autonomous University of Mexico, 04510 Mexico City, Mexico*
[6] *National Institute for Nuclear Physics, 95123 Catania, Italy*
[7] *Akdeniz University, 07058 Antalya, Turkey*
[8] *Sicilian Center of Nuclear Physics and Physics of Matter, 95125 Catania, Italy*
[9] *National Institute for Nuclear Physics, 10125 Turin, Italy*
[10] *Polytechnic University of Turin, 10129 Turin, Italy*
[11] *Laboratoire de Physique Corpusculaire de Caen, 14050 Caen, France*
[12] *Fluminense Federal University, 24210 Niterói, Brazil*
[13] *Karadeniz Technical University, 61080 Trabzon, Turkey*
[14] *Kore University of Enna, 94100 Enna, Italy*
[15] *University of Giessen, 35390 Giessen, Germany*
[16] *Nuclear and Energy Research Institute, 05508 São Paulo, Brazil*
[17] *University of São Paulo, 05508 São Paulo, Brazil*
[18] *University of Ioannina and Hellenic Institute of Nuclear Physics, 45110 Ioannina, Greece*
[19] *Horia Hulubei National Institute for R&D in Physics and Nuclear Engineering, 077125 Bucharest–Măgurele, Romania*
[20] *University of Athens and Hellenic Institute of Nuclear Physics, 15784 Zografou, Greece*

Abstract. A study of the ^{20}Ne + ^{76}Ge elastic and inelastic scatterings at the incident energy of 306 MeV was performed at the Laboratori Nazionali del Sud (LNS), National Institute for Nuclear Physics (INFN), by the NUMEN Collaboration. The experiment, data reduction, and theoretical analysis presented here are key tools for studying the initial-state interaction of the ^{20}Ne + ^{76}Ge nuclear system at 306 MeV. This task is crucial for a correct description of the reaction mechanism of double-charge-exchange transitions between such heavy ions.

Keywords: neutrinoless double-beta decay; nuclear reactions; elastic scattering
PACS: 23.40.Hc; 24.10.−i; 25.55.Ci

INTRODUCTION

The main goal of the NUMEN (NUclear Matrix Elements for Neutrinoless double-beta decay) project is to study the double-charge-exchange (DCE) nuclear reactions in order to extract information about the nuclear matrix elements (NMEs) of interest in the context of neutrinoless double-beta ($0\nu\beta\beta$) decay [1]. The theoretical basis of the connection between the measured cross sections of DCE reactions and the $0\nu\beta\beta$-decay NMEs is presently under study [2, 3, 4]. The DCE NME is defined as follows:

$$M^{\mathrm{DCE}} = \langle \chi_\beta | \hat{O}^{\mathrm{DCE}} | \chi_\alpha \rangle , \tag{1}$$

where the operator $\hat{O}^{\mathrm{DCE}}$ describes the nuclear DCE transition from the initial distorted wave function $|\chi_\alpha\rangle$ of the incoming partition α to the final state $|\chi_\beta\rangle$ of the outgoing partition β.

A good description of the reaction mechanism depends on the knowledge of the optical potential responsible for the distortion of the wave function for the initial partition. Furthermore, an accurate study of the dependence of theoretical results on the model space used is mandatory. For these purposes, the study of elastic and inelastic transitions is a key tool. Reactions involving a few selected degrees of freedom, keeping the bulk of projectile and target essentially intact, are the most appropriate tools for those investigations and the theory of direct reactions can provide a suitable toolbox. In the past two years, the NUMEN Collaboration started an experimental campaign through the study of DCE reactions and competing transfer, single-charge-exchange, and other quasielastic channels in the ^{76}Ge–^{76}Se pair of isotopes[5]. In this work, we introduce the experiment, data reduction, and theoretical analysis concerning the ^{20}Ne + ^{76}Ge elastic and inelastic scatterings.

EXPERIMENT AND DATA REDUCTION

A beam of $^{20}Ne^{10+}$ ions was accelerated up to 306MeV by the Superconducting Cyclotron at the LNS, INFN. The $^{20}Ne^{10+}$ ions impinged on a target consisting of a $390\,\mu g/cm^2$ layer 98% isotopically enriched in ^{76}Ge, evaporated onto a $60\,\mu g/cm^2$ carbon backing, on the object point of the MAGNEX spectrometer [6]. The ejectiles produced in the reactions were momentum-analyzed in different runs in which the optical axis of MAGNEX was oriented, relative to the beam direction, at the angles $\theta_{\mathrm{opt}} = 8°, 13°, 16°, 19°$. In four runs, at each angle, the MAGNEX-entrance solid angle was set to about 50msr by means of slits at the entrance of the spectrometer. The overall range of polar angles in the center-of-mass framework was $4° < \theta_{\mathrm{c.m.}} < 25°$. The magnetic fields of the dipole and quadrupole magnets were set to transport the $^{20}Ne^{10+}$ ions corresponding to the elastic-scattering events at the center of the Focal-Plane Detector (FPD) [7].

The data-reduction strategy includes a position calibration of the FPD, identification of the $^{20}Ne^{10+}$ ejectiles, and reconstruction of the momentum vector at the target by inversion of the transport equations following the guidelines presented in previous publications [8, 9, 10, 11]. The excitation energy E_x was extracted by means of the

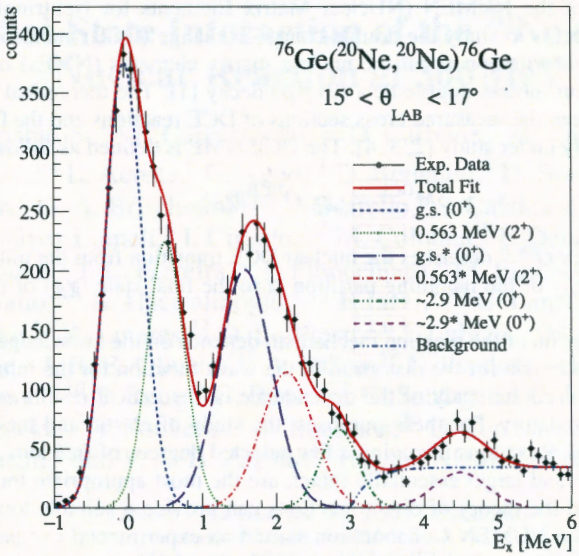

Figure 1. Energy spectrum of ^{76}Ge for the ^{20}Ne + ^{76}Ge elastic-scattering reaction at the bombarding energy of 306 MeV and angle $15° < \theta_{LAB} < 17°$. The total spectrum (red solid line) as well as individual peaks from particular nuclear transitions were obtained by fitting the experimental data (black points). Many states are expected to be populated starting from 3 MeV and are summarized in the fit by the unique background curve. The curves marked with an asterisk correspond to the states in which ^{20}Ne is in the 2^+ state at 1.634 MeV.

relativistic kinematic transformations for binary reactions, adjusted to the projectile and target atomic masses. In Fig. 1, a typical excitation-energy spectrum of $ce^{76}Ge$ for the ^{20}Ne + ^{76}Ge elastic scattering is shown. The energy resolution of about 0.5 MeV is not sufficient to clearly resolve the 0^+ ground state (g.s.) and the 2^+ excited state of the $ce^{76}Ge$ target at 0.563 MeV. At about 1.6 MeV, the structure originates from the sum of a large number of states. The 2^+ excited state of ^{20}Ne at 1.634 MeV is dominant and the contribution at $(0.563 + 1.634)$ MeV that corresponds to the excitation of both the target and the projectile 2^+ states is also important. In the same structure, another state is present at about 2.9 MeV, also visible at about $(2.9 + 1.634)$ MeV. This state is compatible with the 0^+ state of ^{76}Ge at 2.897 MeV.

The fit shown in Fig. 1 was performed using a function which results from a convolution of many functions. This procedure was performed in different angular slices of almost 0.4° between 5° and 22° in order to extract the number of counts for each state and angle. In this way, it was possible to extract the angular distributions of the differential cross section for the transitions to the g.s. and to the first low-lying excited states

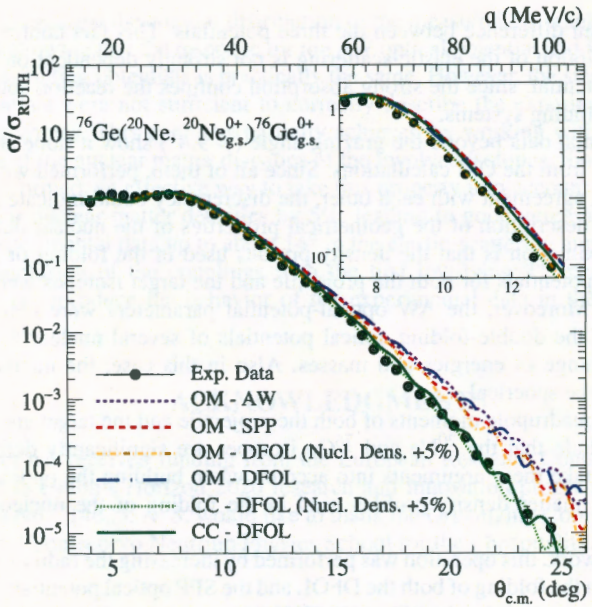

Figure 2. Angular distribution of the elastic differential cross section σ relative to the Rutherford cross section σ_{RUTH}. The curves represent the calculations performed with three different types of optical potentials in the context of the optical-model approximation and in the coupled-channels approach. Two different geometries of the projectile and target nuclear densities were used.

of both the projectile and the target. An example of the g.s.-to-g.s. angular distribution of the differential cross section is shown in Fig. 2 and a description of the underlying theoretical calculations is presented in the next section. More details on the analysis and data reduction are presented in Ref. [12].

THEORETICAL ANALYSIS

The theoretical description of the angular distributions for the elastic and inelastic channels of the $^{20}Ne + ^{76}Ge$ collision was performed using the FRESCO code [13]. The influence of the choice of different types of optical potentials was investigated by comparing the calculation results obtained within the optical model (OM) with the angular distribution of the elastic differential cross section. Three different optical potentials were tested: the parametric Akyüz–Winther (AW) potential [14, 15] as well as two double-folding optical potentials, namely the DFOL potential [16] and the São Paulo potential (SPP) [17, 18, 19, 20].

The results of the OM calculations performed with the three tested optical potentials and the experimental data in the σ/σ_{RUTH} representation are shown in Fig. 2. There is

not any significant difference between the three potentials. This fact confirms that the theoretical description of the elastic scattering is not strongly dependent on the choice of the optical potential, since the strong absorption confines the reaction source on the surface of the colliding systems.

The experimental data beyond the grazing angle ($\sim 9.4°$) show a slope steeper than the one obtained from the OM calculations. Since all of them, performed with different potentials, are in agreement with each other, the discrepancy could indicate a common drawback in the description of the geometrical properties of the nuclear densities. An important approximation is that the density profiles used in the folding of the DFOL and SPP optical potentials for both the projectile and the target isotopes were assumed to be spherical. Moreover, the AW optical-potential parameters were obtained from interpolations of the double-folding optical potentials of several nuclear systems in a relatively large range of energies and masses. Also in this case, the nuclear systems were assumed to be spherical.

Since the g.s. quadrupole moments of both the projectile and the target are large [21], one has to conclude that the ^{20}Ne and ^{76}Ge isotopes are significantly deformed. An effective way to take these arguments into account when building the optical potential is to change the matter density profiles used in the folding of the nucleon–nucleon interactions.

In the present work, this operation was performed by increasing the radii of the nuclear density profiles in the folding of both the DFOL and the SPP optical potentials by 5% and renormalizing the central-density parameter [12]. A comparison between the standard approach and the new one is shown in Fig. 2. The increase in the radii appears to be important in order to correctly describe the experimental shape up to about 14°, where the geometrical properties of the nuclei are more relevant.

However, the change in slope observed in the experimental data above 14° is still not described by the OM framework because of the missing couplings with the first low-lying excited states. This phenomenon can be clearly seen when comparing all the curves in Fig. 2 with the blue one (OM-DFOL). In this calculation, which was performed within the coupled-channel framework, the couplings with the first 2^+ excited states of both the projectile and the target were introduced within the theoretical framework of the macroscopic rotational model (more details on this procedure can be found in Ref. [12]). The optical potential used was the DFOL potential and the modification of the radii of both the projectile and the target nuclear densities was also applied. This result is in good agreement with the experimental data in the whole range of transferred momenta explored by the experiment.

CONCLUSIONS

The elastic and inelastic scatterings of the system $^{20}\mathrm{Ne} + {}^{76}\mathrm{Ge}$ were studied at the incident energy of 306 MeV at LNS, INFN. The g.s.-to-g.s. transition was separated from the other inelastic channels by means of a good resolution achieved through a careful tuning of the experimental setup and the applied advanced analysis. Moreover, the small error bars and the overall quality of the experimental data are such as to justify the attempt to use sophisticated microscopic analysis. The capability of several optical

potentials to describe the angular distribution of the measured differential cross sections was tested, showing that the response for the AW optical potential and for the DFOL and SPP double-folding potentials is practically the same. However, the standard versions of these potentials were not sufficient to correctly describe the experimental data above the grazing angles. This goal was partially achieved by working with the geometrical parameters of the nuclear matter densities of the involved isotopes. Since both ^{20}Ne and ^{76}Ge are deformed, an effective way to take this property into account is to increase the radii of their nuclear-matter densities by 5%, leading to good agreement of the results with the experimental data up to about 14° in the elastic-scattering angular distribution. Only the inclusion of the couplings with the first low-lying 2^+ excited states made it possible to reproduce the behavior of the experimental data in the whole explored angular range.

ACKNOWLEDGMENTS

This project has received funding from the European Research Council (ERC) within the European Union's Horizon 2020 research and innovation programme under Grant Agreement No. 714625. A. S. would like to thank the Organizing Committee of the VIII International Pontecorvo Neutrino Physics School for their hospitality.

REFERENCES

1. F. Cappuzzello et al., "The NUMEN Project: NUclear Matrix Elements for Neutrinoless Double Beta Decay," *Eur. Phys. J. A* **54**, 72 (2018).
2. H. Lenske, J. I. Bellone, M. Colonna, and J.-A. Lay (NUMEN Collaboration), "Theory of Single-Charge Exchange Heavy-Ion Reactions," *Phys. Rev. C* **98**, 044620 (2018).
3. E. Santopinto, H. García-Tecocoatzi, R. I. Magaña-Vsevolodovna, and J. Ferretti (NUMEN Collaboration), "Heavy-Ion Double-Charge-Exchange and Its Relation to Neutrinoless Double-β Decay," *Phys. Rev. C* **98**, 061601(R) (2018).
4. H. Lenske, F. Cappuzzello, M. Cavallaro, and M. Colonna (NUMEN Collaboration), "Heavy Ion Charge Exchange Reactions as Probes for Nuclear β-Decay," *Prog. Part. Nucl. Phys.* **109**, 103716 (2019).
5. M. Cavallaro et al. (NUMEN Collaboration), "Recent Results on Heavy-Ion Induced Reactions of Interest for Neutrinoless Double Beta Decay at INFN-LNS," *EPJ Web Conf.* **223**, 01009 (2019).
6. F. Cappuzzello, C. Agodi, D. Carbone, and M. Cavallaro, "The MAGNEX Spectrometer: Results and Perspectives," *Eur. Phys. J. A* **52**, 167 (2016).
7. M. Cavallaro et al., "The Low-Pressure Focal Plane Detector of the MAGNEX Spectrometer," *Eur. Phys. J. A* **48**, 59 (2012).
8. F. Cappuzzello et al., "A Particle Identification Technique for Large Acceptance Spectrometers," *Nucl. Instrum. Methods Phys. Res. A* **621**, 419–423 (2010).
9. F. Cappuzzello, D. Carbone, and M. Cavallaro, "Measuring the Ions Momentum Vector with a Large Acceptance Magnetic Spectrometer," *Nucl. Instrum. Methods Phys. Res. A* **638**, 74–82 (2011).
10. S. Calabrese et al. (NUMEN Collaboration), "First Measurement of the ^{116}Cd(^{20}Ne, ^{20}O)^{116}Sn Reaction at 15A MeV," *Acta Phys. Pol. B* **49**, 275 (2018).
11. M. Cavallaro et al. (NUMEN Collaboration), "Charge-State Distributions of ^{20}Ne Ions Emerging from Thin Foils," *Results Phys.* **13**, 102191 (2019).
12. A. Spatafora et al. (NUMEN Collaboration), "^{20}Ne + ^{76}Ge Elastic and Inelastic Scattering at 306 MeV," *Phys. Rev. C* **100**, 034620 (2019).

13. I. J. Thompson, "Coupled Reaction Channels Calculations in Nuclear Physics," *Comput. Phys. Commun.* **7**, 167–212 (1988).
14. R. Ö. Akyüz and A. Winther, "Parameterization of the Nucleus–Nucleus Potential," *Proceedings of the International School of Physics "Enrico Fermi,"* Course **LXXVII** "Nuclear Structure and Heavy-Ion Collisions" (Varenna, 1979), p. 491 (1981).
15. R. A. Broglia and A. Winther, *Heavy Ion Reactions: The Elementary Processes*, Addison-Wesley (1991).
16. H. Lenske, personal communication.
17. L. C. Chamon et al., "Toward a Global Description of the Nucleus–Nucleus Interaction," *Phys. Rev. C* **66**, 014610 (2002).
18. D. Pereira, J. Lubian, J. R. B. Oliveira, D. P. de Sousa, and L. C. Chamon, "An Imaginary Potential with Universal Normalization for Dissipative Processes in Heavy-Ion Reactions," *Phys. Lett. B* **670**, 330–335 (2009).
19. J. R. B. Oliveira et al., "Study of the Rainbow-Like Pattern in the Elastic Scattering of ^{16}O on ^{27}Al at $E_{\text{lab.}} = 100\,\text{MeV}$," *J. Phys. G: Nucl. Part. Phys.* **40**, 105101 (2013).
20. L. M. Fonseca et al., "Elastic and Inelastic Scattering of ^{16}O on ^{27}Al and ^{28}Si at 240 MeV," *Phys. Rev. C* **100**, 014604 (2019).
21. B. Pritychenko, M. Birch, B. Singh, and M. Horoi, "Tables of E2 Transition Probabilities from the First 2^+ States in Even–Even Nuclei," *At. Data Nucl. Data Tables* **107**, 1–139 (2016).

AGENDA

Pontecorvo School 2019 – Agenda

Date	Lecture 1 9:00 - 10:30	Lecture 2 11:00 - 12:30	Lecture 3 16:00 - 17:30	Lecture 4 18:00 - 19:30
Su 1.9.	**Arrival; 18:30 - Welcome party; 19:00 – Dinner**			
Mo 2.9.	**Samoil Bilenky** *Introduction to Neutrino*	**Alexei Smirnov** *Theory of ν–masses and mixing - I*	**Boris Kayser** *Neutrino oscillation phenomenology - II*	**Suchita Kulkarni** *Dark matter searches*
Tu 3.9.	**Alexei Smirnov** *Theory of ν–masses and mixing - II*	**Boris Kayser** *Neutrino oscillation phenomenology - II*	**Juan Pablo Yanez** *Atmospheric ν-experiments*	**Nathan Whitehorn** *ν-telescopes*
We 4.9.	**Anna Hayes** *Spectra of ν's from reactor*	**Henry Wong** *Coherent ν-nucleus elastic scattering*	**Jan Sobczyk** *ν-nucleus interactions*	**Guenakh Mitselmakher** *Everything about Higgs boson*
Th 5.9.	**Oleg Smirnov** *Solar ν-experiments*	**Carlo Giunti** *Light sterile ν's - theory*	**Yuri Shitov** *Light sterile ν's - experiments*	**Dmitry Gorbunov** *Heavy sterile ν's*
Fr 6.9.	**Excursion and free time**			
Sa 7.9.	**Pasquale Di Bari** *Leptogenesis*	**Imre Bartos** *Physics of gravitational waves*	**Maury Goodman** *Accelerator ν-experiments*	**Dmitry Naumov** *Reactor ν-experiments*

Su 8.9.	**Thomas Schwetz** *Statistics for ν-experiments -I*	**Kathrin Valerius** *Measurement of ν-mass*	**Andrea Giuliani** *0νββ-decay experiments*	**Javier Menendez** *0νββ-decay nuclear matrix elements*
Mo 9.9.	**Richard Battye** *ν-properties from cosmology*	**Thomas Schwetz** *Statistics for ν-experiments - II*	**Students presentations**	**Students presentations** **and** **Final panel discussion session**
Tu 10.9.	**Departure**			

Evening problem sessions:

- **Tuesday, 3.9.** Boris Kayser: *Neutrino oscillations*
- **Thursday, 5.9.** Alexei Smirnov: *MSW effect and neutrino oscillations*
- **Saturday, 7.9.:** Samoil Bilenky: *Majorana neutrinos*

Daily timetable

8:00-9:00		16:00-19:30
Breakfast	12:30-13:30	Afternoon session
9:00-12:30	Lunch	17:30-18:00
Morning session	13:30-16:00	Coffee break
10:30-11:00	Free time	19:30-20:30
Coffee break		Dinner

LIST OF PARTICIPANTS

List of lectures

	Photo	Name Affiliation Email		Photo	Name Affiliation Email
1		Bilenky Samoil JINR Dubna, Russia *bilenky@gmail.com*	2		Bartos Imre Univ. of Florida, USA *imrebartos@ufl.edu*
3		Battye Richard Univ. of Manchester, UK *richard.battye@manchester.ac.uk*	4		DiBari Pasquale Univ. of Southampton, UK *P.Di-Bari@soton.ac.uk*
5		Giuliani Andrea CSNSM in Paris, France *andrea.giuliani@csnsm.in2p3.fr*	6		Giunti Carlo INFN Torino, Italy *giunti.carlo@gmail.com*
7		Goodman Maury Argonne National Lab., USA *maury.goodman@anl.gov*	8		Gorbunov Dmitry INR RAS Moscow, Russia *gorby@inr.ac.ru*
9		Hayes Anna Los Alamos National Lab., USA *anna_hayes@lanl.gov*	10		Kulkarni Suchita HEPHY Vienna, Austria *Suchita.Kulkarni@oeaw.ac.at*
11		Kayser Boris Fermilab, USA *boris@fnal.gov*	12		Menendez Javier Univ. of Barcelona, Spain *menendez@fqa.ub.edu*

13		Mitselmakher Guenakh Univ. of Florida, USA *mitselmakher@phys.ufl.edu*	14		Naumov Dmitry JINR Dubna, Russia *dmitryvnaumov@gmail.com*
15		Shitov Yuri JINR Dubna, Russia *shitov@jinr.ru*	16		Smirnov Alexei MPI Heidelberg, Germany *smirnov@mpi-hd.mpg.de*
17		Smirnov Oleg JINR Dubna, Russia *osmirnov@jinr.ru*	18		Sobczyk Jan Univ. of Wroclaw, Poland *jan.sobczyk@uwr.edu.pl*
19		Schwetz Thomas KIT in Karlsruhe, Germany *schwetz@kit.edu*	20		Valerius Kathrin KIT in Karlsruhe, Germany *kathrin.valerius@kit.edu*
21		Whitehorn Nathan Univ. of California, USA *nwhitehorn@physics.ucla.edu*	22		Wong Henry Academia Sinica, Taipei, Taiwan *htwong@phys.sinica.edu.tw*
23		Yanez Juan Pablo Univ. of Alberta, Canada *j.p.yanez@ualberta.ca*			

List of participants

№	Last name	First name	Affiliation	Country	E-mail
1	Aker	Max	KIT, Karlsruhe	Germany	*max.aker@kit.edu*
2	Álvarez	Alejandro Uribe	IEAP CTU in Prague	Czech Republic	*aalvar54@eafit.edu.co*
3	Anghel	Claudia-Ioana	IFIN-HH, Bucharest	Romania	*claudia.anghel@theory.nipne.ro*
4	Antonova	Maria	Inst. de Física Corpuscular, Paterna	Spain	*maria.antonova@ific.uv.es*
5	Astalos	Robert	Comenius Univ., Bratislava	Slovakia	*robcoas@gmail.com*
6	Avrorin	Alexander	INR, Moscow	Russia	*avrorin@jinr.ru*
7	Babic	Andrej	IEAP CTU in Prague	Czech Republic	*andrej.babic@utef.cvut.cz*
8	Bardacova	Zuzana	Comenius Univ., Bratislava	Slovakia	*zuzanabardacova@gmail.com*
9	Belov	Viacheslav	JINR, Dubna	Russia	*vvbelov@jinr.ru*
10	Benso	Cristina	MPI, Heidelberg	Germany	*cristina.benso@mpi-hd.mpg.de*
11	Blazek	Tomas	Comenius Univ., Bratislava	Slovakia	*blazek@fmph.uniba.sk*
12	Bonciu	Anca Florina	INFLPR, Măgurele	Romania	*anca.bonciu.ub@gmail.com*
13	Chiriacescu	Ana	Univ. of Bucharest	Romania	*anachiriacescu@gmail.com*
14	Dmitrievsky	Sergey	JINR, Dubna	Russia	*dmitr@jinr.ru*
15	Dolzhikov	Dmitrii	JINR, Dubna	Russia	*dolzhikov.d.a@gmail.com*
16	Dvornicky	Rastislav	Comenius Univ. Bratislava	Slovakia	*rastonator@gmail.com*
17	Eckerova	Eliska	Comenius Univ., Bratislava	Slovakia	*eliska.eckerova@gmail.com*
18	Ershova	Anna	MIPT, Moscow	Russia	*anna.ershova@phystech.edu*
19	Fomina	Maria	JINR, Dubna	Russia	*masjnj.89@mail.ru*
20	Ghinescu	Stefan-Alexandru	CIFRA, Bucharest	Romania	*ghinescustefanalexandru95@gmail.com*
21	Helej	Markus	Comenius Univ., Bratislava	Slovakia	*Markus.Helej@fmph.uniba.sk*
22	Helis	Dounia	CEA , Paris	France	dounia.helis@cea.fr
23	Huang	Guihong	IHEP, Beijing	China	*huanggh@ihep.ac.cn*
24	Hussain	Hamzah	Univ. College London	UK	*ucapmhh@ucl.ac.uk*
25	Ilyasov	Aidar	MEPhI, Moscow	Russia	*ilyasovaid@yandex.ru*
26	Jokiniemi	Lotta Maria	Univ. of Jyväskylä	Finland	*lotta.m.jokiniemi@jyu.fi*
27	Kakorin	Igor	JINR, Dubna	Russia	*idkakorin@gmail.com*

28	Kalitkina	Anastasiia	JINR, Dubna	Russia	*mir8796@gmail.com*
29	Karl	Christian	MPI, Munich	Germany	*karlch@mpp.mpg.de*
30	Kasperovych	Dmytro	INR, Kyiv	Ukraine	*casper.phys@gmail.com*
31	Kazartsev	Sergey	JINR, Dubna	Russia	*kazarcevs@gmail.com*
32	Kis	Stefan Tiberiu	West Univ., Timişoara	Romania	*stefan.kis@e-uvt.ro*
33	Klavdiienko	Volodymyr	INR, Kyiv	Ukraine	*klavdiienko.volodymyr@gmail.com*
34	Lebert	Manuel	MPP, Munich	Germany	lebert@mpp.mpg.de
35	Lukashevich	Svetlana	Gomel State Univ.	Belarus	*lukashevich@gsu.by*
36	Macko	Miroslav	Czech Technical Univ., Prague	Czech Republic	*macko.mire@gmail.com*
37	Mare	Adrian Sorin	IFIN-HH, Bucharest	Romania	*adrian.mare@nipne.ro*
38	Marsteller	Alexander	KIT, Karlsruhe	Germany	*alexander.marsteller@kit.edu*
39	Matak	Peter	Comenius Univ., Bratislava	Slovakia	*peter.matak@gmail.com*
40	Meszaros	Peter	Comenius Univ., Bratislava	Slovakia	*meszaros317@gmail.com*
41	Mihalceanu	Stelian	Univ. of Bucharest	Romania	*stelian.physics@gmail.com*
42	Nagu	Srishti	Univ. of Lucknow	India	*srishtinagu19@gmail.com*
43	Neacsu	Andrei	IFIN-HH, Bucharest	Romania	*nandrei@theory.nipne.ro*
44	Niewczas	Kajetan	Univ. of Wrocław	Poland	*kajetan.niewczas@uwr.edu.pl*
45	Nitescu	Ovidiu-Vasile	CIFRA, Bucharest	Romania	*nitescu.ovidiuvasile@gmail.com*
46	Nosek	Tomas	Charles Univ., Prague	Czech Republic	*xnosekt@seznam.cz*
47	Novotny	Dominik	Comenius Univ., Bratislava	Slovakia	*do39minik@gmail.com*
48	Nugmanov	Radik	Kurchatov Inst., Moscow	Russia	*rrnugmanov@gmail.com*
49	Nurtayeva	Ulkhanym	JINR, Dubna	Russia	*nurtaeva@jinr.ru*
50	Parvu	Mihaela	Univ. of Bucharest	Romania	*mihaela.parvu@drd.unibuc.ro*
51	Paun	Alice-Mihaela	INFLPR, Măgurele	Romania	*alice.paun@spacescience.ro*
52	Petro	Maroš	IEAP CTU in Prague	Czech Republic	*maros.petro@cvut.cz*
53	Petropavlova	Maria	JINR, Dubna	Russia	*maria.petropavlova@gmail.com*
54	Picciau	Emmanuele	Univ. of Cagliari	Italy	*emmanuele.picciau@ca.infn.it*
55	Poenaru	Robert	IFIN-HH, Bucharest	Romania	*robert.poenaru@theory.nipne.ro*
56	Prisco	Renato Maria	Univ. of Naples Federico II	Italy	*priscorenato@gmail.com*

57	Romanyuk	Maria	Kiev institute for Nuclear Research	Ukraine	*romanyukmariya@ukr.net*
58	Rumyantseva	Nadezda	JINR, Dubna	Russia	*rumyantseva.nads@gmail.com*
59	Scafes	Adela Consuela	IFIN-HH, Bucharest	Romania	*ascafes@tandem.nipne.ro*
60	Schweizer	Konstantin	TUM, Munich	Germany	*k.schweizer@tum.de*
61	Shelepov	Mark	INR, Moscow	Russia	*Shelepov-1992@mail.ru*
62	Shevchik	Egor	JINR, Dubna	Russia	*egor.shevchik@gmail.com*
63	Siemaszko	Michal Mateusz	Univ. of Wrocław	Poland	*michal.siemaszko@ift.uni.wroc.pl*
64	Singh	Jaydip	Univ. of Lucknow	India	*jaydip.singh@gmail.com*
65	Sitnikova	Elizaveta	MIPT, Moscow	Russia	*sitnikova.ea@phystech.edu*
66	Smetana	Adam	IEAP CTU in Prague	Czech Republic	*adam.smetana@cvut.cz*
67	Sokur	Nazar	Taras Shevchenko National Univ., Kyiv	Ukraine	*nazar147@ukr.net*
68	Sorokovikov	Maksim	JINR, Dubna	Russia	*sorokovikov@jinr.ru*
69	Spatafora	Alessandro	INFN, Catania	Italy	*alessandro.spatafora@lns.infn.it*
70	Strobl	Patrick	TUM, Munich	Germany	*patrick1.strobl@tum.de*
71	Suchy	Daniel	Comenius Univ., Bratislava	Slovakia	*suchy.daniel@gmail.com*
72	Sushenok	Evgenii	JINR, Dubna	Russia	*sushenok.eo@gmail.com*
73	Titov	Oleg	Kurchatov Inst., Moscow	Russia	*titov-o@mail.ru*
74	Ur Rehman	Junaid	COMSATS Univ., Islamabad	Pakistan	*junaidurrehman329@gmail.com*
75	Urban	Korbinian	MPP, Munich	Germany	*kurban@mpp.mpg.de*
76	Wang	Yakun	Peking Univ.	China	*wangyk15@pku.edu.cn*
77	Wu	Di	Sichuan Univ., Chengdu	China	*di.wu@stu.scu.edu.cn*
78	Zhu	Yi	Inst. of Modern Physics, Lanzhou	China	*1027231899@qq.com*

	Photo	Name Affiliation Email		Photo	Name Affiliation Email

Plenipotentiary of Romania by the JINR Dubna

		Buzatu Florian-Dorian Institute of Atomic Physics, Bucharest, Romania f.buzatu@ifa-mg.ro

Organizing committee: vice-chairmen and members

1		Samoil Bilenky JINR Dubna, Russia bilenky@gmail.com	2		Giunti Carlo INFN Torino, Italy giunti.carlo@gmail.com
3		Olshevskiy Alexander JINR Dubna, Russia olshevsk@gmail.com	4		Stoica Sabin CIFRA, Bucharest, Romania Sabin.stoica@cifra-c2unesco.ro
5		Šimkovic Fedor Comenius University in Bratislava, Slovakia and JINR Dubna, Russia simkovic@fmph.uniba.sk	6		Štekl Ivan IEAP, Czech Technical University in Prague, Czechia Ivan.Stekl@utef.cvut.cz

Organizing committee: secretaries

1		Ali Deniz Bucharest	2		Babič Andrej JINR Dubna, Russia and IAEP, CTU in Prague, Czechia
	hisame.artwork@gmail.com			*andrejbabic@centrum.sk*	
3		Militaru Cristina CIFRA, Bucharest, Romania	4		Neacsu Andrei CIFRA, Bucharest, Romania
	cristina.militaru@infim.ro			*jneandrei@gmail.com*	
5		Nitescu Ovidiu CIFRA, Bucharest, Romania			
	Ovidiu.nitescu@infim.ro				

POSTERS OF PREVIOUS SCHOOLS

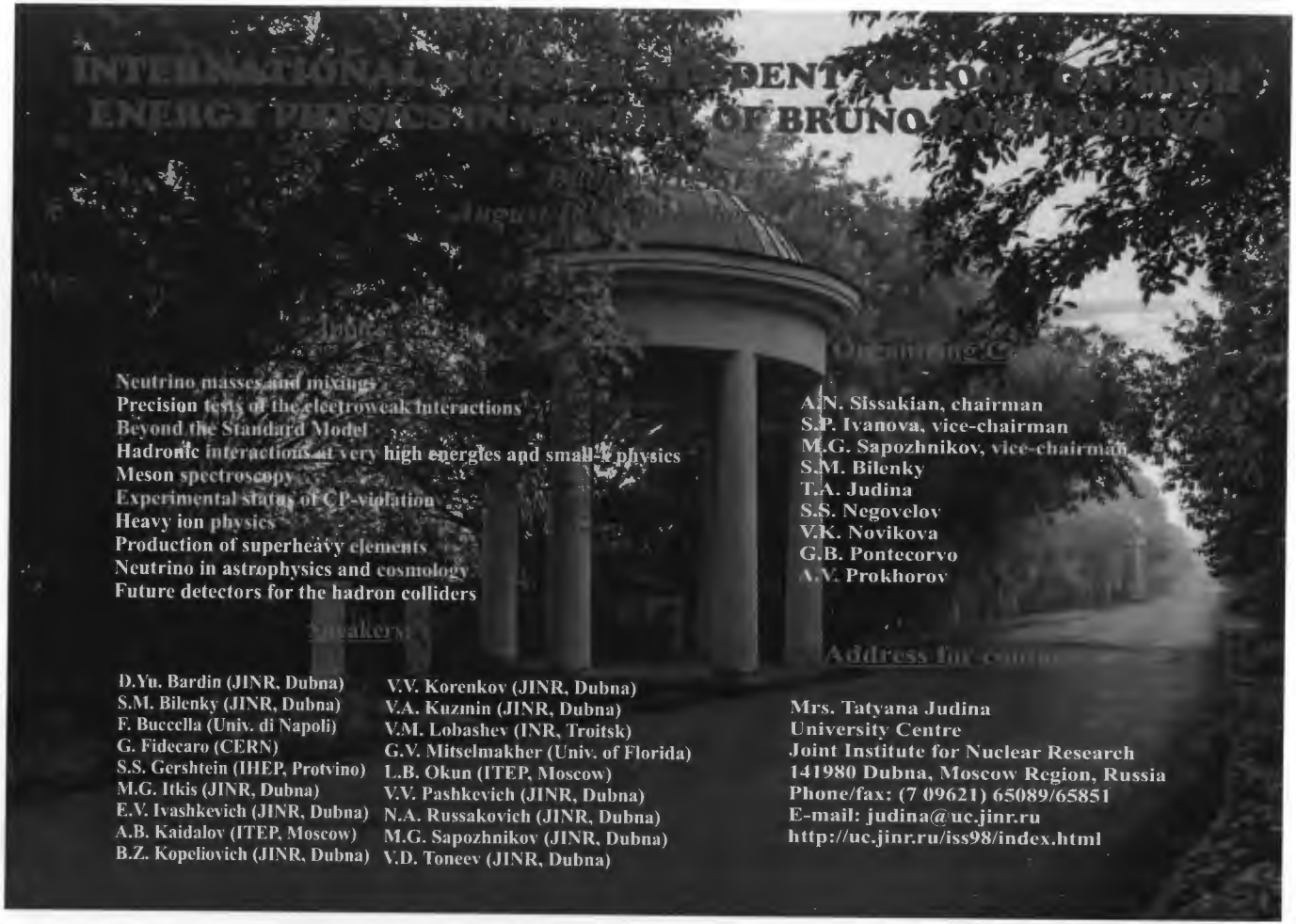

Neutrino masses and mixings
Precision tests of the electroweak interactions
Beyond the Standard Model
Hadronic interactions at very high energies and small-x physics
Meson spectroscopy
Experimental status of CP-violation
Heavy ion physics
Production of superheavy elements
Neutrino in astrophysics and cosmology
Future detectors for the hadron colliders

A.N. Sissakian, chairman
S.P. Ivanova, vice-chairman
M.G. Sapozhnikov, vice-chairman
S.M. Bilenky
T.A. Judina
S.S. Negovelov
V.K. Novikova
G.B. Pontecorvo
A.V. Prokhorov

Speakers:

D.Yu. Bardin (JINR, Dubna)
S.M. Bilenky (JINR, Dubna)
F. Buccella (Univ. di Napoli)
G. Fidecaro (CERN)
S.S. Gershtein (IHEP, Protvino)
M.G. Itkis (JINR, Dubna)
E.V. Ivashkevich (JINR, Dubna)
A.B. Kaidalov (ITEP, Moscow)
B.Z. Kopeliovich (JINR, Dubna)
V.V. Korenkov (JINR, Dubna)
V.A. Kuzmin (JINR, Dubna)
V.M. Lobashev (INR, Troitsk)
G.V. Mitselmakher (Univ. of Florida)
L.B. Okun (ITEP, Moscow)
V.V. Pashkevich (JINR, Dubna)
N.A. Russakovich (JINR, Dubna)
M.G. Sapozhnikov (JINR, Dubna)
V.D. Toneev (JINR, Dubna)

Address for contact:

Mrs. Tatyana Judina
University Centre
Joint Institute for Nuclear Research
141980 Dubna, Moscow Region, Russia
Phone/fax: (7 09621) 65089/65851
E-mail: judina@uc.jinr.ru
http://uc.jinr.ru/iss98/index.html

1913 - 1993

Joint Institute for Nuclear Research
University Centre

Second International Summer Student School on Neutrino Physics in Memory of Bruno Pontecorvo

7-18 September, 2003
Alushta, Ukraine

TOPICS

- Phenomenology of neutrino and lepton mixing
- Nature of neutrino masses
- Neutrinos and astrophysics
- Neutrinos from the Sun
- Atmospheric neutrinos
- Long-baseline experiments with neutrinos
- Neutrinoless double beta decay
- Direct measurements of neutrino mass in tritium decay
- Neutrino factories
- Life of Bruno Pontecorvo

A request for registration should be sent to the School secretaries:
Mr. Mikhail Zhabitsky and Mrs. Elena Russakovich
University Centre
Joint Institute for Nuclear Research
141980 Dubna, Moscow Region, Russia
Phone/fax (7 09621)65089/65851
E-mail: zhabitsk@nusun.jinr.ru
rusakovich@jinr.ru
http://uc.jinr.ru/iss2003/

Бруно Понтекорво

III Interational Pontecorvo Neutrino Physics School

16 - 26 September, 2007

Resort House "Dubna" in Alushta, Crimea, Ukraine

Organized by the Joint Institute for Nuclear Research

Contacts:

Tatyana DONSKOVA
Tatyana.Donskova@jinr.ru

Anastasia BOLSHAKOVA
nst@nusun.jinr.ru

http://www.jinr.ru/pontecorvo07/

The program of the school will cover modern topics of neutrino physics including phenomenology, experimental results and theory.

Organizing Committee:

A. Sissakian - chairman

S. Bilenky - member of the Committee

A. Bolshakova - scientific secretary

T. Donskova - secretary

A. Olchevski - vice-chairman

Topics:

- Phenomenology of neutrino mixing and oscillations;
- Neutrino oscillation results and prospects;
- Neutrinoless double beta decay;
- Theory of neutrino mass and mixing;
- Direct determination of neutrino masses.

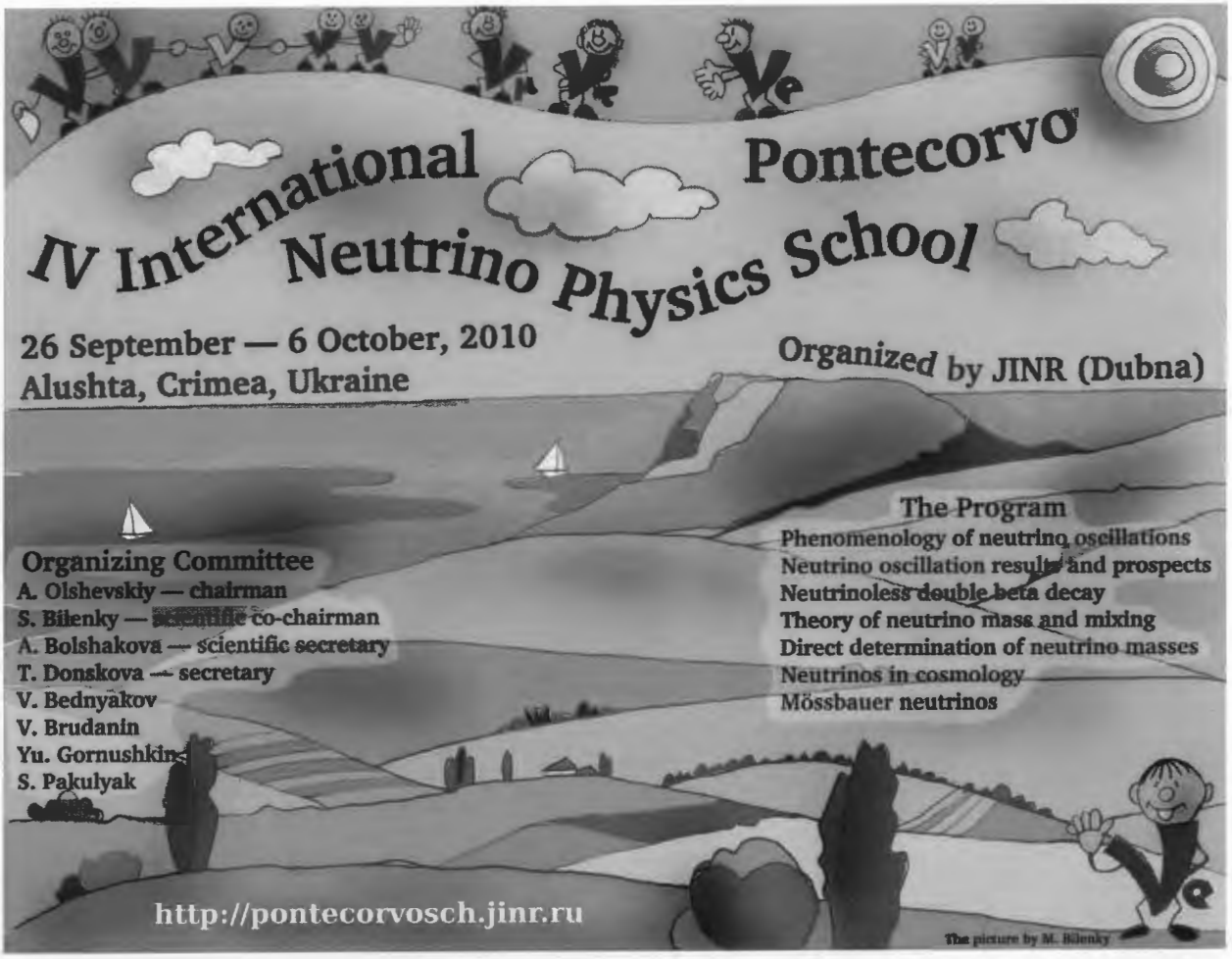
IV International Pontecorvo Neutrino Physics School
26 September — 6 October, 2010
Alushta, Crimea, Ukraine
Organized by JINR (Dubna)
Organizing Committee
A. Olshevskiy — chairman
S. Bilenky — scientific co-chairman
A. Bolshakova — scientific secretary
T. Donskova — secretary
V. Bednyakov
V. Brudanin
Yu. Gornushkin
S. Pakulyak
The Program
Phenomenology of neutrino oscillations
Neutrino oscillation results and prospects
Neutrinoless double beta decay
Theory of neutrino mass and mixing
Direct determination of neutrino masses
Neutrinos in cosmology
Mössbauer neutrinos
http://pontecorvosch.jinr.ru
The picture by M. Bilenky

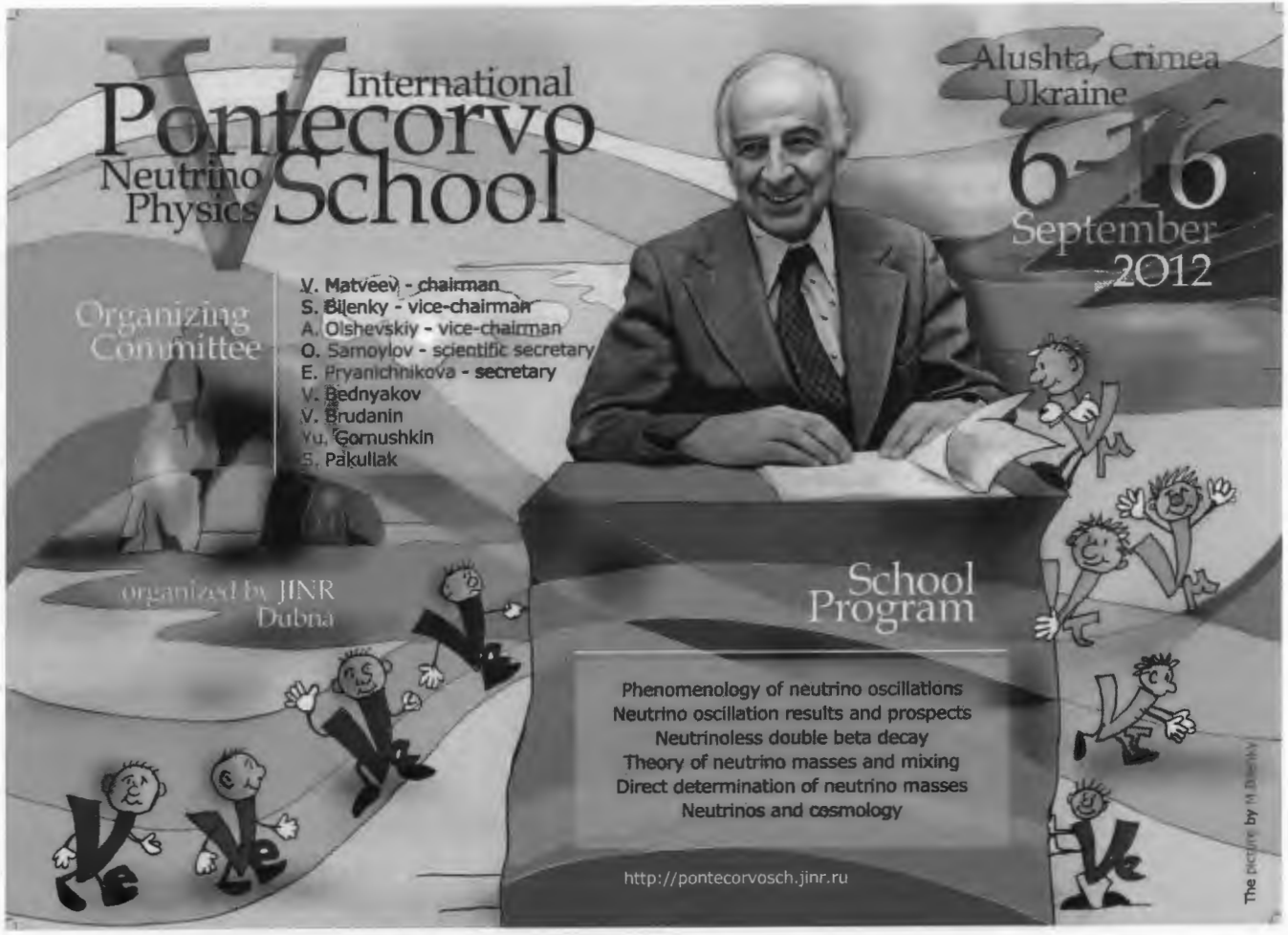
V International
Pontecorvo
Neutrino Physics School
Alushta, Crimea
Ukraine
6-16
September
2012
Organizing Committee
V. Matveev - chairman
S. Bilenky - vice-chairman
A. Olshevskiy - vice-chairman
O. Samoylov - scientific secretary
E. Pryanichnikova - secretary
V. Bednyakov
V. Brudanin
Yu. Gornushkin
S. Pakuliak
organized by JINR
Dubna
School Program
Phenomenology of neutrino oscillations
Neutrino oscillation results and prospects
Neutrinoless double beta decay
Theory of neutrino masses and mixing
Direct determination of neutrino masses
Neutrinos and cosmology
http://pontecorvosch.jinr.ru
The picture by M.Bilenky

VI International Pontecorvo Neutrino Physics School

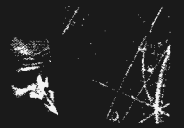

August 27 – September 4, 2015
Horný Smokovec, Slovakia

(http://theor.jinr.ru/~neutrino15/)

Organizing Committee:

V. A. Matveev chairman
S. M. Bilenky - scientific program
F. Šimkovic - vice-chairman
A. G. Olshevskiy - vice-chairman
I. Štekl - vice-chairman
V. A. Bednyakov

R. Leitner
V. B. Brudanin
E. A. Kolganova
O. Matyukhina
D. Štefanik
A.E. Bolshakova
R. Dvornicky

Lectures at School:

Neutrinos in SM and beyond:	Samoil Bilenky (JINR Dubna)	*0νββ-decay: EXO and KamLAND-Zen:*	Andreas Piepke (U. of Alabama)
Phenomenology of ν-mixing and oscillations:	Serguey Petcov (SISSA)	0νββ-decay : GERDA:	Stefan Schoenert (TU Muenchen)
Long baseline ν-oscillation experiments:	David Wark (Oxford U.)	*Neutrinos in cosmology and astronomy:*	Steen Hannestadt (Aarhus U.)
Reactor ν experiments:	Rupert Leitner (Charles U.)	*Physics at IceCube:*	Elisa Resconi (TU Muenchen)
Atmospheric neutrinos:	Yoichiro Suzuki (U. of Tokyo)	*Baikal experiment:*	Zhan-Arys Dzhilkibaev (INR Moscow)
Solar- and geo-neutrinos:	Oleg Smirnov (JINR Dubna)	*Supernova and relic neutrinos:*	Petr Vogel (CATLTECH)
Theory of ν–masses:	Werner Rodejohann (MPI Heidelberg)	*Dark Matter:*	Walter Potzel (TU Muenchen)
Baryogenesis from Leptogenesis:	Sasha Davidson (IPNL Lyon)	*News from CERN:*	Sergio Bertolucci (CERN)
Direct ν-mass search:	Christian Weinheimer (U. of Muenster)	*Progressive detection techniques:*	Ettore Fiorini (U. di Milano-Bicocca)
Theory of 0νbb-decay :	Martin Hirsch (U. of Valencia)	*Progressive detection techniques II:*	Ivan Štekl (CTU Prague)
Double Beta Decay Matrix Elements:	Fedor Šimkovic (Comenius U.)	*Statistics for Nuclear and Particle Physics:*	Louis Lyons (U. of Oxford)

VII International Pontecorvo Neutrino Physics School 2017

http://theor.jinr.ru/~neutrino17

August 20 – September 1, 2017

Prague, Czech Republic

Introduction to ν-physics	Bilenky S. (JINR Dubna)
Theory of ν-masses and mixing	King S.F. (Southampton Univ.)
ν-oscillation phenomenology	Kayser B. (Fermilab)
Solar ν-experiments and theory	Smirnov A. (MPI Heidelberg)
Accelerator ν-experiments	Feldman G.J. (Harvard Univ.)
Reactor ν-experiments	Wang Y. (IHEP)
Measurement of ν-mass	Tkachev I. (INR RAS, Moscow)
	Gastaldo L. (Heidelberg Univ.)
0νββ-decay experiments	Barabash A. (ITEP Moscow)
0νββ-decay nuclear matrix elements	Vogel P. (Caltech)
ν-nucleus interactions	Sobczyk J. (Wroclaw Univ.)
Sterile neutrinos	Link J. (Virginia Tech.)
	Giunti C. (INFN Torino)
Leptogenesis	Davidson S. (IPNL Lyon)
ν-astronomy	Tamborra I. (Copenhagen Univ.)
ν-telescopes	Spiering C. (DESY)
ν-cosmology	Mangano G. (INFN Naples)
Dark matter experiments	Fornengo N. (INFN Torino)
Observation of gravitational waves	Barish B. (CALTECH)
Neutrino physics at CERN	Elsen E. (CERN)
Future colliders	Blondel A. (CERN)
Statistics for Nucl. and Particle Phys.	Dyk D.V. (IC, London)

Organized by

Joint Institute for Nuclear Research (Dubna, Russia)
Czech Technical University (Prague, Czech Republic)
Charles University (Prague, Czech Republic)
Comenius University (Bratislava, Slovakia)
Institute of Nuclear Physics (Krakow, Poland)

Organizing Committee

Matveev V.A. (JINR)	- chairman
Bilenky S.M. (JINR)	- scientific program
Štekl I. (CTU)	- vice-chairman
Olshevskiy A.G. (JINR)	- vice-chairman
Šimkovic F. (CU/JINR)	- vice-chairman
Jezabek M. (INP)	- vice-chairman

Members

Bednyakov V.A. (JINR) Leitner R. (ChU)
Zalewska A. (INP) Brudanin V.B. (JINR)
Rondio E. (NCBJ, Swierk) Kolganova E.A. (JINR)

Secretaries

Hodák R. (CTU) Rusakovich E. (JINR)
Rukhadze E. (CTU) Vanišová M. (CTU)

150 =

Научное издание

VIII INTERNATIONAL PONTECORVO NEUTRINO PHYSICS SCHOOL

Proceedings of Student Poster Session

VIII МЕЖДУНАРОДНАЯ ШКОЛА ПО ФИЗИКЕ НЕЙТРИНО ИМ. Б. М. ПОНТЕКОРВО

Труды студенческой постерной сессии

Ответственная за подготовку сборника к печати *А. В. Малых*.

Сборник отпечатан методом прямого репродуцирования с оригиналов, предоставленных оргкомитетом.

E1,2,4-2020-16

Подписано в печать 5.08.2020.
Формат 60×90/16. Бумага офсетная. Печать офсетная.
Усл. печ. л. 11,88. Уч.-изд. л. 19,23. Тираж 135 экз. Заказ 59966.

Издательский отдел Объединенного института ядерных исследований
141980, г. Дубна, Московская обл., ул. Жолио-Кюри, 6.
E-mail: publish@jinr.ru
www.jinr.ru/publish/